2013

Turbulent Structure in Open Channel Flow

Mohammad H. Asgari Kaji
University of Windsor

TURBULENCE STRUCTURE IN NON-UNIFORM OPEN CHANNEL FLOW

by

Mohammad H. Asgari Kaji

A Thesis
Submitted to the Faculty of Graduate Studies
through the Department of Civil and Environmental Engineering
in Partial Fulfillment of the Requirements for
the Degree of Master of Applied Science at the
University of Windsor

Windsor, Ontario, Canada

2013

Turbulence Structure in Non-uniform Open Channel Flow

by

Mohammad H. Asgari Kaji

APPROVED BY:

_____

Ronald M. Barron
Department of Mechanical, Automotive and Material Engineering

_____

Tirupati Bolisetti
Department of Civil and Environmental Engineering

_____

Vesselina Roussinova, Co-Advisor
Department of Civil and Environmental Engineering

_____

Ramaswami Balachandar, Advisor
Department of Civil and Environmental Engineering

DECLARATION OF ORIGINALITY

I hereby certify that I am the sole author of this thesis and that no part of this thesis has been published or submitted for publication.

I certify that, to the best of my knowledge, my thesis does not infringe upon anyone's copyright nor violate any proprietary rights and that any ideas, techniques, quotations, or any other material from the work of other people included in my thesis, published or otherwise, are fully acknowledged in accordance with the standard referencing practices. Furthermore, to the extent that I have included copyrighted material that surpasses the bounds of fair dealing within the meaning of the Canada Copyright Act, I certify that I have obtained a written permission from the copyright owner(s) to include such material(s) in my thesis and have included copies of such copyright clearances to my appendix.

I declare that this is a true copy of my thesis, including any final revisions, as approved by my thesis committee and the Graduate Studies office, and that this thesis has not been submitted for a higher degree to any other University or Institution.

ABSTRACT

This thesis investigates the effects of pressure gradient and roughness on the mean and turbulence characteristics in non-uniform open channel flow. The flow and turbulence structure over three successive beds with accelerating, near uniform (near zero pressure gradient) and decelerating flow sections were investigated using a two-component laser Doppler velocimetry. The Clauser chart method was considered for evaluating the friction velocity. Inspection of the velocity profiles confirms existence of the overlap region for all flow cases. The upstream condition emanating from the accelerating flow section affects the turbulence characteristics in the near zero pressure gradient section. The outer layer of the velocity distribution of the decelerating section was strongly affected by the pressure gradient, where a large wake was noted. In the outer layer, higher turbulence intensities were noted for the adverse pressure gradient flow. The combined effects of the pressure gradient and roughness on turbulence quantities were further investigated.

DEDICATION

In loving memory of my father, Ghodratollah (1940 - 2011).

To my mother, Mahpasand, for her love and endless support

and

To my wife Somayeh, who supported me each step of the way

Thanks for your support.

ACKNOWLEDGEMENTS

I would like to extend my deepest appreciation to my advisors Prof. Ramaswami Balachandar and Dr. Vesselina Roussinova for giving me the opportunity to study with them. Furthermore, thanks are also due to their invaluable advices, inspiration, inventive ideas, encouragement and supports throughout my research. It has been a pleasure to work with and learn from such extraordinary individuals.

I would like to extend my gratitude to my graduate committee members: Prof. Ronald Barron and Dr. Tirupati Bolisetti for their useful suggestions, careful review.

My sincere thanks are for Mr. Matt St. Louis for his enthusiastic and brilliant solutions to make and maintain the experimental setup.

Without financial supports this study would not be possible. In fact, all financial supports from my supervisors and University of Windsor are really appreciated.

I owe my deepest thanks to my family; my mother, my wife, my sisters and brother who have always stood by me and guided me through my career.

Lastly, thank God!

TABLE OF CONTENTS

LIST OF TABLES

LIST OF FIGURES

NOMENCLATURE

ACRONIMS

ADV	Acoustic Doppler Velocimetry
APG	Adverse Pressure Gradient
FPG	Favourable Pressure Gradient
LDV	Laser Doppler Velocimetry
NZPG	Near Zero Pressure Gradient
OCF	Open Channel Flow
PIV	Particle Image Velocimetry
ZPG	Zero Pressure Gradient

ENDLISH SYMBOLS

a	power-law constant
B	log-law constant
B_i	power-law constant
B_o	power-law constant
C	power-law constant
C_i	power-law constant
C_o	power-law constant
C_s	power-law constant
E	power-law constant
f	logarithmic function related to the inner layer
Fr	Froude number
g	gravitational acceleration (m/s^2)
h	depth of flow (mm)
H	boundary layer shape factor
k_s	equivalent sand roughness height (mm)
K	favourable pressure gradient parameter
P	pressure (N/m^2)
Re	Reynolds number
Re_x	Reynolds number based on distance from the start of the bed
Re_h	Reynolds number based on depth of flow

Re_θ	Reynolds number based momentum thickness
T	temperature ($^\circ$C)
u	streamwise turbulence intensities (m/s)
u^*	friction velocity (m/s)
u'	streamwise velocity fluctuation (m/s)
u_h	streamwise velocity at the free surface (m/s)
U	streamwise component of mean velocity (m/s)
U_e	maximum streamwise component of mean velocity (m/s)
v	vertical turbulence intensities (m/s)
v'	vertical velocity fluctuation (m/s)
v_h	vertical velocity at the free surface (m/s)
V	vertical component of mean velocity (m/s)
x	streamwise direction
y	vertical or wall normal direction

GREEK SYMBOLS

α	power-law constant
β	adverse pressure gradient parameter
β_i	power-law constant
β_o	power-law constant
ΔU^+	roughness function
γ	power-law constant
Γ	power-law constant
δ	boundary layer thickness (mm)
δ^*	boundary layer displacement thickness (mm)
ε	shift in position from the vertical coordinate (mm)
θ	boundary layer momentum thickness (mm) or angle of the channel bed made with the horizontal axis (degree)
κ	von Karman constant
μ	dynamic viscosity (N.s/m^2)
ν	kinematic viscosity (m^2/s)
ξ	power-law constant

Π	Coles wake parameter
ρ	density (kg/ m^3)
σ	Reynolds normal stress (N/ m^2)
τ	shear stress (N/ m^2)
τ_w	wall shear stress (N/ m^2)
ω	wake function which is universal function of y/ δ

SUBCRIPT

max	maximum
RMS	root mean square

SUPERCRIPT

+	normalized by viscous units

CHAPTER I

INTRODUCTION

1.1 Open Channel Flow

Open channel flow is a flow in a channel (conduit) that is not completely filled and a free surface is formed between the flowing fluid (water) and the air. The gravity force is the main force that drives such flows. Most open channel flow correlations have been obtained from laboratory small-scale models under uniform flow conditions.

Significant attention has been given to the study of open channel flow and its turbulence characteristics. The flow in open channel can be classified, based on different criteria such as developing, fully developed, uniform, non-uniform laminar, turbulent, and so on. The existence of the free surface also allows the fluid to self-select its configuration (Munson, 2011). It is important to pay attention to uniform and non-uniform open channel flows, so this study mainly focuses on these two types of open channel flows. An open channel flow can be classified as uniform flow if the depth of flow (h) does not vary along the channel, and it is a non-uniform flow if the depth varies along the channel. Depending on various conditions, as well as the Reynolds number, open channel flow can also be laminar, transitional, or turbulent. Since 1970, extensive experimental and theoretical investigations of turbulent flows over smooth and rough surfaces have been completed by Grass (1971), Krogstad *et al.(*1992), Nezu and Nakagawa (1993a), Balachandar and Tachie (2001), Castillo and George (2001), Tachie (2001), Nezu (2005), Balachandar and Bhuiyan (2007), Afzal *et al*. (2009), and Emamzadeh *et al.* (2010) among many others.

1.2 Uniform and Non-uniform Open Channel Flow

A uniform flow is one in which the velocity and depth remain constant over distance while in non-uniform flow, both velocity and depth vary. Due to changes in the channel cross-section from point to point, uniform flow condition rarely occurs in either naturally occurring or man-made channels. Uniform flow can occur only in a channel of constant cross-section, roughness, and slope in the flow direction. Non-uniform flow can occur in both man-made and natural channel with variable geometrical properties. The presence of the pressure gradient is the main cause of non-uniformity and has a global influence on the flow. Although moderate non-uniform open channel flows do actually exists, such case are usually assumed as uniform flow. At the river each bed slope can cause the depth and velocity to vary from upstream to downstream as a result, the water surface will not be parallel to the bed. If the channel's cross-sectional area decreases in the downstream direction, the flow is going to accelerate flow with a positive velocity dU_e/dx gradient and negative pressure gradient. On the other hand, if the channel's cross-sectional area increases, decelerating flow will be generated and negative velocity gradients and positive pressure gradients will occur. Mathematically, pressure p(x) is linked to the free stream velocity U(x) according to the Bernoulli's equation and the pressure gradient is:

$$-\frac{dp}{dx} \propto \rho U \frac{dU}{dx} \tag{1.1}$$

Accelerating flow ($\frac{\mathrm{dU}}{\mathrm{dx}} > 0$) corresponds to a negative or favourable pressure gradient, and decelerating flow ($\frac{\mathrm{dU}}{\mathrm{dx}} < 0$) yields a positive or adverse pressure gradient that can lead to separation of the boundary layer of the surface. Alternatively, if $\frac{\mathrm{dU}}{\mathrm{dx}} = 0$, then uniform flow with zero pressure gradient will be achieved.

Recently, zero pressure gradient (ZPG) turbulent boundary flows on a flat plate with constant surface velocity have received considerable attention. Many studies such as song and Chiew (2001), Yang and Chow (2008), and Emamzadeh *et al.* (2010) have focused on understanding how turbulent boundary layer characteristics change once the boundary layer meets a favourable pressure gradient (FPG) or adverse pressure gradient (APG).

1.3 Turbulent Boundary Layer in an Open Channel Flow

Turbulence transport of momentum, heat and mass have important influences on many flows investigated in, fluid mechanics, hydraulic engineering and environmental sciences. Turbulence measurements in open channel flows started in the 1970s (Nezu and Nakagawa, 1993). Application of the laser Doppler velocimetry (LDV) enabled researchers to accurately measure turbulence quantities in one, two or three dimensions.

With a vertical organization of the flow structure in open channel flows (Fig 1.1), it is reasonable to postulate that in two-dimensional open channel flow, which is the topic of this thesis, velocity profile shape can be deduced from an inner and outer layer plus an intermediate overlapping region between the two. In the region near the viscous (molecular) shear layer, where the viscosity is dominant, and the wall (bed) bounded flow is controlled by the inner variables such as kinematic viscosity (ν) and friction velocity (u^*). Accurate estimate of friction velocity is very important since it is used as a velocity scaling parameter to collapse velocity distribution ant test for self-preservation. Furthermore, friction velocity can be used to estimate several boundary layer parameters, such as skin friction coefficient and shape factor. For open channel flows, the friction

velocity is used to calculate the flow resistance and estimate the initiation of the sediment transport.

Away from the bed, in the outer layer, the turbulence (eddy) shear dominates and the flow is controlled by the depth (h) and the maximum streamwise velocity (U_e) near the free surface. Unlike the turbulent boundary layers, the outer region in open channel flow is influenced by the free surface. Nezu and Nakagawa, 1993b observed that the free surface dampen the vertical velocity fluctuations. In the overlap layer, the logarithmic layer exists and the velocity profile smoothly connects the inner and outer regions.

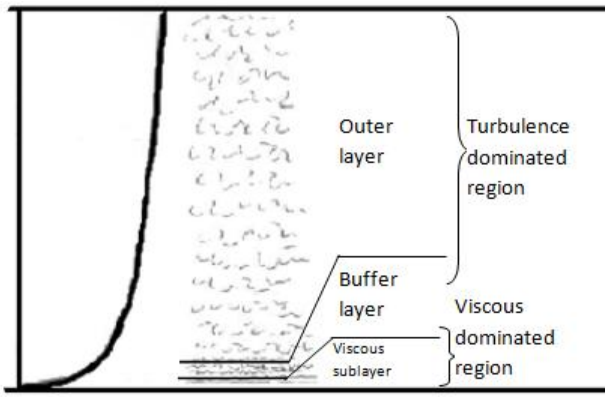

Figure 1.1 Division of turbulent open channel flow on the basis of turbulent flow (adapted from http://water.me.vccs.edu).

For the inner layer, Prandtl (1925) found that the profile would depend upon wall shear stress, fluid properties (viscosity and density), and distance from the wall (y), but not upon free stream parameters:

$$\overline{U} = f(\tau_w, \rho, \mu, y) \tag{1.2}$$

Conversely, for the outer layer, von Karman (1930) deduced that the wall acts only in reducing local velocity U(y) below the free stream velocity. As such velocity profile is independent of viscosity (μ) but depends upon wall shear stress (τ_w), boundary layer thickness (δ) and free stream pressure gradient (dp_e/dx):

$$U_e - \overline{U} = f(\tau_w, \rho, y, \delta, \frac{dp_e}{dx}) \quad (1.3)$$

Finally, for the overlap layer, a smooth matching of the inner and outer functions are invoked over some finite intermediate region:

$$\overline{U}_{inner} = \overline{U}_{outer} \quad (1.4)$$

Two other thin layers can be identified. The first is the viscous sublayer, which is a thin layer of flow next to the boundary in which viscous shear stress predominates over turbulent shear stress. Shear in the viscous sublayer, is characterized by the rate of change of the velocity which becomes very high as one move away from the wall. This is due to the rapid mixing of the fast-moving fluid right down to the top of the viscous sublayer by turbulent diffusion. The second layer is the buffer layer, which is a zone just outside and adjacent to the viscous sublayer. In the buffer layer, the velocity gradient is still very high but the flow is also turbulent. Its outstanding characteristic is that both viscous shear stress and turbulent shear stress are important and cannot be ignored.

1.4 Motivations and Objectives of the Thesis

This research investigates the characteristics of turbulence structures in smooth and rough bed open channel flows with and without pressure gradient effects. The overall purposes of this research are:

1. To study of the effect of bed roughness in non-uniform open channel flow by measuring the mean flow and various turbulence quantities such as turbulence intensities and Reynolds shear stresses.
2. To examine the applicability of power-laws to describe the mean velocity in the overlap region under the non-uniform conditions.
3. To produce a database that can be used in the development and calibration of numerical models for open channel flows .

1.5 Organization of the Thesis

A literature review on open channel flow with and without a pressure gradient over both smooth and rough beds is presented in Chapter II. Furthermore, the effects of roughness and non-uniformity on the turbulence characteristics in open channel flow are investigated. Chapter III describes experimental setup with details for the flume setup and the laser Doppler velocimetry (LDV) technique which is used to acquire velocity measurements. In Chapter IV, the results obtained from the LDV measurements are discussed. The effect of roughness and pressure gradient (favourable, zero and adverse) in open channel flow on turbulence intensities Reynolds stress are also examined in Chapter IV. Finally, conclusions, recommendations for future studies are presented in Chapter V.

CHAPTER II

LITERATURE REVIEW

This chapter contains a review of the theoretical developments of the scaling laws for the mean velocity of uniform open channel flows. A description of the scaling laws of the overlap region of the turbulent boundary layer proposed by the classical theories, and power-law formulations are carefully reviewed. A review of the literature pertaining to the effects of the pressure gradient and bed roughness is also discussed.

2.1 Law of the Wall and Defect Law

Experimental observations in a turbulent boundary layer flow growing on a smooth bed under a constant pressure (zero pressure gradient) show that there is a thin viscous sublayer that is formed near the boundary surrounded by a turbulent (outer) layer. The thickness of the viscous sublayer depends on the characteristics of the particular flow and fluid properties. Using dimensional analysis and equations (1.2) and (1.3), an equation that describing the inner layer becomes:

$$\frac{U}{u^*} = f\left(\frac{yu^*}{\upsilon}\right) \text{ and } u^* = \sqrt{\frac{\tau_w}{\rho}} \tag{2.1}$$

Here, u^* is the wall friction velocity, and for a boundary layer flow, in the region closest to the wall, it is established as the appropriate velocity scale. The appropriate viscous length scale is defined as ν/u^* for flow over a smooth surface. In the case of the rough surface the height k of the roughness needs to taken into account. Here, ν is the fluid kinematic viscosity. If the mean velocity is normalized by the friction velocity ($U^+ = U/u^*$) and vertical distance y is normalized by the viscous length scale ($y^+ = yu^*/\nu$), for the viscous sublayer in wide channel it can be shown that:

$$\frac{U}{u^*} = \frac{yu^*}{\upsilon} \quad \text{or} \quad U^+ = y^+ \tag{2.2}$$

In Eq. (2.1), function f is a multiplicative logarithmic function. The universal law of the wall has the following form:

$$\frac{U}{u^*} = \frac{1}{\kappa} \ln \frac{yu^*}{\upsilon} + B \tag{2.3}$$

Hinze (1959) stated that the parameter B in equation (2.3) is 5.0, whereas other studies have reported different values for B. Nezu and Rodi (1986) reported a value of B = 5.29, while Steffler *et al*. (1985) found that the value of B is 5.5. Values ranging from 5.0 to 5.5 have been commonly used (Roussinova *et al*. 2006). The other constant, κ, appearing in the equation (2.3) is the von Karman constant that has value of 0.41 and it is dependent of the wall surface conditions (Krogstad *et al.* 1992). Balachandar and Ramachandran (1999) verified that κ = 0.41 for shallow, low Reynolds number, open channel flow. Both B and κ have also been adopted by Roussinova *et al*. (2006) for the case of fully developed uniform open channel flow. Above the viscous sublayer, the velocity deviates from $U^+ = y^+$ and the region is referred to as the buffer layer. Balachandar and Patel (2002) have shown that this layer is in the range of $5 \leq y^+ \leq 0.2\frac{hu^*}{\nu}$, and in most studies it is assumed to range from $y^+ = 5$ to 30.

As mentioned in Chapter I, distribution of the velocity in the turbulent boundary layer far from the wall, is not influenced by viscosity and maximum velocity (U_e) is the proper characteristic to scale the velocity profile. The characteristic length scale is the boundary layer thickness, δ. A combination of two universal functions; law of the wall and law of the wake has been proposed by Coles (1956). The velocity profile can be expressed as

$$\frac{U}{u^*} = \frac{1}{\kappa}\ln y^+ + B - \Delta U^+ + \frac{2\Pi}{\kappa}\omega\left(\frac{y}{\delta}\right) \tag{2.4}$$

In equation (2.4) the dimensionless parameter Π is known as the Coles' wake parameter, ω is a universal function of ΔU^+ is the roughness shift. ΔU^+ denotes the downward shift in the rough wall profile which is zero for the smooth wall profiles. The last term in the right hand side of the equation (2.4) shows the deviation from the log-law in the outer region. Krogstad *et al.* (1992) and Balachandar *et al.* (2000) reported that the wall roughness modifies the value of the wake parameter. Small values of the wake parameter are reported for uniform open channel flow.

For decades, separate formulae were used for the viscous sublayer, the buffer layer and the log layer, until Spalding (1961) deduced a single composite formula which covered the entire wall related region.

$$y^+ = U^+ + e^{-\kappa B}\left[e^{-\kappa U^+} - 1 - \kappa U^+ - \frac{(\kappa U^+)^2}{2} - \frac{(\kappa U^+)^3}{6}\right] \tag{2.5}$$

This expression describes the velocity distribution all the way from the wall to the point where the outer layer begins (usually for $y^+ < 100$). However, Eq. (2.5) is not function of the wake parameter, so it is not a proper equation in the outer layer. Considering the outer layer of the turbulent boundary layer, which extends inward from the outer limit of $y \approx \delta$ to the distance up to which fluid viscosity is important, it can be noted that the velocity defect in the boundary layer $(U_e - U)$ is a function of wall shear stress, τ_w, density of the fluid, ρ, the boundary layer thickness, δ, and the distance from the wall (for the constant pressure boundary layer). In this layer, the velocity u^* is still considered to be appropriate velocity scale, but the characteristic length scale is replaced by the boundary layer thickness δ. For the outer layer, equation (1.3) may be non-dimensionalized as follows:

$$\frac{U_e - U}{u^*} = g\left(\frac{y}{\delta}\right) \tag{2.6}$$

Equation (2.6) is known as the velocity defect law, with $(U_e - U)$ being the defect due to the inclusion of the wall effect. The parameter U_e is the free stream velocity at the outer edge of the boundary layer. As it will be discussed later at any streamwise location x, the wake function g(y/δ) will depend upon the local pressure gradient. It should be mentioned that g is another multiplicative function that can have different form. Krogstad *et al*. (1992) proposed the following velocity defect relationship for the smooth wall:

$$\frac{U_e - U}{u^*} = \frac{2\Pi}{\kappa}\left[\omega(1) - \omega\left(\frac{y}{\delta}\right)\right] - \frac{1}{\kappa}\ln\left(\frac{y}{\delta}\right) \tag{2.7}$$

where

$$\omega\left(\frac{y}{\delta}\right) = \frac{1}{2\Pi}\left[(1 + 6\Pi) - (1 + 4\Pi)\left(\frac{y}{\delta}\right)\right]\left(\frac{y}{\delta}\right)^2 \tag{2.8}$$

The mean velocity defect shown in equation (2.7) depends on two boundary layer parameters; wake parameter and friction velocity. Roughness can influence both of these parameters. Coles (1956) initially proposed that for zero pressure gradient turbulent boundary layers, the wake parameter, Π should be 0.55 at high Reynolds numbers. In addition, he also gave a value of 0.62 for the wake parameter. Cebeci and Smith (1974) found experimentally that Π increases monotonically with an increase of the Reynolds number in zero pressure gradient boundary layers, attaining an asymptotic value of 0.55 at high Re. This parameter depends strongly on the pressure gradient, with Π increasing in adverse pressure gradients (decelerating flow) and decreasing in favorable pressure gradients (accelerating flow). Tani *et al.* (1988) obtained different values of Π ranging from 0.4 to 0.7 for two-dimensional k-type rib surfaces and got even higher values for d-type-rib roughness. Balachandar and Tachie (2001) and Tachie *et al*. (2000) have applied equations (2.7) and (2.8) for flow in an open channel, and by optimization of both

parameters, Π and u^*, they found different values of Π. Tachie *et al*. (2003) has shown that, the value of the wake parameter depends strongly on the bed conditions. Larger values of Π are obtained on rough surfaces providing an indication that the roughness effects are not confined only to the near wall region.

As mentioned above, the outer layer in open channel flow is subjected to the free surface. Some experimental studies have been carried out to study the effect of the free surface at shallow open channel flow. Balachandar and Ramachandran (1999) have focused on this effect and determined the friction velocity using the near wall data, and noted that the extent of the log-law decreases with decreasing Reynolds number. Rashidi *et al.* (1990) have found two effects from the free surface on the turbulence characteristics. The first effect is similar to the effect of the solid boundary where velocity fluctuations in the direction normal to the boundary are suppressed. They also found that contrary to the solid boundary, the velocity fluctuations parallel to the free surface are relatively unchanged at lower Fraud number since the free surface behaves as elastic membrane. Balachandar and Patel (2002) noted a region of constant streamwise turbulence intensity near the free surface and they suggested a new length scale (which is 11% smaller than the boundary layer thickness).

2.2 Effects of Roughness in Open Channel Flows

Most of the theoretical considerations and relations presented above are applicable to both smooth and rough bed open channel flows. One of the most important topics in hydraulic engineering is turbulent flow over rough beds because almost all riverbeds contain sand grains and have complicated bed configurations. Therefore, turbulent flows over rough surfaces have been extensively studied in the past, as

indicated by reviews of Raupacham *et al*. (1991), Nikora *et al.* (2001), and Balachandar and Patel (2002).Some studies; for example, by Jimenez (2004) and Amir and Castro (2011) support the wall similarity hypothesis of Townsend (1976), which suggests that it is only the inner layer of the order of five roughness heights that is affected. Other researches such as Krogstad *et al*. (1992) and Volino *et al*. (2009) have suggested that the entire boundary layer is affected by the roughness when the roughness consists of long spanwise bars. Tachie (2000) noticed that the effects of surface roughness are confined to the immediate vicinity of the roughness elements so that the turbulence structure over a significant portion of the boundary layer should be unchanged in spite of substantial alterations to the surface characteristics of the wall.

The mean velocity profiles and turbulence intensities in rough bed open channel flows differ considerably from the profiles over smooth bed open channel flows since the bottom effects are significant when roughness elements are present. Nezu and Nakagawa (1991) and Nezu *et al*. (1993b) found that the overshooting properties of the bed shear stress occurred just behind the abrupt change of roughness, i.e., from the smooth to the rough beds. Although most of the turbulent energy is generated close to the wall, large roughness affects the turbulence structure throughout the flow depth. Nezu and Nakagawa (1993c) mentioned that two questions must be answered in order to describe accurately turbulence structure over rough beds. The first one is how to find a proper parameter, which represents the size of roughness elements. Nikuradse determined the equivalent sand roughness k_s based on the systematic experiments in rough pipes. Nezu and Nakagawa (1993a) proposed that for uniform rough beds, the sand grain diameter can be used instead of k_s. If roughness is considered, the turbulent structure in the wall region

may be composed of multiple length scales such as k_s and ν/u^*. By defining $k_s^+ = k_s u^*/\nu$ the effects of roughness elements are usually classified in three categories; $k_s^+ < 5$ for hydraulically smooth wall, $5 \leq k_s^+ \leq 70$ for transitional roughness regime, and $k_s^+ > 70$ for fully rough regime. Because of the existence of the viscous sub layer, roughness effects disappear in the hydraulically smooth wall. In the case of completely rough bed, viscous effects disappear because the roughness elements penetrate the fully turbulent logarithmic layer. A transitional roughness regime is affected by both viscosity and roughness. The second question is how to find the theoretical wall position (i.e., y = 0). There is no standard definition available for finding the location of the virtual origin. As shown in Figure 2.1, the theoretical wall level can be set at a t-position below the top of the roughness elements. The range of t/k_s is between 0.15-0.3 depending on the different studies; for instance, Grass (1971) found that $t/k_s = 0.18$, Blinco and Partheniades (1971) found that $t/k_s = 0.27$, and Nakagawa *et al*. (1975) reported that $t/k_s = 0.25$.

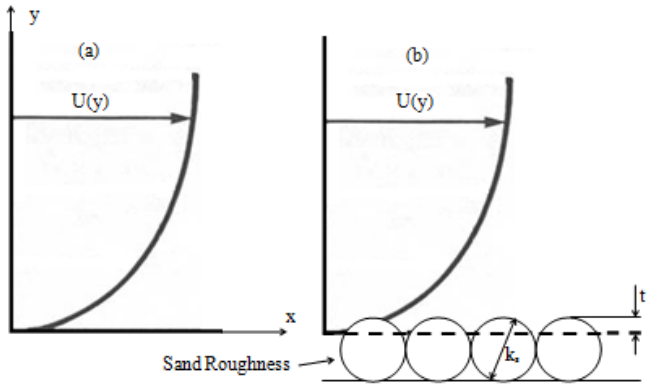

Figure 2.1 Schematic descriptions of turbulent flow over (a) smooth bed, (b) rough bed (Adapted from Nezu and Nakagawa, 1993a).

For fully rough beds, like some of the experimental tests in this study ($k_s^+ > 70$), the viscous sublayer disappears and the roughness layer penetrates into the logarithmic

region. Equivalent sand grain roughness can be determined from the friction law derived from the log-law or by using mean velocity distribution in the region where it coincides with the log-law. This parameter influences the roughness function (ΔU^+) in equation (2.4), and it depends on the reduction in the thickness of the viscous sublayer as the roughness effect increases. Hence, it measures how the intersection point between the logarithmic region and the viscous sublayer shifts as the boundary condition changes. The conventional expression for the shift due to the roughness, the roughness function, is usually expressed as

$$\Delta U^+ = \frac{1}{\kappa} \ln {k_s}^+ - 3.2 \qquad (2.9)$$

Raupacham *et al*. (1991) found k_s=3.2k for his experiments. Other studies (Long and Chen, 1981) proposed a universal velocity profile in which an overlap region exists and the mean velocity varies logarithmically with the normal distance from the wall. Therefore, we can rewrite equation (2.4) for the rough wall as

$$U^+ = \frac{1}{\kappa} \ln \frac{u^*(y+\epsilon)}{\nu} + B - \Delta U^+ + \frac{2\Pi}{\kappa} \omega \left(\frac{y+\epsilon}{\delta}\right) \qquad (2.10)$$

Here, ε is the shift in the vertical position y where the effective wall is expected to exist. The shift accounts for the reduction in the thickness of the viscous sublayer as the roughness effect increases. Krogstad *et al*. (1992) and Tachie *et al*. (2000) have used equation (2.10) together with equations (2.7) and (2.8) for boundary layers and open channel flows respectively, on smooth and rough surfaces. For the current study it was decided to use a formulation that allows Π to be optimized. This formulation proposed by Krogstad *et al*. (1992) is:

$$f = \frac{U}{U_e} = 1 + \frac{u^*}{\kappa U_e} \left\{ \ln\left(\frac{y+\epsilon}{\delta}\right) - (1+6\Pi)\left[1 - \left(\frac{y+\epsilon}{\delta}\right)^2\right] + (1+4\Pi)\left[1 - \left(\frac{y+\epsilon}{\delta}\right)^3\right] \right\} \qquad (2.11)$$

Tachie *et al*. (2003) showed that although the boundary layer in an open channel flow is affected by the free surface, roughness effects on the velocity field were similar to those observed in a zero pressure gradient turbulent boundary layer. Balachandar and Patel (2002) indicated that the streamwise mean velocity profiles follow the classical logarithmic law for the smooth surface, and with an appropriate shift, for the rough surface. Tachie *et al*. (2003) noted that roughness enhances the level of the turbulence over most of the flow. They also noted that surface roughness enhances the level of the Reynolds stresses over most of the flow and suggested a stronger interaction between the inner and outer regions of the flow than would be implied by the wall similarity hypothesis.

Nezu (2005) investigated the effects of the roughness on Reynolds shear stress and defined a parameter named correlation coefficient of the Reynolds shear stress ($R = \frac{-\overline{uv}}{u*v}$). Here, u and v are the turbulence intensity in streamwise direction and normal to the bed, respectively. He noted that R is universal and independent of the properties of the mean flow and the wall roughness. Bigillon *et al*. (2006) observed that the Reynolds stress reaches a maximum and decreases towards the bed in the wall region. They explained that in the case of smooth walls, this behaviour was due to the viscous effects, while for rough walls it was due to the existence of a roughness sublayer where additional mechanisms for momentum extraction emerge.

2.3 Effects of Pressure Gradient on Turbulent Open Channel Flows

Research of flow in open channels has been performed theoretically, experimentally and numerically considering that the flow is uniform. However, flows in nature such as rivers are non-uniform and a few studies have addressed the effect of

pressure gradient or non-uniformity and their effect on turbulence characteristics. Though there are some similarities, the results obtained from the studies for uniform open channel flows may not be directly applicable to the non-uniform open channel flow. Particularly, the turbulence structure in a non-uniform open channel flow would be much more complicated.

The Navier–Stokes equation for a 2-dimensional, steady non-uniform flow is given by:

$$\rho\left[U\frac{\partial U}{\partial x}+V\frac{\partial U}{\partial y}\right]=-\frac{\partial P}{\partial x}+\left[\frac{\partial \sigma_x}{\partial x}+\frac{\partial \tau_{xy}}{\partial y}\right] \tag{2.12}$$

In the equation (2.12), U and V are mean velocities in the streamwise and wall normal directions, respectively, ρ is density, P is pressure, τ_{xy} is Reynolds shear stresses and σ_x is Reynolds normal stress. This equation was outlined by Emamzadeh *et al.* (2010) for a 3-dimensional, steady non-uniform flow. On the bed, the mean flow velocities are zero, i.e., U = V = 0, so the left hand side of equation (2.12) is zero. Since the evolution of the turbulent shear stress in the x direction may be considered to be small when compared to that in the y direction, the terms ($\partial\sigma_x/\partial x$) will be negligible in comparison with the term ($\partial\tau_{xy}/\partial z$). Therefore, equation (2.12) is reduced to:

$$-\frac{\partial P}{\partial x}=\frac{\partial \tau_{xy}}{\partial z} \tag{2.13}$$

The boundary conditions are assumed as: y = 0 ⇒ $\tau_{xy} = \tau_w$ and y = h (depth) ⇒ τ_{xy} = 0, therefore, integration of Eq. (2.13) results

$$\tau_{xy}=\tau_w+\left(\frac{\partial P}{\partial x}\right)y \tag{2.14}$$

In the accelerating flow, the velocity (U) increases in the longitudinal direction, the equation (2.13) results $\partial\tau_{xy}/\partial z < 0$ and equation (2.14) yields ($\tau_{xy} < \tau_w$). In addition, the shear stress distribution reaches its peak values at the bed and reduces in a non-linear

form towards the free surface. According to the equation (2.14) the boundary shear stress τ_w in the accelerating flow is smaller than that in uniform flow. On the other hand, in the decelerating flow, according to the equations (2.13) and (2.15) it can be deduced that $\partial\tau_{xy}/\partial z > 0$ and $\tau_{xy} > \tau_w$ (Emamzadeh *et al.* 2010). Thus, the boundary shear stress τ_w in decelerating flows is larger than that in uniform flow. Here, the shear stress distribution is progressively increasing near the channel bed, and after reaching its maximum values, it diminishes towards the free surface. This distribution is consistent with previous studies by Song (1994), Kironoto and Graf (1995), Song and Chiew (2001), Emamzadeh *et al.* (2010), and Afzalimehr *et al*. (2007, 2009). The decelerating flow generates an upward wall-normal velocity whereas the accelerating flow yields a downward velocity. The wall-normal velocity is zero at the wall and becomes non-zero in the main flow region under non-uniform flow (Song and Chiew, 2001). It is important to mention here that the boundary shear stress for the uniform flow is larger than that in accelerating flow, and smaller than that in the decelerating flow.

Most of the previous rough and smooth wall studies were conducted in fully developed channel flows and zero pressure gradient boundary layers (Raupacham *et al*. 1991 and Bakken *et al*. 2005). The turbulence structure of non-uniform open channel flow has been a subject of fewer experimental and numerical investigations. Cardoso *et al.* (1991) carried out experiments to study the structure of accelerating flows in a smooth open channel flow. Kironoto and Graf (1995) studied velocity distribution in favourable and adverse pressure gradient flows over rough bed. They applied Coles wake function (Coles 1956) to describe velocity in the outer region. Balachandar *et al.* (2002) used laser Doppler velocimetry technique to study the turbulent boundary layer formed in a

decelerating open channel flow over a smooth surface and also over three rough surfaces. They concluded that the inner region of the boundary layer is not influenced by the channel slope. Tsujimoto *et al*. (1990) studied the effect of flow acceleration and deceleration of the longitudinal velocity fluctuations (root mean square values), and shear stress by performing experiments in non-uniform open channel flows.

Recently several studies have examined the turbulence characteristics of non-uniform flows. Notable amongst them are those by Nezu *et al*. (1994), Yang *et al*. (2006), Yang and Chow (2008), Tachie and Shah (2008), and Pearce *et al*. (2013). Some studies like Song and Graf (1994) and Kironoto and Graf (1995), used an acoustic Doppler velocimetry profiler (ADVP) to measure the instantaneous velocity over a fixed gravel-bed under equilibrium conditions, in accelerating and decelerating flows over hydraulically rough beds. They found that in equilibrium condition velocity profiles are self-similar at different cross sections for each measuring run.

Yang *et al.* (2006) used mean-flow equations derived by Nezu and Nakagawa (1993b) to derive the Reynolds shear stress ($-\overline{u'v'}$) distribution. They stated that for a steady flow using Leibnitz's theorem, the vertical velocity at the free surface can be expressed as

$$v_h = u_h \frac{d(h(x))}{dx} \tag{2.15}$$

where, h(x) = water depth, u_h and v_h are mean velocities at the free surface along x and y axis, respectively. Equation (2.15) indicates that v_h is zero in uniform flows (dh/dx = 0), but it becomes positive or upward in decelerating flows (dh/dx > 0), it is downward or negative in accelerating flows (dh/dx < 0). For the wall shear stress (U = V = 0 and $\tau = -\rho\overline{u'v'} = \tau_w = \rho u^{*^2}$):

$$\frac{\tau_w}{\rho} = -\frac{d}{dx}\int_{y_0}^{h} U^2 dy - gh(\frac{dh}{dx}\cos\theta - \sin\theta) \quad (2.16)$$

Here, θ is the angle made by the channel bed with the horizontal axis and g is the gravitational acceleration. In order to determine the friction velocity u^*, equation (2.10) can be used. Yang *et al.* (2006) reported that the Reynolds shear stress can be expressed as:

$$\overline{u'v'} + UV + u^{*^2} = -fy - g(\frac{dh}{dx}\cos\theta - \sin\theta)y \quad (2.17)$$

Here f is the mean value of $\partial^2 U/\partial x^2$ on the interval (0, y). In a gradually varied flow, it can be assumed that $\partial^2 U/\partial x$ is not significant, or that f is not very large relative to g(dh/dx cosθ - sinθ). Equation (2.17) can be rewritten as follows:

$$-\frac{\overline{u'v'}}{u^{*^2}} = \left(1 - \frac{y}{h}\right) + b\frac{y}{h} + \frac{UV}{u^{*^2}} \quad (2.18)$$

Here,

$$b = 1 + (\frac{f}{g} + \frac{dh}{dx}\cos\theta - \sin\theta)\frac{gh}{u^{*^2}} \quad (2.19)$$

As indicated by Yang *et al.* (2006) Equation (2.18) can be written as follows:

$$\frac{\overline{u'v'}+UV}{u^{*^2}} = (1 - \frac{y}{h}) + b\frac{y}{h} \quad (2.20)$$

Equations (2.18) and (2.19) show that in the case of non-uniform open channel flow the Reynolds shear stress will deviate from the standard linear distribution. As Yang *et al.* (2006) reported, this is because the non-zero vertical velocity will result in an additional momentum term or -UV, therefore, the Reynolds stress distribution will have different forms in decelerating and accelerating flows. It can be seen from equation (2.20) that the modified term $-(\overline{u'v'} + UV)/u^{*^2}$ is linear with respect to the relative height y/h. The unknown parameter b can be determined using the boundary condition: at the free surface where y = h, $-\overline{u'v'} = 0$ then b is obtained from equation (2.20) as

$$b = -\frac{v_h u_h}{u^{*^2}} \quad (2.21)$$

Equation (2.21) indicates that the coefficient *b* depends on the vertical velocity at the free surface. Inserting Eq. (2.15) into (2.21), one could express the coefficient *b* in the following way:

$$b = -(\frac{u_h}{u^*})^2 \frac{dh}{dx} \tag{2.22}$$

Equation (2.22) shows that b is always positive in an accelerating flow (dh/dx < 0), but it becomes negative in a decelerating flow (dh/dx > 0). Emamzadeh *et al*. (2010) found that the Reynolds shear stress distributions for both accelerating flow can be divided into two regions. The shear stresses in the first region increase from the bed until a maximum value, followed by a transition to the second region, where shear stresses decrease from the maximum value towards the water surface. Tachie *et al.* (2003) studied the effect of the non-uniformity on the wake parameter and found that Π strongly depends on the wall condition. Cebeci and Smith (1974) found experimentally that Π increased monotonically with an increase of Reynolds number in zero pressure gradient boundary layers. In addition, Π depends strongly on the pressure gradient, with Π increasing in the adverse pressure gradient flow and decreasing in the favourable pressure gradient flow. Krogstad and Skare (1995) and Lee and Sung (2009) found that the 'constants' κ and A in the log-law of the wall equation (see section 2.2), are affected by pressure gradients. In the next two sections, effects of the accelerating and decelerating flows on the turbulence structure will be discussed in detail.

2.3.1 Favourable Pressure Gradient in the Turbulent Open Channel Flow

Favourable pressure gradient turbulent flows (FPG) over smooth and rough surfaces are encountered frequently in fluid engineering applications. Tachie (2008) argued that when near-wall turbulent flows are subjected to streamwise pressure gradient,

it is the inner-layer velocity gradient and Reynolds stresses that are immediately altered. By considering wall roughness effects in the near-wall region, the interaction between the inner and outer layers of FPG turbulent flows over rough surfaces becomes fundamentally important. Coleman *et al*. (1977) found that FPG decreased the normalized Reynolds stresses and made the turbulence field less isotropic than in zero pressure gradient (ZPG) turbulent flow over rough surfaces. Cal *et al*. (2006) investigated the FPG open channel turbulent flows and reported that pressure gradient changed the shape of the Reynolds shear stresses. The effects of FPG along with roughness and effects of FPG on smooth wall open channel flows have yet to be resolved. In the favourable pressure gradient or accelerating flow, the pressure gradient along the streamwise direction is negative ($dp/dx < 0$), and velocity gradient is positive. Launder (1964) proposed an acceleration parameter for favourable pressure gradient flows given as:

$$K = \frac{\nu}{U_e^2}\frac{dU_e}{dx} \tag{2.23}$$

Here existence of the non-zero wall-normal velocity, assumes as one of the most important characteristic in non-uniform flow (Bourassa and Thomas, 2009). Sreenivasan and Narasimha (1982) pointed out that K cannot truly be a fundamental parameter since it contains no boundary layer information. Bourassa and Thomas (2009) pointed out that as K starts to increase slightly, relaminarization appears to occur gradually. They explained that the relaminarization may be caused by many factors such as a thinning of the boundary layer, a departure of the mean velocity profile from both the standard law of the wall and law of the wake, an initial decrease followed by a rapid increase in the shape factor and finally a decrease in the relative turbulence intensity.

2.3.2 Adverse Pressure Gradient in the Turbulent Open Channel Flow

The effect of adverse pressure gradients on the flow and turbulence characteristics, such as turbulence intensities and Reynolds shear stress over a smooth wall, have been documented in Skare and Krogstad, (1994), Nagano *et al*. (1998), Lee and Sung, (2008), and Lee *et al*. (2010). Perhaps, one of the first studies addressing the simultaneous effects of the roughness and APG was carried out by Perry *et al*. (1969). They reported the effects on the streamwise mean velocity profiles. Recently, Tsikata and Tachie (2013) have used PIV to evaluate the combined effects of roughness (sand grains and gravel) and APG. The statistics reported includes the mean velocity, Reynolds stresses, eddy viscosity, mixing length and production term for the turbulence kinetic energy and the Reynolds shear stress. Their results confirm that APG changes the equivalent roughness height. A combination of APG and roughness would enhance the turbulence level. Emamzadeh *et al*. (2010) reported that in decelerating flows with positive pressure gradients, increasing the bed-slope results in larger pressure gradients and therefore higher shear stress. Most of the researchers still use the universal logarithmic law of the wall in APG flows, and confirm a pressure gradient dependence of the logarithmic region. Spalart and Watmuff (1993) and Nagano *et al*. (1998) reported that in the case of strong pressure gradients a shift appears in the profile above or below the classical log-law followed by a change in the profile's shape. Marusic and Perry (1995) have shown that the turbulence intensity in the outer region also increases with pressure gradient when scaled with the friction velocity. Spalart and Watmuff (1993) noted that the apparent value of κ (von-Karman constant) decreased with pressure gradient. In the next chapter it will be shown that the shape factor (H) of the mean

velocity profile, which is usually used to characterize the boundary layer, increases in the presence of an adverse pressure gradient.

The most recognisable feature of an APG flow in the outer region is the amplified wake of the mean velocity profile and increase in the turbulence intensities. Durbin and Belcher (1992) explained that the APG boundary layer profile may have an initially steep rise near the wall, but it is then affected by the pressure gradient, so that it has a large wake deficit. Nagano *et al*. (1998) and Aubertine and Eaton (2005) have shown that as pressure gradient increases, the wake strength increases. Clauser (1954) introduced the following pressure gradient parameter (β) as

$$\beta = \frac{\delta^*}{\tau_w}\frac{dP}{dx} \tag{2.24}$$

Here, δ^* is the displacement thickness, P the static pressure, x the streamwise coordinate and τ_w the wall shear stress. This is the most commonly discussed of the parameters affecting pressure gradient boundary layers. For an equilibrium boundary layer, β does not change along the flow direction.

2.4 Power-laws

The mean velocity profile of a turbulent boundary layer at high Reynolds number can be divided to three distinct regions namely inner overlap and outer layer. The scaling law for each region is different. For instance, in the inner layer, where viscous effects are dominant, the proper scaling law is logarithmic law of the wall, and for the outer layer, where inertia effects dominate; velocity defect law is used as the scaling law. Tennekes and Lumley (1972) suggested that, in order to control the dynamics of the flow in the overlap region, neither inner nor outer scales can be used since inner length scale (ν/u^*) is too small and boundary layer thickness (δ) is too large. Therefore, fluid dynamics

researchers have been interested to investigate different scaling laws for this region. This scaling law should be gained by matching the inner scaling law in conjunction with the outer scaling law. Barenblatt (1993) and George and Castillo (1997) proposed a power-law to describe the velocity profile in the overlap region of the turbulent boundary layer. The two approaches have been applied by many researchers to describe the overlap region of the velocity profile. Although from the log-law point of view the velocity profile in the main part of the flow is independent of molecular viscosity, on the other hand, power-law assumes that the velocity profile in the main part of the flow remains dependent on viscosity at finite Reynolds number (Barenblatt and Prostokishin, 1993). Tachie *et al.*(2000) have pointed out that the friction velocity obtained using power-law formulations for smooth wall data have been comparable to the values obtained by other reliable techniques. Afzal (2001) has provided a power-law theory for turbulent boundary layers, and his functional equation is represented by an inner power-law velocity profile, an outer velocity defect law layer, and a skin friction power-law in the overlap region. It is important to note that a Reynolds number dependency of the mean velocity profile cannot be excluded in general and it seems much more complex functional forms are needed to describe the profile. Buschmann and Gad-el-Hak (2006) proposed a higher-order approach which is based on the assumption that at sufficiently high Reynolds numbers, the influence of the outer turbulence-structures scaling (δ) reduces in the inner region, and the influence of the inner viscosity dominated structures scaling (ν/u^*) reduces in the outer region.

The overlap region between the viscous inner and outer layers is characterized by inertia. However, Long and Chen (1981) remarked that this region does not depend on

both inertia and viscosity, and it only depends on inertia. Recent measurements at low Reynolds numbers and direct numerical simulation (DNS) results show that as Reynolds number decreases, the overlap region starts to gradually disappear. It follows that a log-law region may not be apparent at low Reynolds number (Tachie, 2000). Power-law and its applicability; and also different methods for determining the friction velocity have been studied by many researchers (Barenblatt 1997, 2000, Buschmann and Meinert 1999, Österlund *et al.* 2000, Balachandar *et al.* 2002, Buschmann and Gad-el-Hak, 2003 and 2006).

2.4.1 Power-law by Barenblatt

A power-law scaling for the mean velocity profile of the zero pressure gradient turbulent boundary layer and pipe flow has been proposed by Barenblatt *et al*. (1993, 1997) in a series of papers. Their main idea is the distinction between complete and incomplete similarity, and using incomplete similarity for the overlap region, which is Reynolds number dependent. According to their study, the effect of the viscosity remains at arbitrary large Reynolds number not only in the viscous sublayer, but also in the entire boundary layer. They proposed a power-law for a smooth surface,

$$U^{+} = Cy^{+\alpha} \tag{2.25}$$

Introducing u^{*} as friction velocity, $U^{+}=U/u^{*}$ and y^{+} can be used to define a local Reynolds number with respect to the wall-normal coordinate. The parameters C and α are Reynolds number dependent and given by,

$$C = \frac{1}{\sqrt{3}} \ln \mathrm{Re} + \frac{5}{2} \tag{2.26}$$

$$\alpha = \frac{3}{2 \ln \mathrm{Re}} \tag{2.27}$$

Barenblatt (1993) reported that Equations (2.26) and (2.27) can be determined from classical pipe flow data of Nikuradse (1933). Zagarola *et al*. (1997) re-examined the power-law proposed by Barenblatt and found,

$$C = 0.7053 \ln \mathrm{Re} + 0.3055 \tag{2.28}$$

$$\alpha = \frac{1.085}{\ln \mathrm{Re}} + \frac{6.5355}{\ln \mathrm{Re}^2} \tag{2.29}$$

Balachandar *et al.* (2002) found no Reynolds number dependence over a range of Reynolds numbers ($10000 < Re_h < 90000$) used in their open channel study. They determined that the power-law coefficients were near constant, which values C = 7.957 and $\alpha = 0.155$, and provide for an accurate distribution in the range $50 < y+ < 500$ at all Froude numbers. In order to apply power-law for rough wall boundary layers, a downward shift parameter (ΔU^+) must be used to modify equation (2.25). A power-law equation has been adopted by Balachandar *et al*. (2002) to determined u^* for rough surfaces,

$$U^+ = 7.975 y^{+0.155} - \Delta U^+ \tag{2.30}$$

Kotey *et al*. (2003) found a power-law velocity profile in the overlap region for a rough wall boundary layer,

$$U^+ = \frac{C_i}{E} (y'^+)^{\gamma+\xi} \tag{2.31}$$

Here, E and ξ are roughness parameters (both non-negative) and C_i and γ are the multiplicative constant and the exponent for a smooth surface.

2.4.2 Power-law by George and Castillo

George and Castillo (1997) developed a power-law for the zero pressure gradient boundary layer, which is derived from the Prandtl's boundary layer equation. Their approach is different from that proposed by Barenblatt *et al.* (1997). They used two key assumptions for their approach. First one is the asymptotic invariance principle (AIP)

which explains that, as Re → ∞, the Reynolds number dependent term in the mean momentum equation will disappear. In addition, when Re→∞, the mean momentum equations for the inner and the outer regions are exactly valid, this leads to complete similarity in the inner and outer layers. The second assumption that they used is for the overlap region, is the near asymptotic (NS). In this assumption they considered a parameter which affected related to mesolayer, where neither dissipation nor Reynolds stress are independent of viscosity. They also assumed that the appropriate velocity scale for the inner and outer layers is friction velocity (u^*) and surface velocity (U_e) respectively. They obtained a power-law description of the mean velocity in inner and outer coordinate as follows:

$$U^+ = C_i(y^+ + a^+)^\gamma \tag{2.32}$$

$$\frac{U-U_e}{U_e} = C_o\left(\frac{y+a}{\delta}\right)^\gamma \tag{2.33}$$

Parameters C_o, C_i, and γ are functions with a weak dependence on the Reynolds number ($\delta^+ = \delta u^*/\nu$). The parameter a or a^+ is introduced to make the expressions invariant to coordinate transformation of the form y → (y+a) (George and Castillo, 1997), and represents a shift in the origin for measuring y associated with the growth of the mesolayer region (30 < y+ < 300). Such a layer is assumed as a region where neither dissipation nor Reynolds stress will become independent of viscosity regardless of how high the Reynolds number is. They also proposed a composite empirical velocity profile which defines mean velocity in the inner (viscous sublayer and buffer layer) and overlap layers:

$$U^+ = [y^+ + C_4y^{+4} + C_5y^{+5}]\exp(-dy^{+6}) +$$
$$C_iy^{+\gamma}\left[1 + \gamma a^+y^{+-1} + \frac{1}{2}\gamma(\gamma-1)a^{+2}y^{+-2}\right]\left(1-\exp(-dy^{+6})\right) \tag{2.34}$$

Here, $a^+ = -16$ and d is a damping parameter selected as $d = 8\times10^{-8}$ to fix the transition from the viscous wall region to the overlap region. The dependency of y^{+6} into the exponentials, allows not only the no-slip condition to be satisfied at the wall, but also the boundary conditions on velocity derivatives. They found also another value of $a^+ = -37$ and $C_4 = 0.00074$, however this value of a^+ is very difficult to determine. Balachandar *et al*. (2002) used an iterative procedure with the best available value for u^* and introduced a value off $C_4 = -0.27\times10^{-3}$. Wosnik *et al*. (2000) found a logarithmic law for pipe and channel flows based on asymptotic invariance principle and near asymptotic, and introduced the following formulations:

$$U^+ = \frac{1}{\kappa(\delta^+)}\ln(y^+ + a^+) + B_i(\delta^+) \tag{2.35}$$

$$\frac{U_e - U}{u_e} = \frac{1}{\kappa(\delta^+)}\ln(\bar{y} + a) + B_o(\delta^+) \tag{2.36}$$

George and Castillo (1997) proposed:

$$\frac{u^*}{U_e} = \left(\frac{C_o}{C_i}\right)^{\frac{1}{1+\gamma}}\left(\frac{U_e\delta}{\upsilon}\right)^{\frac{-\gamma}{1+\gamma}} \tag{2.37}$$

2.4.3 Higher order Approach by Buschmann and Gad-el-Hak

Two major hypotheses were employed by Buschmann and Gad-el-Hak (2003), first one is that the classical two layer assumption is sufficient to describe a wall-bounded flow and the second one is that asymptotic matching can be applied to obtain higher-order solutions for the mean velocity profile in the overlap region. Thus, for inner and outer region, asymptotic expansions are:

$$U^+ \sim \sum_{i=0}^{\infty} u_0^+(y^+)\gamma_0(\delta^+) \tag{2.38}$$

$$U \sim \sum_{i=0}^{\infty} U_0(\eta)\Gamma_0(\delta^+) \tag{2.39}$$

Here γ_i and Γ_i represent functions which depend only on δ^+ but do not necessarily have the same functional shape. The strong assumption here is the separation of the Reynolds number dependence and the dependence on the wall-normal coordinate into multiplicative functions.

2.5 Summary

In nature, uniform flow conditions are rarely attained and the flow is influenced by the bed roughness and by the constantly changing flow depth. These warrant further investigations of the flow and turbulence characteristics in the presence of pressure gradient. In this Chapter, the scaling laws for the mean flow and turbulence quantities in both inner and outer coordinates have been reviewed. Standard approaches such as log-law and power-law which are used to predict velocity distribution in non-uniform open channel flows have been also discussed. Literature review of the open channel flow studies have shown that most of the experimental studies considered uniform flow conditions in equilibrium FPG and APG flows. Those studies have not considered non-equilibrium conditions in the open channel flows. In this study, the main motivation is to investigate a flow field which consists of three connected non-uniform flows including FPG, NZPG and APG. This allows considering effects from upstream and downstream conditions on the main flow. The combined effects of the pressure gradient (non-uniformity) and surface roughness on the mean and turbulence quantities are discussed in this study. Furthermore, application of the log-law is justified and the applicability of the power-law is also investigated in the case of rough non-uniform open channel flow.

CHAPTER III

EXPERIMENTAL SETUP

3.1 General comments

Traditionally, knowledge of the structure of the turbulent boundary layer in open channel flows is gained from experimental measurements over a wide variety of flow and channel geometry conditions. This chapter describes the laboratory experiments carried out in this research and includes a description of the flume and flow facilities, as well as detailed descriptions of the laser Doppler velocimetry (LDV). The measurement procedure and a summary of test conditions for all flow fields are also presented.

3.2 Open Channel Flume

The desired flow fields includes zero, favourable, and adverse pressure gradient turbulent open channel flows. The flow field was established in a 9.5 m long and 1.24 m wide open channel flume, which is shown in Figure 3.1, in the Civil Engineering Hydraulic Engineering Laboratory at the University of Windsor.

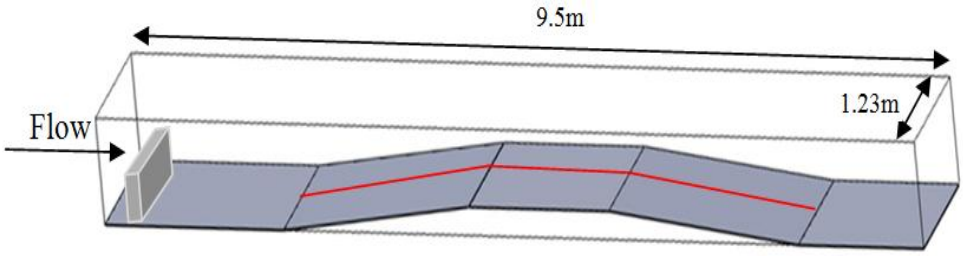

Figure 3.1 Schematic of the open channel flume.

The flume has Plexiglas on the sidewalls and bottom to provide optical access from all sides. The supply system includes two pumps with flow control valves and a reservoir located below the flume. Additionally, a sluice gate located at the exit part of the flume was used to control and adjust the depth of the flow. To reduce the turbulence

levels in the flow and to condition the flow, a set of flow straighteners made of packed plastic straws was located at the entrance section of the flume. To obtain uniform and non-uniform flows, the flume was equipped with a long polished smooth bed, which includes three distinct sections with different slopes. The first part has a positive longitudinal bed slope (2 degrees) to maintain a favourable pressure gradient flow or accelerating flow, followed by a flat wooden plate to provide near-zero pressure gradient flow or uniform flow. The last section was a negative longitudinal bed slope (-2 degrees) to obtain an adverse pressure gradient or decelerating flow. Figure 3.2 shows a schematic of the flow field. The mean velocity and the bed shear stress increase in the streamwise direction of the first cross-section (the accelerating bed); while, these two parameters decrease along the third cross section (the decelerating bed).

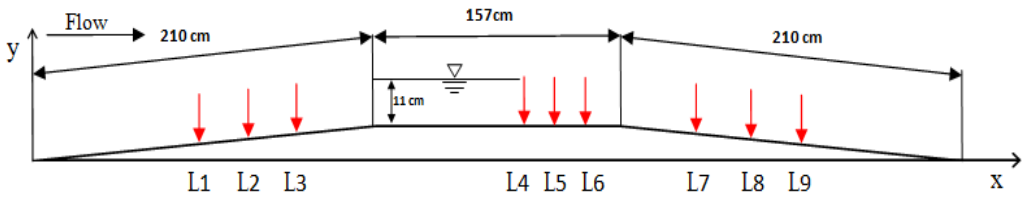

Figure 3.2 Sketch of position of the measuring stations.

To maintain a rough surface, a thin layer of sand roughness was glued on to the bottom of the channel. This roughness reduced the local depth by 3 mm. The reason for choosing this roughness is to allow comparison between our results with those obtained by Faruque (2009) with the same bed particles. The Reynolds number of the flow based on the distance from the beginning of each bed varied from 2.39×10^5 to 5.9×10^5 for the smooth bed experiments, and from 1.94×10^5 to 7.6×10^5 for the rough bed experiments. Nine stations were chosen for measurement of velocity along the flume including three for the accelerating part of the flow, three for the flat plate, and three other on the

decelerating ramp, as indicated in Fig. 3.2. For all experiments, the measurement stations were located in the middle of the channel where the secondary flow effects are expected to be negligible. In addition, the selected aspect ratio was 11.2, which is large enough to reduce secondary currents (Nezu and Nakagawa, (1993b), Knight and Patel. (1985). The details are tabulated in Tables 3.1 and 3.2, for smooth and rough experiments, respectively. In these tables, test locations are along the x-axis, and represent the distance of the measurement location from the starting edge of each bed. The flow depth (h) for all experiments was varied, thus each test case has a certain Froude number (Fr) and Reynolds number (Re). In all cases, boundary layer thickness (δ), momentum thickness (θ), and boundary layer shape factor (H) as well as the Reynolds number based on momentum thickness (Re_θ) has been determined. Boundary layer thickness was determined directly from the acquired data (where U = 0.99 U_e). The two parameters, θ and Re_θ, are defined as

$$\theta = \int_0^h \frac{U}{U_e}\left(1 - \frac{U}{U_e}\right) dy \tag{3.1}$$

$$Re_\theta = U_e\theta/v \tag{3.2}$$

In the above equations, U is the local velocity and U_e is the maximum velocity at each measurement station. Based on these data, the flow conditions are fully turbulent and also subcritical.

3.3 Measurement locations and details

For this study, sixteen different series of experiments under three categories were performed. The first category consists of three smooth and three rough experiments on the accelerating part of the bed to study the effect of favourable pressure gradient on open channel flows. These locations are named L1, L2, and L3 in Fig. 3.2 and in Tables 3.1

and 3.2. In order to investigate the effect of adverse pressure gradient, another three locations were established on the decelerating part. A total of six series of experiments were performed: three tests for the smooth case and three tests for the rough wall. Subsequently, three locations were selected on the flat section and conducted six series of experiments were conducted on both smooth and rough surfaces (two tests for each case). It should be mentioned that all of the rough tests were carried out at the same locations as the smooth ones.

The LDV measures the flow velocity by tracking particles, which are moving in the water, so prior to each experiment the water in the flume was filtered. Then the water was seeded with hollow glass bead particles with a specific gravity of 1.1 and a mean diameter of 12 μm. The size of particles is very important because, on one hand, it should be smaller than the measurement volume of the LDV so that the particles can follow the flow velocity faithfully and, on the other hand, it should be large enough to reflect enough light to be captured. The other important property of the particles is density, which may influence the particle's ability to follow the flow feature. In this study the particle density is 1.13 g/cc. Figure 3.3 includes four pictures of the flume and shows the smooth and rough wall as well as two images of the accelerating and decelerating sections.

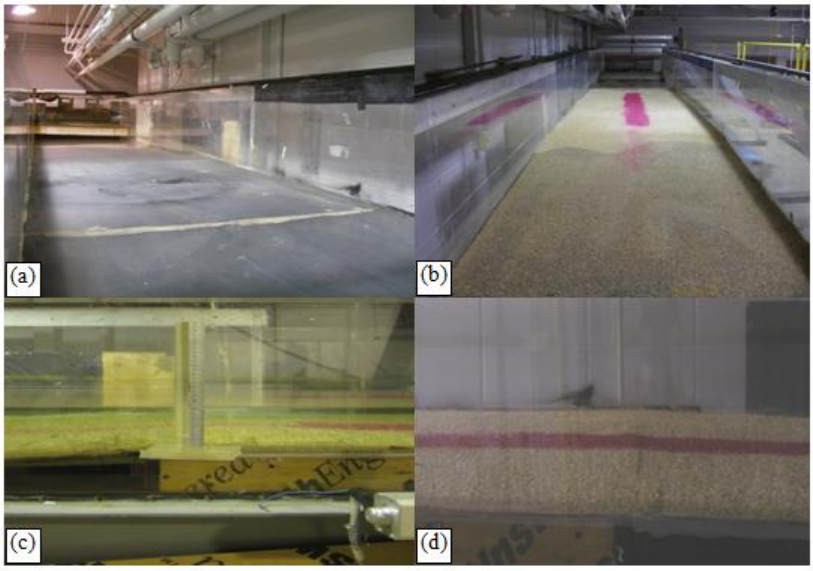

Figure 3.3 Pictures of flume bed, a) smooth wall view, b) rough wall view, c) Joint section of the Accelerating ramp with the flat plate, d) joint section of the flat plate and the decelerating ramp.

3.4 Laser Doppler Velocimetry (LDV)

The LDV system is an appropriate instrument for collecting thousands of instantaneous velocity samples in a certain region of space and therefore is capable of providing accurate single point measurement of turbulence quantities of interest. In this study, a commercial two-component fiber-optic LDV in which the velocity determined based on the principal of the Doppler effect was used. This system (DANTEC Dynamics) powered by a 300 mW Argon-Ion laser, and its optical component includes a Bragg cell and a 500 mm focusing lens. The beam spacing was 38 mm and the beam half angle was 2.2 degrees. At each measurement location, 10000 validated samples were acquired while the system was operated at 1000 μs coincidence window. The data rate varied from 6 Hz close to the bed to 250 Hz near the water surface. Prior to each experiment, water was seeded with 12 μm particles and sidewalls were cleaned to avoid any extraneous light

scattered from particles distributed throughout the illuminating beams. Due to the transmitting optics limitation of the LDV, two-component velocity measurement was not performed through the whole depth, so only 75% of the depth was used for this purpose. However, the entire depth was used to measure the streamwise velocity component. The LDV probe was tilted 2 degree toward the bottom wall to capture data very close to the wall for one-component velocity measurements (Fig. 3.4). This technique has been successfully adopted by Kaftori *et al.* (1995), Tachie (2001) and Faruque (2009) to access locations closer to the bed. When seeding particles move randomly through the measurement volume, raw instantaneous velocity can be collected as a function of time. In addition, normal distribution of arrival particles increases the accuracy of the data acquisition process. It should be noted that any incorrect setting of the LDV system, such as burst validation criteria, processor dead time, or velocity bias, leads to deviation from a normal distribution. The other parameter which may cause false detection of velocity is multi-detection, and it occurs when two particles enter the measurement volume simultaneously. Detailed uncertainty analysis for LDV measurements is discussed in Appendix A.

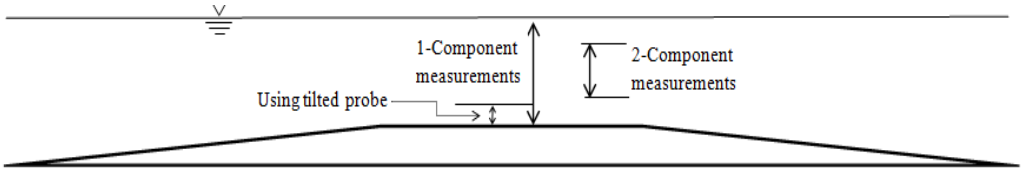

Figure 3.4 Sketch of the measurement zones.

Table 3.1 Summary of the smooth wall experimental conditions

Flow type	FPG			ZPG			APG		
Bed type	Smooth			Smooth			Smooth		
Distance (mm)	1320	1450	1650	620	970	1070	420	620	860
Depth (mm)	153	147	127	110	110	110	130	143	153
$\delta_{(U=0.99Ue)}$ (mm)	140	120	110	90	90	90	80	85	90
U_e (m/s)	0.319	0.327	0.338	0.401	0.414	0.427	0.359	0.344	0.328
T (°C)	25	23	21.5	17.5	23	25	23	25	24
u^* / U_e	0.041	0.043	0.041	0.045	0.043	0.045	0.053	0.058	0.064
ν (m^2/s) $\times 10^{-7}$	8.71	9.12	9.45	10.41	9.12	8.71	9.12	8.71	8.91
δ^* (mm)	14	15	11	6	7	5	15	16	17
θ (mm)	13	12	10	4	5	4	10	11	12
$Re_{(x)}$	483,263	519,500	590,795	238,777	440,558	525,067	165,133	244,520	316,460
$Re_{(\delta)}$	50,523	44,784	37,596	34,661	40,877	44,164	31,454	33,523	33,118
$Re_{(h)}$	56,015	52,667	45,473	42,364	49,960	53,979	51,113	56,397	56,300
$Re_{(\theta)}$	4643	4257	3422	1907	2240	2106	4060	4267	4320
Fr	0.26	0.27	0.30	0.39	0.40	0.41	0.32	0.29	0.27

Table 3.2 Summary of the rough wall experimental conditions

Flow type	FPG			ZPG			APG		
Bed type	Rough			Rough			Rough		
Distance (mm)	1320	1450	1650	620	970	1070	420	620	860
Depth (mm)	153	147	127	110	110	110	130	143	153
$\delta_{(U=0.99Ue)}$ (mm)	110	100	90	80	80	80	120	130	140
U_e (m/s)	0.287	0.354	0.375	0.428	0.418	0.413	0.394	0.378	0.364
T (°C)	28	29	28	26	27	27	26	26	29
u^* / U_e	0.08	0.059	0.061	0.063	0.06	0.061	0.078	0.082	0.088
ν (m^2/s) $\times 10^{-7}$	8.15	7.98	8.15	8.52	8.33	8.33	8.52	8.52	7.9
δ^* (mm)	8	16	12	10	14	14	29	30	35
θ (mm)	6	10	11	7	9	9	17	18	21
$Re_{(x)}$	464,228	644,156	760,080	311,490	487,241	529,895	194,213	275,483	392,835
$Re_{(\delta)}$	38,334	44,425	38,695	37,680	37,673	37,142	54,564	55,541	61,666
$Re_{(h)}$	53,808	65,304	58,503	53,757	53,747	52,989	60,113	63,539	69,888
$Re_{(\theta)}$	2206	4762	4461	3439	4601	4637	7935	7826	9461
Fr	0.23	0.30	0.34	0.42	0.41	0.40	0.35	0.32	0.30

CHAPTER IV

ANALYSIS OF RESULTS

In accordance with the objectives of this study, the effect of pressure gradient and surface roughness effects on the turbulence characteristics of the open channel flow boundary layer are analyzed. To this extent, two types of bed surfaces smooth and rough are used. The near zero pressure gradient (NZPG) case on the smooth wall is first considered and serves to validate the measurement and analysis procedures used in this research. Subsequently, the study goes on to clarify roughness effects and pressure gradient (favourable and adverse) influences. The variables of interest include mean velocity, turbulence intensity and Reynolds shear stress. Finally, the appropriateness of power-law to describe the mean velocity profile on both smooth and rough beds is assessed. Some abbreviations and symbols are used here to represent the flow and surface conditions: S represents the smooth wall, R represents the rough wall, NZPG denotes near-zero pressure gradient, FPG represents favorable pressure gradient, and APG represents adverse pressure gradient flow.

4.1 Verification and Validation

In this part, streamwise component of the mean velocity and the turbulent statistics for smooth and rough wall measurements are reported.

4.1.1 Mean velocity Profile

Figure 4.1 shows the distribution of the streamwise component of the mean velocity profile in the outer scaling along the centreline of the flow. In order to non-dimensionalize the mean velocity (U) and the wall normal distance (y), maximum

velocity (U_e) and maximum depth of flow (h) are respectively used. In the outer region, as expected, the maximum velocity usually occurs near the free surface where the velocity gradient dU/dy is close to zero. The Reynolds number based on the flow depth is of the order of 45,000 and the flow can be expected to be in the fully turbulent region. It can be seen from Figure 4.1 that all velocity profiles follow the trend expected in a standard uniform flow. However, the profiles do not completely overlap on to each other. This could be related to several factors including the proximity of the measurement stations to the surface discontinuity occurring at locations where the bed slope changes. For example, the test station L4 is located close to the accelerating ramp (5.6h from the end of accelerating flow or start of zero bed slope). The test station L6 is located 9.7h from the start of the zero bed slope or 5.2h from the intersection of the flat bed with the decelerating ramp. Furthermore, the profiles are not necessarily in fully developed flow regions when compared to those in classical open channel flows. A longer channel length, generally in excess of 70 times the flow depth is required to attain a fully developed status (Kirkgoz and Ardichoglu, 1997). One should also note that the flow on a zero bed slope is mildly accelerating. As such the mean profiles need cautionary interpretation. The velocity defect profiles in the outer scaling are shown as an inset in Figure 4.1. As flow moves farther downstream in the streamwise direction, the velocity defect is decreased systematically, which was also noticed by Nezu and Rodi (1986) and Tachie *et al.* (2003). From Eq. (2.7) in Chapter II, the velocity defect profile depends on the Coles' wake parameter (Π) and is a measure of the deviation of the velocity distribution from the log-law in the outer region. The effect of mild acceleration

occurring due to a mild decrease in water depth (though the nominal depth is 110 mm) is reflected in the Π values reported in Table 4.1.

The distribution of the streamwise component of the mean velocity profile in inner scaling at the three test stations is shown in Figure 4.2. The shear velocity was calculated using the Clauser chart method and the method presented by Krogstad *et al*. (1992). The mean velocity profile was fitted with the classical log-law, $U^+ = \kappa^{-1} \ln y^+ + B$, where $U^+ = U/u^*$ and $y^+ = yu^*/\nu$, $\kappa = 0.41$ and $B = 5.1$. The values of u^* used for the velocity scales, are shown in Tables 3.1 and 3.2 for smooth and rough surfaces, respectively. As can be seen, all three plots agree with the classical log-law in the overlap region ($30 < y^+ < 250$). The present velocity profiles are compared with the uniform open channel flow data reported by Roussinova *et al*. (2006). They examined effect of the channel aspect ratio on different smooth open channel flow (OCF) velocity profiles and showed that all profiles follow the universal law of the wall in the range between $y^+ > 30$ and $y/h > 0.2$. As Reynolds number based on the distance from the beginning of the flat plate (Re_x) increases, the wake part falls below the classical log-law. This might be due to the mild acceleration of the flow. The other reason is due to the effects of the upstream conditions (FPG), which influences the wake region of the profiles. Although stations L5 and L6 are located far from the accelerated ramp, 97 cm and 107 cm respectively, the effect of non-uniformity is visible when they are compared with the uniform OCF results of Roussinova *et al.* (2006). As Reynolds number increases from Re_x =4.4E+5 for L5 to Re_x=5.2E+5 for L6, the plots approach each other and overlap in the medium part of the profile ($50 < y^+ < 300$) and in the wake region as well.

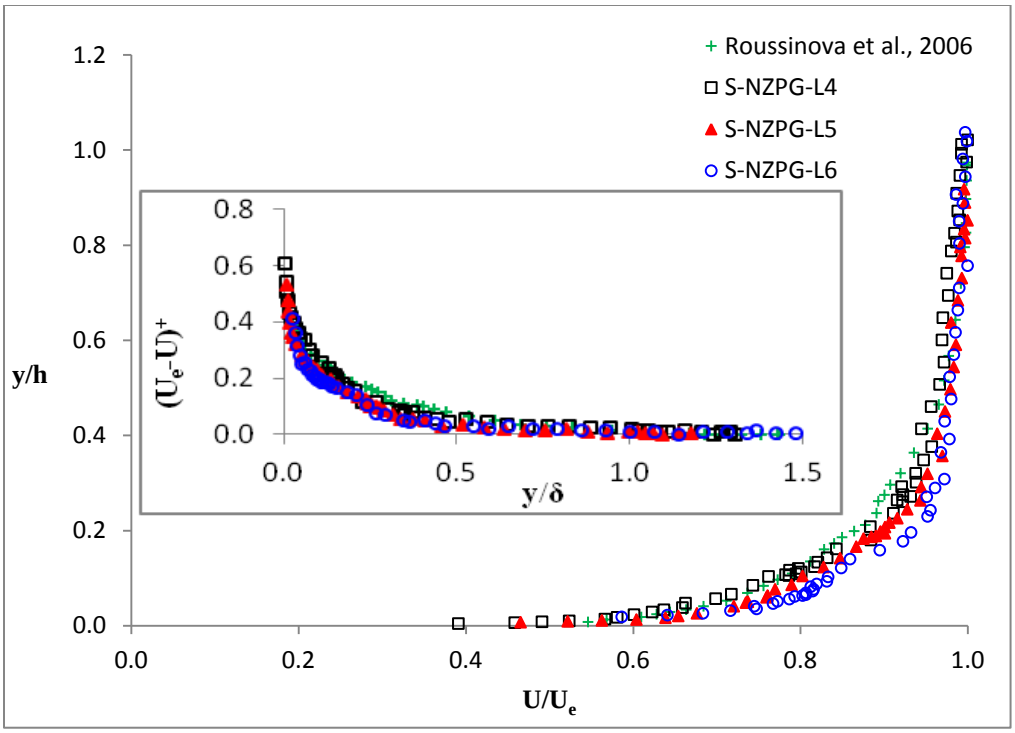

Figure 4.1 Streamwise mean velocity profiles for flow over a smooth flat plate.

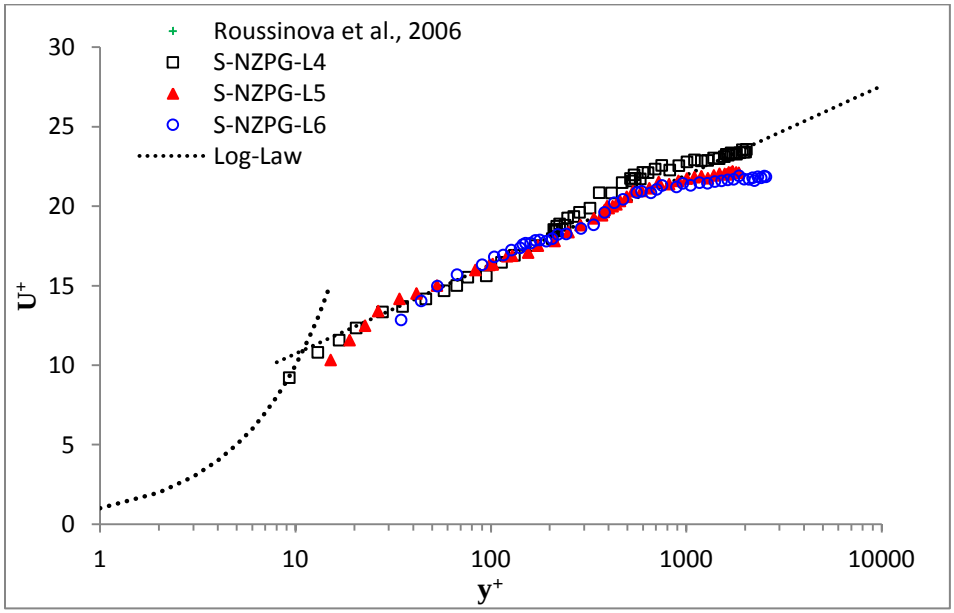

Figure 4.2 Mean velocity profile in inner scaling for flow at different stations over smooth flat plate.

4.1.2 Turbulence Intensity

4.1.2.1 Streamwise Turbulence Intensity

Streamwise turbulence intensity for flow over smooth wall is shown in the Figure 4.3. In Figure 4.3(a), depth of the flow (h) and maximum velocity (U_e) are used as length scale and velocity scale, respectively. These two parameters are directly measured quantities and any inaccuracies associated with the calculated scaling parameters are minimized. In Figure 4.3(b), boundary layer thickness (δ) and friction velocity (u^*) were used for scaling the length and turbulence intensity, respectively. For all test conditions, one can note that the maximum turbulence intensity occurs very close to the bed. Moreover, from the bed to the free surface, the turbulence intensity decreases up to a certain value in the mid-depth region ($y/\delta \approx 0.4$), then remains almost constant towards the free surface. From station L4 to L6, as Reynolds number (Re_x) increases, the turbulence intensity decreases. As it can be seen from both Figures 4.3(a) and (b), the test station L6 which is the farthest location from the bed entrance is less affected by the upstream conditions than other test stations. The existence of the free surface and bed condition generates various distributions of the turbulent intensities, which influence the turbulent conditions in the outer region. One of the reasons to use mean velocity scaling in Figure 4.3(a) is to eliminate or reduce the effect of the free surface, thus the edge of the boundary layer could be define on the basis of the region of constant turbulent intensity. The uniform OCF data reported by Roussinova *et al.* (2006) shows lower values of the velocity fluctuations close to the free surface.

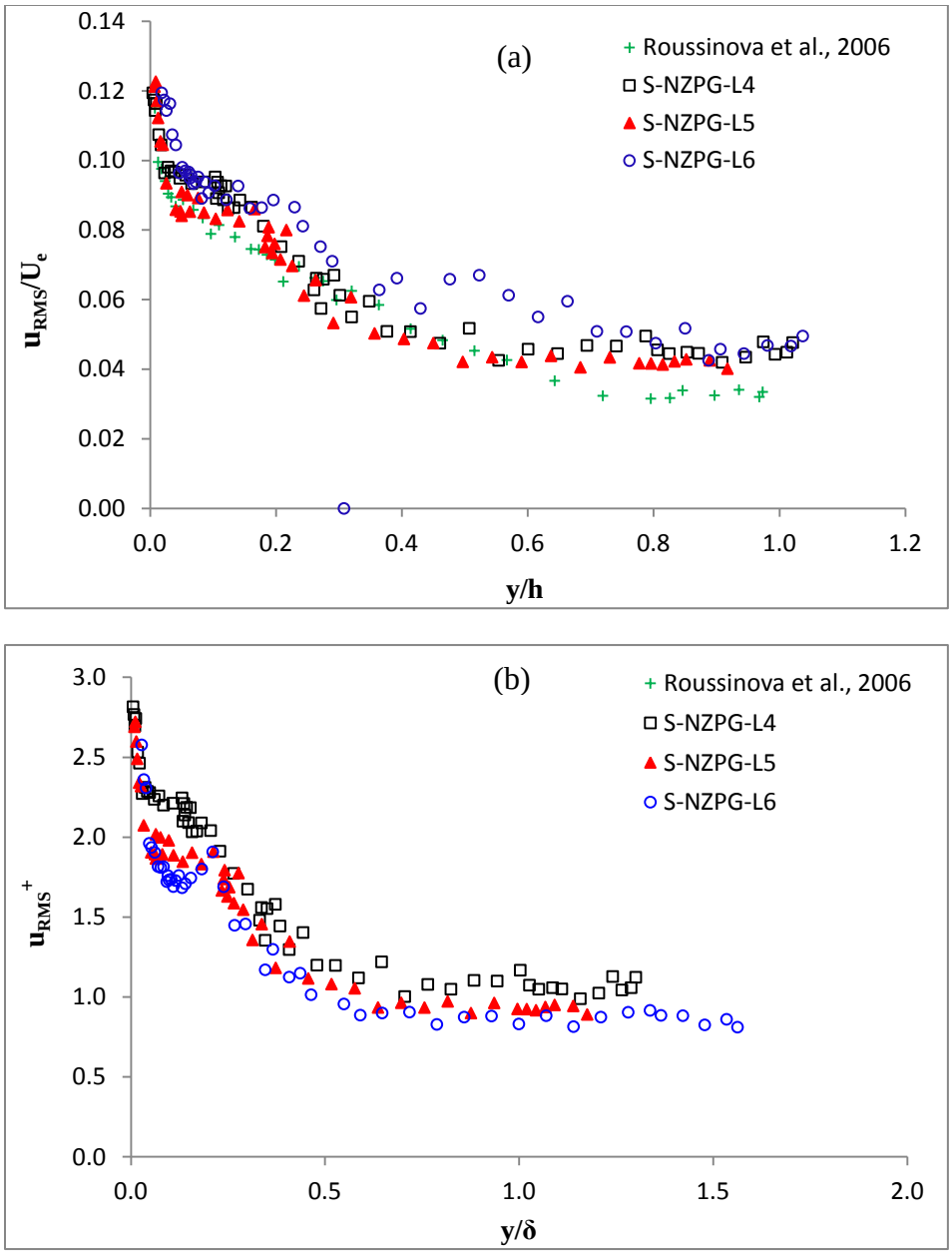

Figure 4.3 Streamwise turbulence intensity in outer scaling for flow at different locations over a smooth flat plate.

4.1.2.2 Vertical Turbulence Intensity

Figure 4.4 shows the distribution of the vertical turbulence intensity. The general trend is similar to the streamwise turbulent intensity profile, however very close to the bed and also near to the free surface, the data show different behaviour. The vertical

turbulence intensity reduces from the bed to about y/h = 0.2, and then remains constant in the range of 0.3 < y/h < 0.7 and then decreases again to its lowest values near the free surface. The first decreasing trend is due to the suppression of turbulence in the vertical direction by the bed, and the second one is due to the free surface effects. A comparison between Fig. 4.3(a) and Fig. 4.4 and also the data of Table 3.1 show that for the entire depth, both streamwise and vertical turbulence intensities decrease as Reynolds number (Re_x) increases. The uniform OCF results of Roussinova *et al.* (2006) shows a linear variation of vertical turbulence intensity. Thus, the non-uniformity of the data of the current study due to the upstream conditions (FPG flow) is clearly visible, especially in the range of 0.4 < y/h < 0.9. In this range it can be seen that the highest level of turbulence intensity belongs to the test station L4, which is more influenced by the upstream conditions (FPG flow). These comparisons also demonstrate how pressure gradient or non-uniformity increases the level of turbulence in an open channel flow. However, in the range of y/h < 0.4 all sets of data indicate similar values of vertical turbulence intensity.

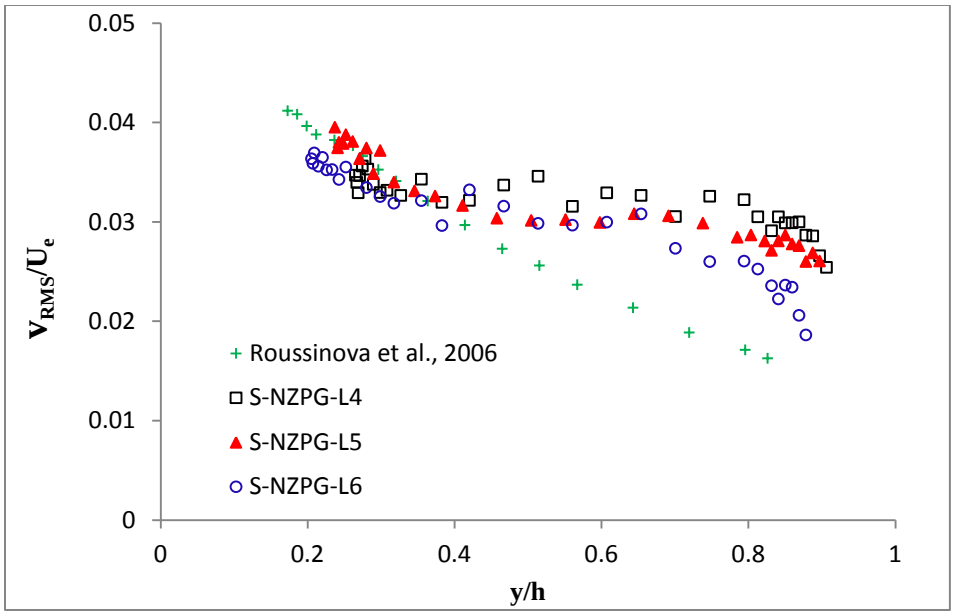

Figure 4.4 Vertical turbulence intensity in outer scaling, for flow at different locations over smooth flat plate.

4.1.3 Reynolds Shear Stress

Figure 4.5 shows the Reynolds shear stress on the smooth wall in outer coordinates. It appears that the Reynolds shear stress for all of the test cases reaches to a maximum value near the bed ($0.2 < y/h < 0.3$). Although the free stream velocity is used for velocity scaling, the effect of Reynolds number is still visible for the entire depth of the flow. This behaviour is significantly noticeable for the outer layer ($y/h > 0.3$). The test station L6, which is located far from the beginning of the bed (1070 mm) has minimum values of Reynolds shear stress in the outer region. The reduction of the Reynolds shear stress from L4 to L6 shows that the flow over the flat plate seems to be mildly accelerated. Comparing data of the current study with the uniform OCF results of Roussinova *et al.* (2006) shows that in the range of $y/h > 0.5$, non-uniform flow has higher values of Reynolds shear stresses. This is a consequence of the carry over of turbulence from the upstream non-uniform flow. However, in the range of $0.2 < y/h <$

0.5, uniform OCF has higher values of Reynolds shear stress. Tachie *et al.* (2003) have found influence of bed condition on the Reynolds shear stress penetrates up to y/h ~ 0.3, which is similar to the results of the present study.

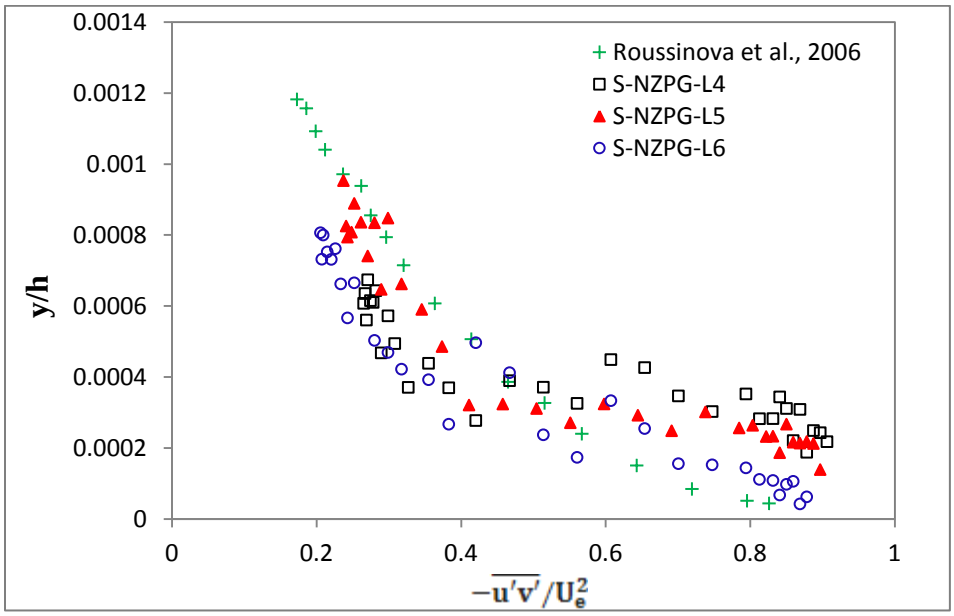

Figure 4.5 Distribution of Reynolds shear stress for flow at different location over smooth flat plate.

4.2 Effect of Roughness on the NZPG

To investigate the effects of the surface roughness on the mean velocity and turbulence intensities, three sets of data were obtained over different test stations. The discussion presented in this part provides understanding into the effects of the surface roughness on the turbulence structure over the NZPG flow.

4.2.1 Mean Velocity Profile

The distribution of the streamwise component of the mean velocity in the outer scaling is shown in Figure 4.6. These data are compared with a set of smooth data as reported in section 4.1 and also compared with a set of rough experiment data reported by

Faruque (2009). The rough wall results of the current study are consistent with the results of Faruque (2009). However, the data of Faruque (2009), show a slight velocity dip in the outer region, where the local maximum value of U_e occurs below the free surface. The rough wall profiles are displaced upwards compared to the smooth profile. Tachie *et al.* (2000) pointed out that one of the effects of roughness is to increase the surface drag, resulting a deviation in the mean velocity profile of the rough wall in comparison with the smooth wall profile. This trend is consistent with observations made in zero pressure gradient boundary layer measurements, e.g. Krogstad and Antonia (1999) and Tachie *et al.* (2003). One can note from Figure 4.6 that profiles of the test stations L5 and L6 are well matched over the depth. However, for the test station L4, which is the closest station to the bed entrance, the velocity profile is close to the smooth bed results in the outer region. The reason is that this station is influenced by the upstream FPG condition which increases the velocity magnitude.

The distributions of the streamwise mean velocity profile in the inner coordinates at the three test stations is shown in Figure 4.7. Friction velocity for rough bed data was calculated using the Clauser method by fitting the mean velocity profile with the universal log-law. $U^+ = \kappa^{-1} \ln y^+ + B - \Delta U^+$. Here $U^+ = U/u^*$ and $y^+ = yu^*/\nu$, $\kappa = 0.41$ and $B = 5.1$ are the log-law constants and ΔU^+ is the roughness function representing the downward shift of the velocity profile from the smooth wall data ($\Delta U^+ = 9$). Compared to the smooth wall data, the rough wall data shows a limited overlap region. The test stations L4 and L6 follow the logarithmic profile in the range $80 < y^+ < 500$, however the test station L5 has an extended overlap region which follows the logarithmic profile in the range $40 < y^+ < 500$. Tachie (2001) pointed out that as Re_θ increases, the extent over

which the experimental data collapse onto the logarithmic law increases. One can note from Figure 4.7 that the wake region for the rough wall data is larger than that for the smooth wall data. The other important note from this figure is that the upstream FPG conditions affects the velocity profile of the test station L4 and causes a collapse in the wake region of this profile.

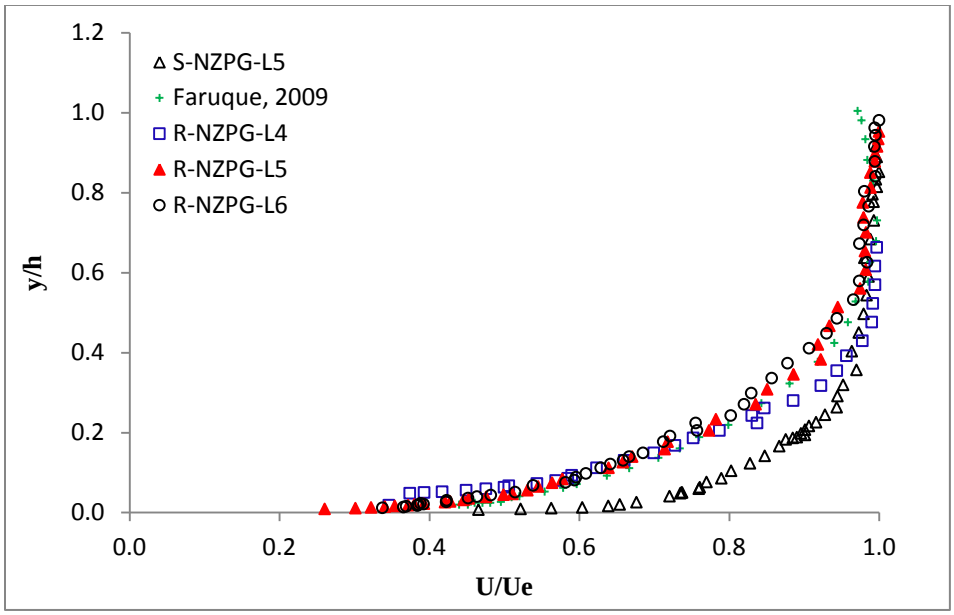

Figure 4.6 Distribution of mean velocity in outer variables, smooth and rough wall data.

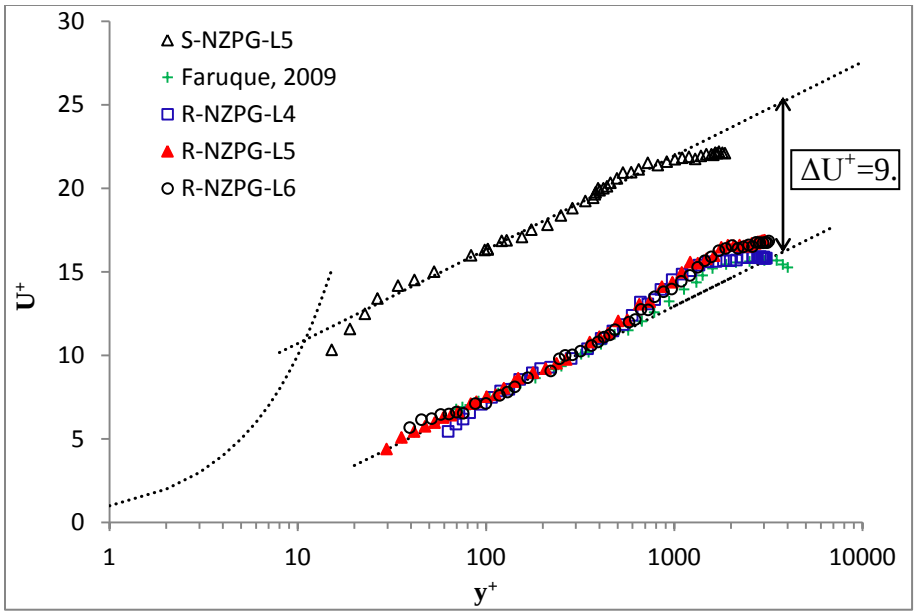

Figure 4.7 Mean velocity distribution in inner variables, comparison between smooth and rough wall data.

4.2.2 Turbulence Intensity

4.2.2.1 Streamwise Turbulence Intensity

Figure 4.8 compares the streamwise turbulence intensity for flow over the smooth wall data and three sets of data over a rough bed normalized by the free stream velocity (U_e). This figure demonstrates that the rough wall turbulence intensities are clearly higher than that for the smooth wall condition. The difference between the rough and the smooth wall data continues over most of the open channel flow boundary layer. The results reported by Faruque (2009) have a similar trend, however there is a difference between these data in the outer layer ($0.4 < y/h < 1.0$), which is because of the higher free surface velocity of the data reported by Faruque (2009). For the test station L4, the data show noticeably lower values of the turbulence intensity from $y/h = 0.2$ to $y/h = 0.6$. This behaviour suggests that the extent to which roughness influences the turbulence structure depends on the Reynolds number and the distance of the measurement stations from the

beginning of the horizontal bed. Figure 4.8 also shows that in the range of $0.7 < y/h < 1.0$, roughness has no significant effect on the production of turbulence, and the smooth and rough data indicate the same values of turbulence intensities in the present measurements. Among all rough data, the flow at the station L6 shows the largest values over the entire depth, and also shows the largest peak very close to the bed, followed by the results of test station L5.

The streamwise turbulence intensity normalized by the friction velocity ($u_{RMS}^{+} = u_{RMS} / u^{*}$), is shown in Figure 4.9. It can be seen from Figure 4.9 that the peak value for the rough wall data ($u_{RMS}^{+} = 2.28$ at $y/\delta = 0.067$ for L6) are lower than observed for the smooth wall data ($u_{RMS}^{+} = 2.7$ at $y/\delta = 0.01$). These values agree well with the values obtained by Tachie (2001). On the other hand, rough wall data shows substantially higher values than smooth wall data over most portion of the depth excluding a region close to the free surface ($y/\delta > 0.9$). Moreover, the maximum deviation from the smooth wall is in the range $0.2 < y/\delta < 0.6$. It can be noted that Figures 4.8 and 4.9 clearly demonstrate the usefulness of the scaling proposed by George and Castillo to show the general effects that surface roughness has on the turbulence levels in the OCF boundary layer.

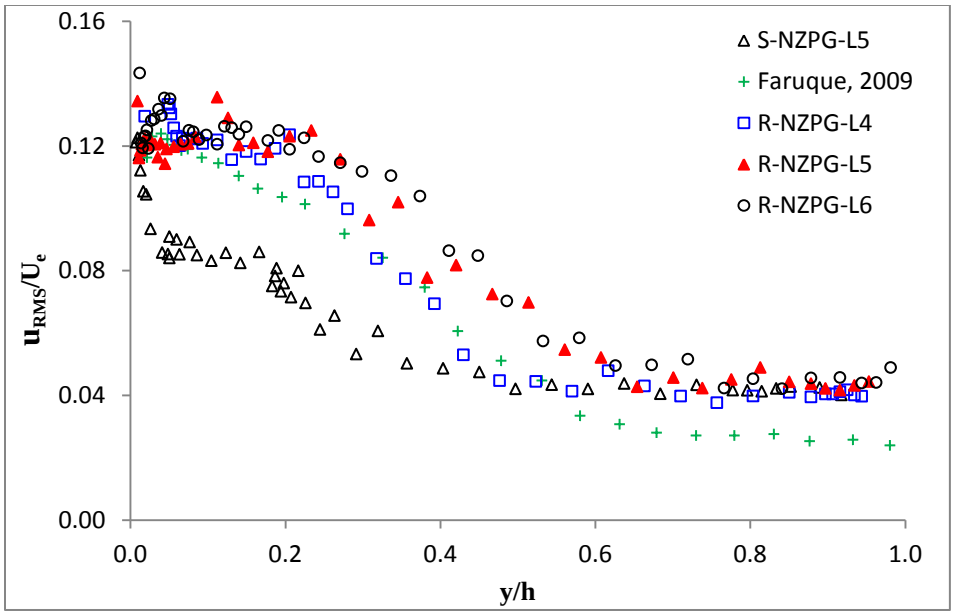

Figure 4.8 Streamwise turbulence intensity in outer scaling, flow over smooth and rough bed condition.

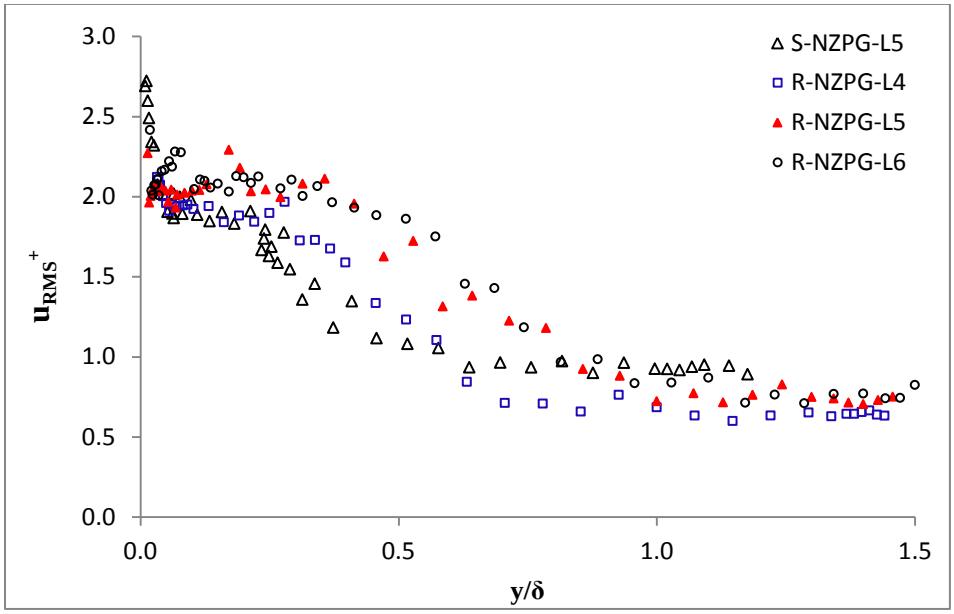

Figure 4.9 Streamwise turbulence intensity for flow over smooth and rough bed using mix scaling.

4.2.2.2 Vertical Turbulence Intensity

The distributions of the wall-normal turbulence intensity in Figure 4.10 show a trend similar to that of the streamwise turbulence intensity profile with the exception of locations very close to the bed. The scaling used here is according to George and Castillo (1997). The vertical turbulence intensity increases at locations close to the wall due to the roughness effect ($y/\delta < 0.4$). However, the streamwise turbulence intensity reduces at locations close to the bed. Because of the LDV limitations in the simultaneous measurement of the two components of velocity close to the bed, the data could not be obtained in the near-wall region ($y/h < 0.2$). The results of Faruque (2009) show a similar trend, but with the lower values from $y/h > 0.3$ towards the free surface. The reason is that his experiment was performed over a natural (permeable) bed, while the experiments of this study were carried out on an impermeable rough bed. In addition, the difference between the smooth and the rough bed data are evident over the most of the boundary layer ($0.2 < y/h < 0.7$). It can be clearly seen that the roughness effect increases the wall normal fluctuations and consequently the level of turbulence production. All of the rough wall data of the present study have very close constant values in the range $y/h > 0.7$ near the free surface. It is important to mention that the effect of surface roughness on the wall- normal turbulence intensity is stronger than that for streamwise turbulence intensity.

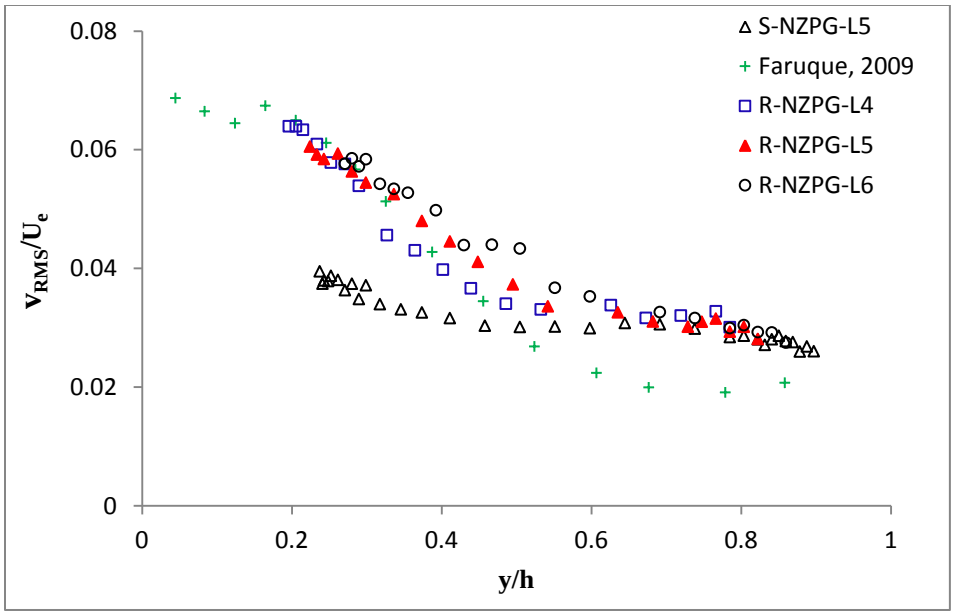

Figure 4.10 Vertical turbulence intensity in outer scaling, for flow at different locations over rough flat plate.

4.2.3 Reynolds Shear Stress

Figure 4.11 shows the distribution of the Reynolds shear stress in outer variables. Tachie (2001), reported that Reynolds shear stress at locations near the bed is highly Reynolds number dependent. However, in the current study as can be seen from Figure 4.11, this effect is not clearly visible. The Reynolds shear stress profile of the smooth wall data is considerably lower than that for the other rough bed data in the range $y/h < 0.5$, so the shear stress shows important sensitivity to the specific wall condition. Close to the free surface ($y/h > 0.6$), the Effect of the roughness on the Reynolds shear stress diminishes. Due to the measurement limitations in this study, unfortunately there is not enough data very close to the bed. The variation of Reynolds shear stress for another Reynolds number (Faruque, 2009) shows a similar trend compared to the results of the present study. However, Faruque's data shows negative values close to the free surface.

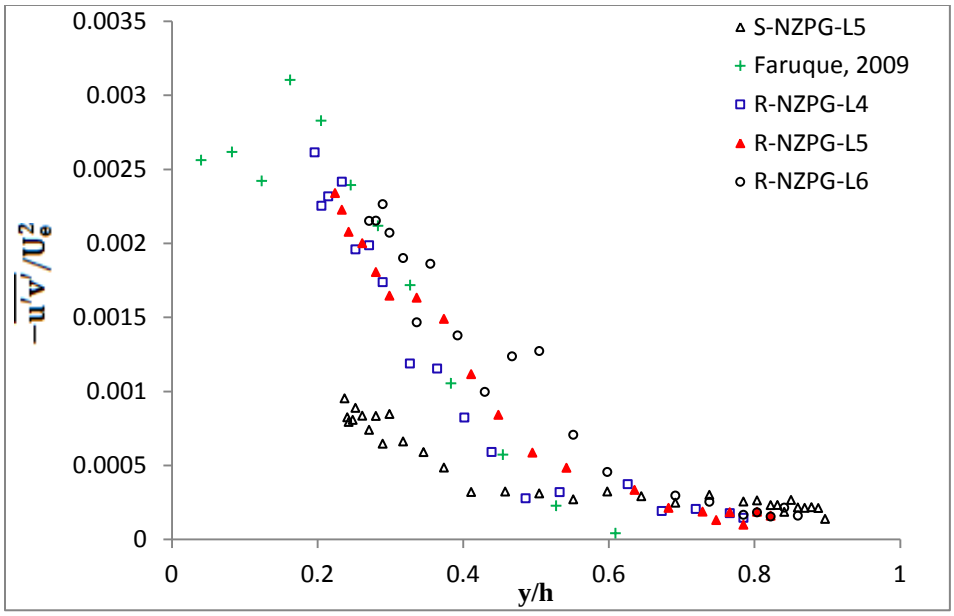

Figure 4.11 Distribution of Reynolds shear stress for flow at different location over rough flat plate.

4.3 Effect of Pressure Gradient on Smooth Bed Open Channel Flows

In this section, effect of pressure gradient (non-uniformity) in open channel flow is investigated. To this end, analysis of the results of flow over a smooth bed under favourable and adverse pressure gradients is discussed. These results provide information about the development of the flow and the influence of the favourable and adverse pressure gradients on the turbulence structure in open channel flow. The variables of interest include mean velocity, streamwise and vertical turbulence intensities, and Reynolds shear stress. The experimental conditions are summarized in Tables 3.1 and 3.2.

4.3.1 Boundary Layer Characteristics of Non-uniform Smooth Open Channel Flow

Flow characteristics of the turbulent boundary layer in open channel flows depend not only on the bed (roughness, slope) but also on the proximity to the free surface. The

depth can influence the flow by restricting the boundary layer in the vertical direction and by triggering secondary currents. Fully developed open channel flow condition is reached in laboratory conditions when the mean velocity profile becomes invariant (independent) of the measurement location Kirkgoz and Ardichoglu (1997) established a criteria for attaining the fully developed flow in open channel flumes. According to Kirkgoz and Ardichoglu (1997) for flow on a smooth bed, the minimum distance required to attain a fully developed condition should be about ~ 70h away from the entrance to the flume. This criterion can also be used as a guideline for establishing the uniform (equilibrium) flow conditions in laboratory flumes. Since most of the experimental data on turbulent boundary layer flows are performed under equilibrium conditions, a uniform fully developed open channel flow can be compared with the existing literature on turbulent boundary layers.

In the present experiments, to maintain the non-uniform flow conditions, the flow was first accelerated (x_a = 2.1 m), then a flat plate was introduced with a total length of x_f = 1.57 m and at the end, the flow was decelerated over a length x_d = 2.1 m. The approach flow condition for the accelerated section was verified to be uniform. The uniform flow characteristics on the smooth bed was investigated previously and details for the boundary layer characteristics can be found at Afzal. *et al,* (2009). It should be also noted that the inlet condition for the flat plate section is not uniform flow since it is affected by the upstream ramp. Similarly, the inlet condition for the decelerated section is also somewhat affected by the upstream flow on the flat plate. In essence, the flow in the present study cannot be separated in three sub-cases due to the non-uniform effects (different inlet conditions) and it needs to be described as a connected system. The

present non-uniform results are also compared with the uniform open channel flow results of Roussinova *et al*. (2006).

The effect of the three connected sections (FPG, NZPG and APG) on the mean flow is examined using the flow parameters summarized in Table 4.1, and 4.2. The values of the acceleration parameter K shows consistent increase with x for L1, L2 and L3 sections. The favourable pressure gradient parameter (K) which is determined from equation (2.23) is 5.25×10^{-6} for test stations L1 and L2, and is 4.55×10^{-6} for test stations L2 and L3. There is also a slight increase of K on the flat plate (from section L4 to L6) since the flow undergoes a mild acceleration. The flow along sections L7 to L9 is decelerating, which is consistent with the negative values of the parameter K. While accelerating flow tends to decrease the boundary layer thicknesses (δ and θ) and the shape parameter (H), the decelerating flow tends to increase these values. The turbulent boundary layer thicknesses are constant along the flat plate. From Table 3.1 it can be seen that the Reynolds number based on momentum thickness is Re_θ = 4643 for station L1 and decrease to Re_θ = 4257 for station L2 and Re_θ = 3422 for station L3. It will be seen that any change in the Reynolds numbers may result in changing the length of the log-law region.

The APG reduces the value of the maximum mean velocity and increases boundary layer thicknesses (δ, δ^* and θ) as presented in Table 3.1. A similar increase in δ and θ was reported by Tachie (2007) for the turbulent boundary layer subjected to external APG. In addition, no major Reynolds number dependency is found for the APG flow. The Reynolds number based on the momentum thickness for test stations L7, L8, and L9 was found to be Re_θ = 4060, 4267, and 4320 respectively. The flow is

decelerating along stations L7, L8 and L9, and the adverse pressure gradient parameter show a slight decrease for these stations. The adverse pressure gradient parameter values (β) for test stations L7 and L8 is 1.93 and for the test stations L8 and L9 is 1.73.

4.3.2. Favourable Pressure Gradient Smooth Open Channel Flows

4.3.2.1 Mean Velocity Profile

Figure 4.12 shows the distribution of the streamwise mean velocity plotted in outer scaling at stations L1, L2 and L3 along the accelerated ramp. In Figure 4.12 (a), profiles representing that in a uniform OCF (Roussinova *et al.* 2006) is also plotted for comparison. When the flow accelerates over the ramp, velocity distributions undergo progressive changes. In Figure 4.12(a), the shape of the velocity profiles deviate from the uniform OCF at $0.2 < y/h < 0.8$. The NZPG flow and the uniform OCF are in good agreement and collapsed onto a single line as expected. All FPG profiles collapse onto a single line (within the range of experimental error) which suggests independence of the Reynolds number. The presence of the inclined bed seems to retard the velocity in the outer region, which contradicts the fact that the flow is accelerating. This deviation from the uniform flow condition could be explained by the insufficient distance of the present measurement stations from the start of the inclined ramp. According to Cardoso *et al.* (1991), the flow once subjected to an inclined ramp starts to accelerate ~ 2 m from the start of the ramp. The effect of the beginning of the ramp can be felt upstream at all locations where the flow is readjusting to the new conditions and the velocities are systematically lower than the corresponding uniform flow. Since the flow is influenced by the inlet conditions it is not in equilibrium. In the near-bed region ($y/h < 0.1$*)* the velocity profiles are not influenced by the edge and all FPG profiles show similar

velocities and compare well with the uniform OCF. The effect of the pressure gradient is visible in Figure 4.12 and it is felt in the region $0.1 < y/h < 0.8$ where the accelerating profiles deviate from the uniform flow.

To investigate the differences in the outer layer of the accelerated flow, velocity defect profiles of all stations are shown as an inset in Figure 4.12(b). The velocity defect is defined as $(U_e\text{-}U)$ and it is normalized by the friction velocity (u^*). The vertical distance is normalized by the boundary layer thickness (y/δ) to conform to boundary layer literature. Except for the velocity profile at station L1, the rest of the favourable pressure gradient profiles collapse within experimental error at $y/\delta < 0.1$. In the outer region, all profiles deviate from the uniform flow case suggesting that the flow is strongly affected by the accelerated ramp. It appears that the use of the friction velocity does not absorb the effect of the pressure gradient.

It has been generally accepted that the velocity distribution obeys the classical logarithmic law of the wall even in the presence of a mild pressure gradient (non-uniform) condition. In Figure 4.13, the FPG velocity profiles are shown in a classical log-law format. Values of the friction velocity for all FPG smooth cases were calculated using the Clauser chart method and validated by the Krogstad method (Krogstad *et al.* 1992) as well. Mean velocity profile was fitted with the classical log-law given by

$$U^+ = \kappa^{-1} \ln y^+ + B \qquad (4.1)$$

Here, $U^+ = U/u^*$, $y^+ = yu^*/\nu$, $\kappa = 0.41$ and $B = 5.1$. The FPG profiles are deviated at the wake region ($y/\delta > 0.22$) and the mean flow conforms reasonably well to the theoretical logarithmic law-of-the-wall given by Eq. (4.1). The values of wake parameter Π for all FPG flow cases were obtained by fitting the velocity profiles using Eq. (2.10)

which was proposed by Krogstad *et al*. (1992). The values of the wake parameter for L1, L2 and L3 are found to be 0.475, 0.302 and 0.199, respectively. As the flow accelerates, the Π values decrease and the wake becomes smaller.

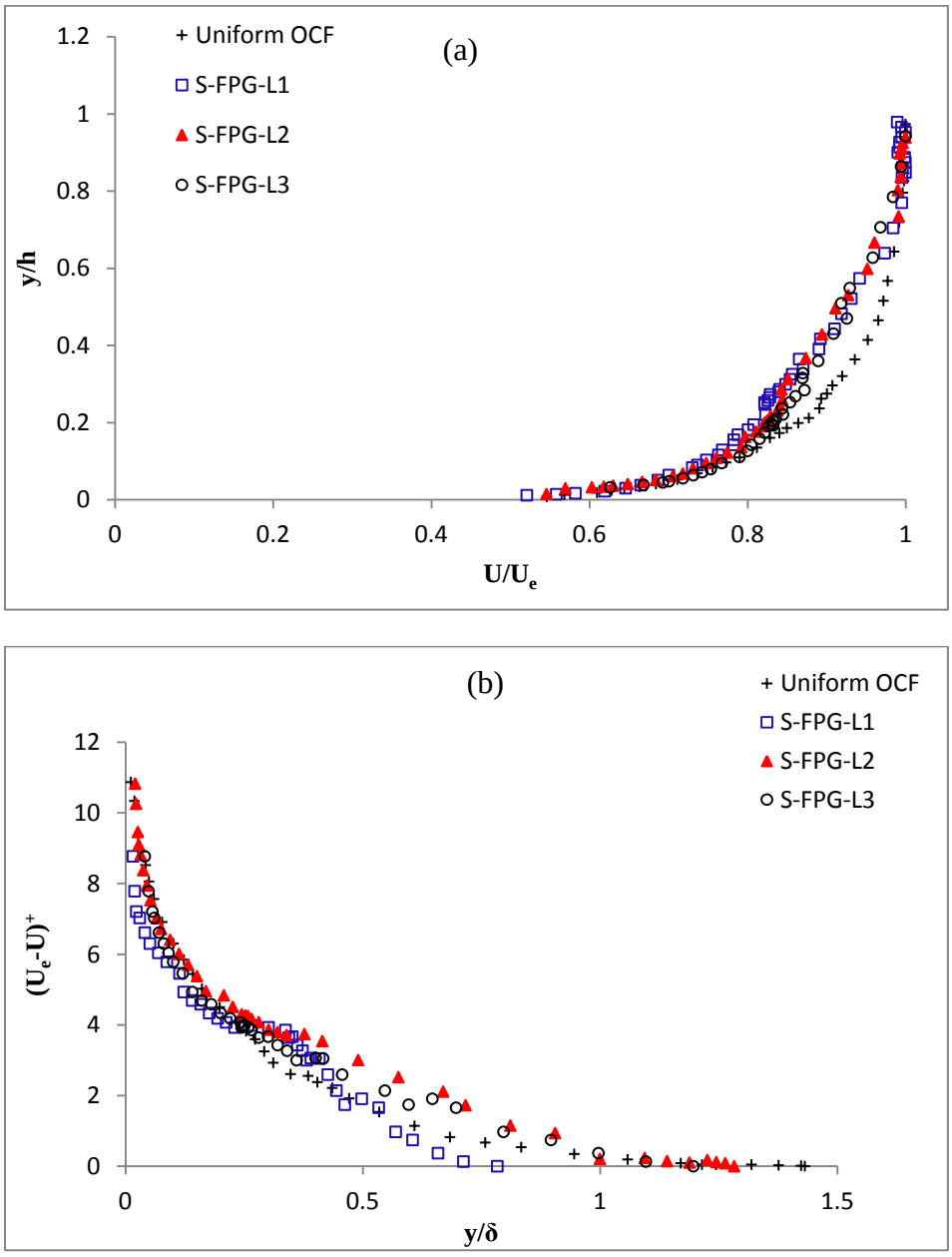

Figure 4.12 (a) Mean velocity profile and (b) velocity defect profile for the FPG flow over a smooth bed.

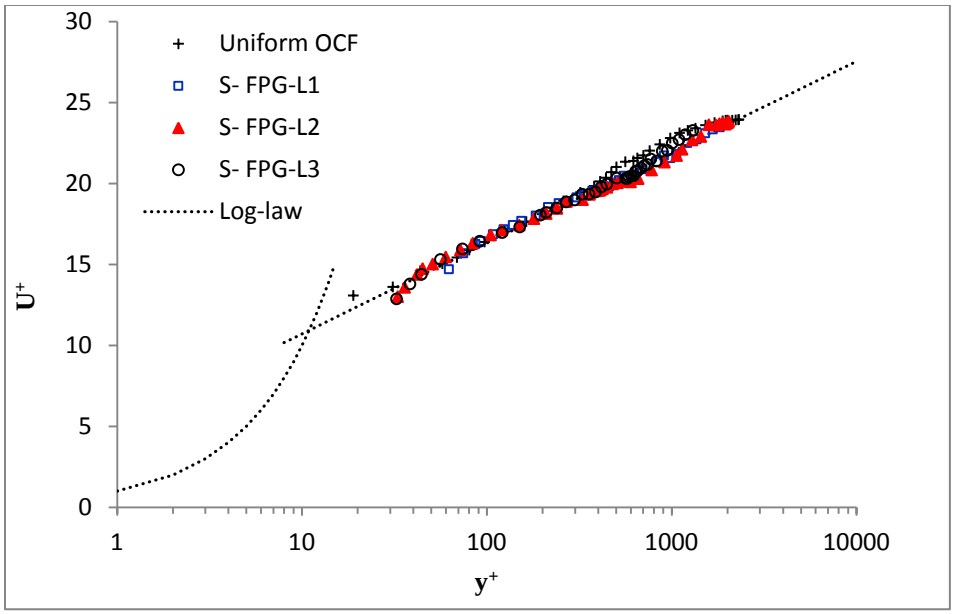

Figure 4.13 Mean FPG velocity profiles over smooth bed in inner scaling.

4.3.2.2 Turbulence Intensity

4.3.2.2.1 Streamwise Turbulence Intensity

The streamwise turbulence intensity profiles for smooth FPG flow cases are presented in Figure 4.14(a). The u_{RMS} distributions of the uniform OCF (Roussinova *et al.* 2006) are also included for comparison. For all FPG test sections, it can be noted that the maximum turbulence intensity occurs very close to the bed ($y/\delta < 0.1$). Near the wall, all data agree with the uniform flow case. Away from the bed, turbulence intensity profiles show different patterns consistent with the turbulence changing along the ramp. One can note a reduction in the turbulence intensity at $0.1 < y/\delta < 0.5$. The reduction is consistent with the dumping of the turbulence intensities observed in accelerated flows (Cardoso *et al.* 1991). The turbulence fluctuations at the mid-depth are also affected by the reduction of the flow depth as the flow accelerates. To accommodate these changes, the turbulence intensity slightly increases at $y/\delta = 0.6$. This increase is less noticeable for the flow at L3. For $y/\delta > 0.6$, turbulence intensities continue to decrease towards the free surface, but are

consistently higher than the uniform flow case. The turbulence intensity profiles scaled with U_e are shown in Figure 4.14(b). The data also shows that the velocity fluctuations at the test station L1 are less scattered than those for stations L2 and L3, located near the edge of the horizontal bed. The trends of the FPG turbulence profiles, shown in Figure 4 14(b), are similar to the one discussed previously. Effect of the FPG on the u_{RMS} distributions influences the entire flow depth except for a small region close to the bed ($y/\delta < 0.1$). It is found that no self-similarity exists for the turbulence intensity due to the proximity of the measurement locations to the start of the accelerated ramp. It appears that a longer ramp would be required to attain equilibrium flow conditions. The change of the bed slope (accelerated ramp) and reduction of the depth influence the turbulence intensities in the outer region.

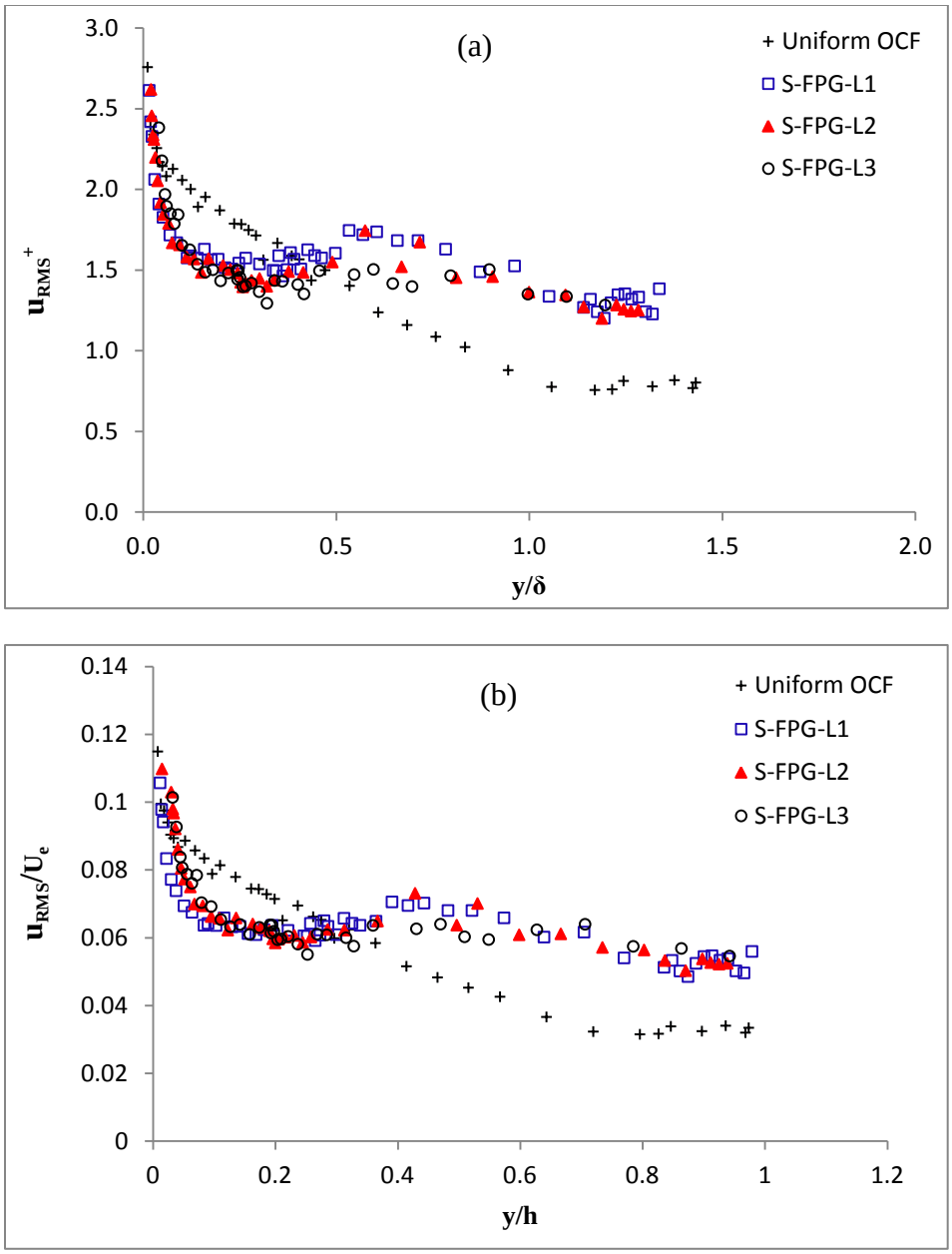

Figure 4.14 Streamwise turbulence intensity over smooth FPG flow in (a) inner scaling, and (b) outer scaling.

4.3.2.2.2 Vertical Turbulence Intensity

Figure 4.15 shows the distribution of the vertical turbulence intensity in outer coordinates for the FPG open channel flow. As the present LDV system did not allow for 2-D measurements close to the wall, simultaneous measurements of the two velocity

components were obtained for y/h > 0.2 (outer region) for all test cases. In the outer layer (0.2 < y/h < 0.5) it was observed that the v_{RMS} increases and attains maximum ($v_{RMS}/U_e \approx$ 0.05). A comparison between FPG flows and uniform flows shows that the favourable pressure gradient has a global effect on the vertical turbulence intensity, and the characteristics over the entire depth are affected.

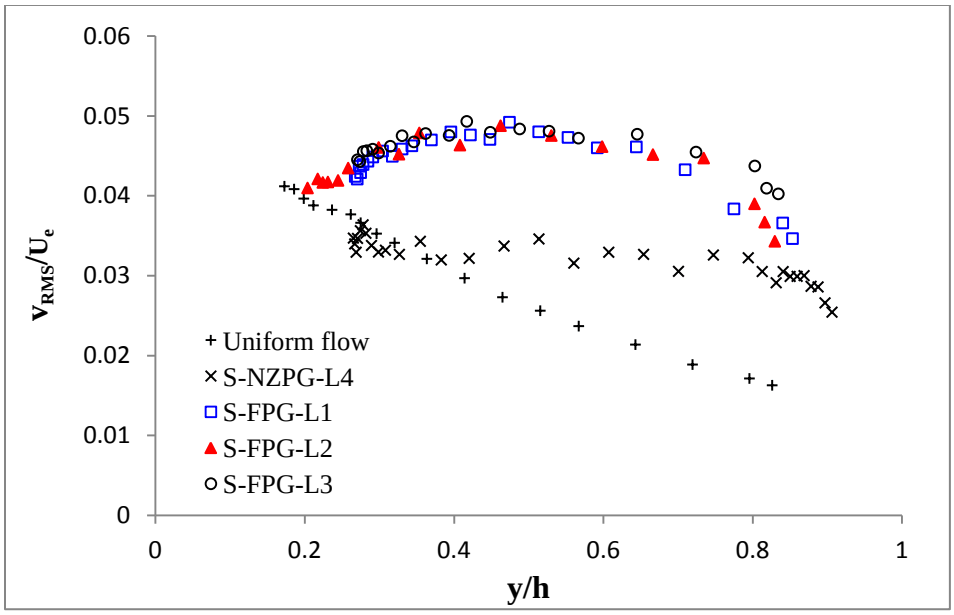

Figure 4.15 Vertical turbulence intensity over smooth FPG flow in outer scaling.

4.3.2.3 Reynolds Shear Stress

The Reynolds stresses distributions normalized by U_e^2 are shown in Figure 4.16. The Reynolds shear stress has smaller value (~ 0.0008) close to the bed, which increases and reaches a maximum value (~ 0.0014) around y/h ≈ 0.45. For y/h > 0.45, the Reynolds shear stresses decrease towards the free surface. Similar trend of the Reynolds shear stress distributions under external pressure gradient was reported by Song and Chiew (2001). The maximum values of the Reynolds shear stress occurred at y/h ≈ 0.1 which was smaller than that for the current study. Song (1994) and Song and Chiew (2001) reported that the maximum shear stress occurs on the bed, which is different from the

results of this study. One of the reasons may be because of the difference in their test conditions in comparison with experiment conditions of the current study. For example, the values of Π, which is very sensitive against the pressure gradient, for their study was very small (-0.052 to -0.11), whereas in this study Π changes from 0.19 to 0.475. The fact that the maximum shear stress occurs just above the bed around y/h = 0.4 in FPG profiles seems to disagree with Eq. (2.14). This equation demonstrates that the bed shear stress τ_w is larger than the Reynolds shear stress in the FPG flow ($\partial P/\partial x < 0$); therefore, the maximum shear stress should form on the bed. The distribution of Reynolds shear stress for FPG flow is significantly different from that noticed in uniform flow except close to the free surface. For most of the flow ($0.2 < y/h < 0.7$), the favourable pressure gradient causes the Reynolds shear stress to increase. The maximum Reynolds shear stress for FPG flow occurs in the middle part of the flow ($y/h \sim 0.5$), but for the uniform flow the maximum occurs near the bed region ($y/h \sim 0.2$).

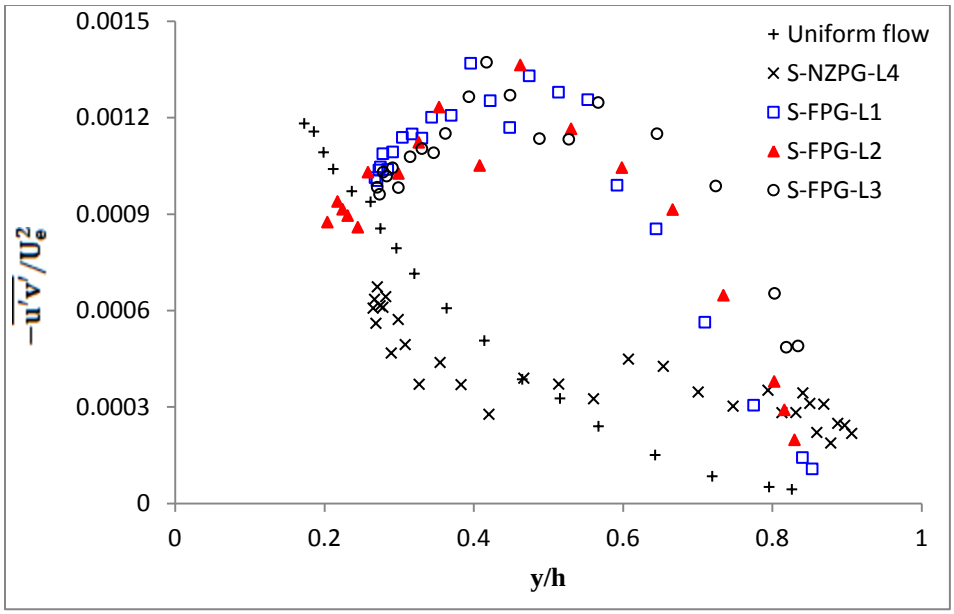

Figure 4.16 Reynolds shear stresses over smooth FPG flow in outer scaling

4.3.3 Adverse Pressure Gradient Smooth Open Channel Flows

4.3.3.1 Mean Velocity Profile

Figure 4.17 shows the distributions of the streamwise mean velocity profiles in outer scaling for APG flow. The free stream velocity (U_e) and the flow depth (h) are chosen as velocity and length scale parameters, respectively. The results of the uniform open channel flow of Roussinova *et al.* (2006) are also plotted in this figure for comparison. Figure 4.17 indicates that in the range of $0.7 < y/h < 0.9$ an upward distribution appears for the velocity profile at the test station L9, which has the minimum velocity values among other stations. Moreover, Figure 4.17 demonstrates that APG changes the velocity profile trends in comparison with the corresponding profiles obtained in the uniform section. This observation can be in the form of an upward spreading of the fluid towards the decelerating bed (Shah and Tachie, 2008).

The defect velocity profiles are shown in inner scaling as an inset in Figure 4.17. It is notable that for the adverse pressure gradient flows, both deficit profiles at the

stations L8 and L9 collapse into a single profile along the depth, however the defects velocity profile of the station L9 deviate from other profiles in the range $0.3 > y/\delta > 0.6$. Therefore, it can be mentioned that although the friction velocity usually absorbs the Reynolds number dependency of the profiles, because of the difference in the Re_θ values (4060, 4267 and 4320 for L7, L8 and L9 respectively), velocity defect profiles show a slight Reynolds number dependency.

The distribution of the streamwise component of the mean velocity profile normalized by inner scaling at three test stations for APG flow are shown in Figure 4.18. The deviation of velocity profiles from the log-law due to the adverse pressure gradient can be seen in this figure. The profile for the APG flow is dominated by an extensive wake region. The values of Π for test stations L7, L8 and L9 which is determined using the Krogstad method (Krogstad *et al.* 1992) are 1.251, 1.192, and 1.476, respectively. In the outer region, the profiles are displaced upwards showing a strong wake region while near the wall the mean flow conforms to the logarithmic law-of-the-wall. Figure 4.18 also shows a good collapse of the APG velocity profiles in the buffer and overlap regions ($y^+ < 100$) all measurement stations. A comparison between APG velocity profiles and uniform OCF velocity profile shows that, in the outer region, the APG mean velocity profiles were shifted higher than that of the uniform OCF flow case. This is consistent with the progressive flow deceleration and the velocity distributions deviate from the classical log-law of the wall This deviation is measured by the 'strength' of the wake Π, obtained from the method proposed by Krogstad *et al.* (1992). The values of Π are included in Table 4.1. Aubertine and Eaton (2005) conducted experiments over an inclined ramp of 4°, and they reported that under certain adverse pressure gradient

conditions the mean velocity still follows the classical log-law within the uncertainty of the experiments. In the present study the logarithmic layer is considered at the region of $20 < y^+ < 150$. On the other hand, for the uniform OCF presented here, the logarithmic region appears to begin at $20 < y^+ < 250$, which is slightly more extended than APG flow.

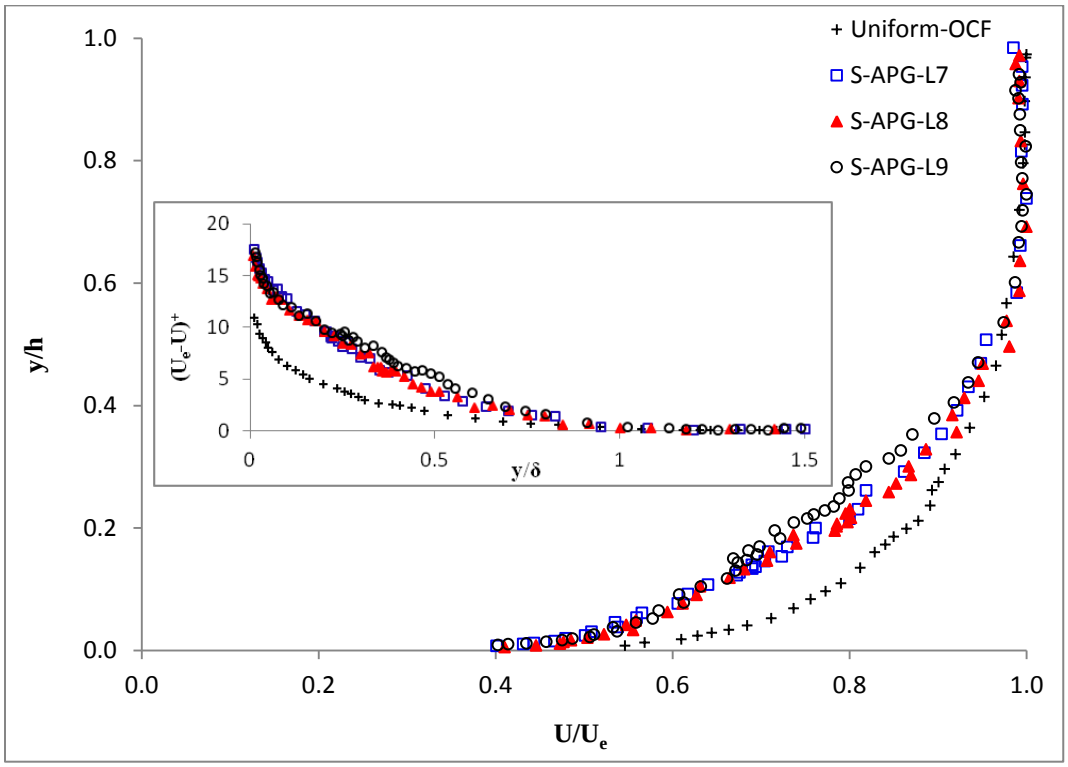

Figure 4.17 Streamwise mean velocity profiles and the velocity defect profiles for the APG flow case over a smooth bed.

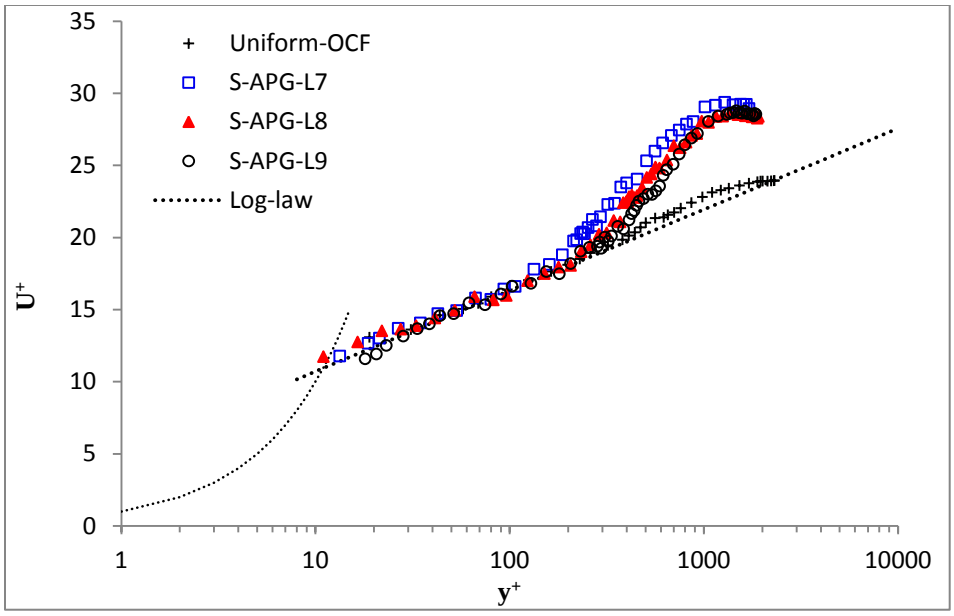

Figure 4.18 Mean velocity profiles for APG flow over smooth bed in the inner scaling.

4.3.3.2 Turbulence Intensities

4.3.3.2.1 Streamwise Turbulence Intensity

Typical profiles of streamwise turbulence intensity in APG flow over a smooth bed is presented in both inner and outer scaling in Figure 4.19. The u_{RMS} profiles are compared with the uniform OCF, bringing out the effect of the pressure gradient. As expected the turbulence intensity is higher throughout the flow for the APG case. This is in agreement with the results reported by Yang and Chow (2008), who also found that the flow is continuously entrained by the turbulence generated by the flow deceleration. Figure 4.19(a) shows that the difference between the streamwise turbulence intensity of APG flow and uniform OCF flow occurs in the whole depth. In Figure 4.19(a), it can be noted that the pressure gradient influences the turbulence intensity also near the channel bed. Figure 4.19(b) illustrates the same results as Figure 4.19(a), highlighting the difference in the turbulence intensity profiles to the effect of the pressure gradient. In

Figure 4.19(b) the maximum values of the turbulence intensity occurs at about y/h = 0.2 for all APG test cases. In contrast, the maximum u_{RMS} for the uniform OCF flow usually occurs near the bed. In conclusion, the flow subjected to an adverse pressure gradient shows increase of the turbulence throughout the entire depth except for the regions very close to the bed and free surface. The free surface tends to reduce the streamwise turbulence fluctuations.

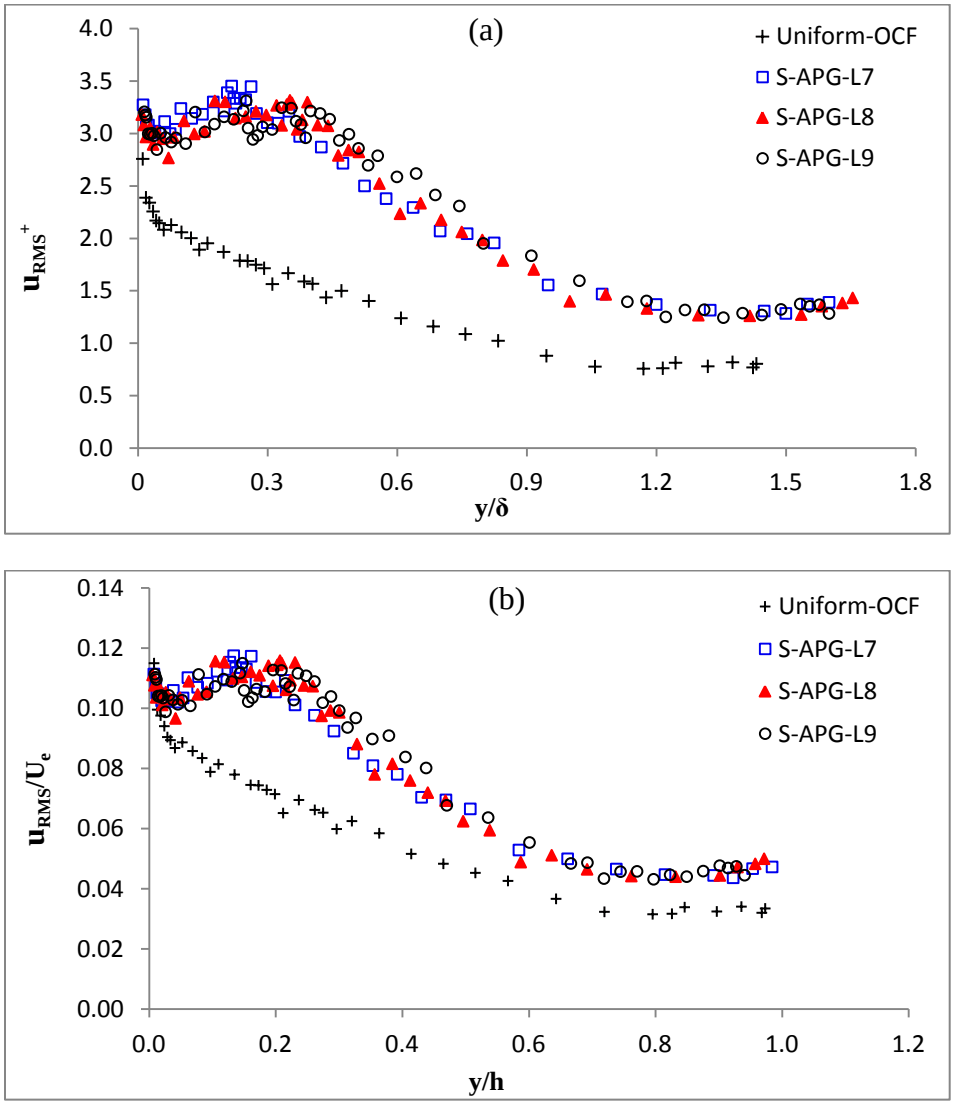

Figure 4.19 Distribution of streamwise turbulence intensity in (a) inner and (b) outer scaling for APG flow over smooth bed.

4.3.3.2.2 Vertical Turbulence Intensity

Figure 4.20 shows the distribution of the vertical turbulence intensity for the smooth APG open channel flow in the outer scaling. Because of the limitations for the two component measurement close to the wall, data was obtained from y/h > 0.2 for all three test cases. For all test stations, vertical turbulence intensity decreases almost linearly from the channel bed to the free surface. These data agree well with Yang *et al*. (2006) and Yang and Lee (2007), which mentioned that very close to the wall, the decelerating flow generates the upward wall-normal velocity. Yang and Chow (2008) also reported that the deviation of the vertical turbulent intensity in APG flow from ZPG flow depends on the ratio of Reynolds shear stress in the APG flow to that in ZPG flow. Figure 4.20 shows a significant deviation of vertical turbulent intensity in APG flow from uniform open channel flow along the bed.

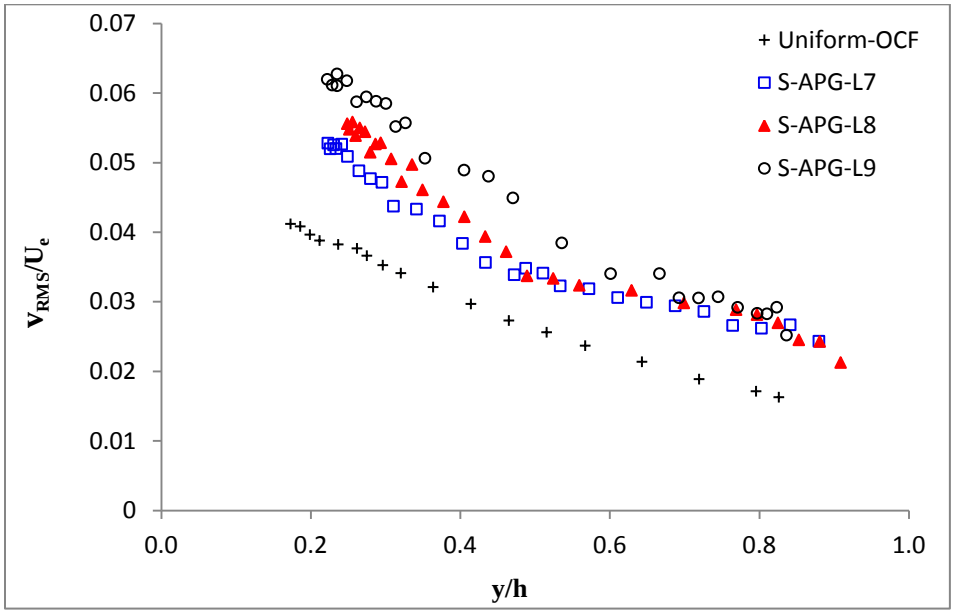

Figure 4.20 Vertical turbulence intensity in outer scaling, for APG flow over a smooth bed.

4.3.3.3 Reynolds Shear Stress

The Reynolds shear stress profiles in outer variables are shown in Figure 4.21. The maximum Reynolds shear stress occurs above the bed at vertical distance of y/h = 0.2 for all APG cases. Figure 4.21 illustrates that in the range of 0.25 < y/h < 0.5 APG flow has higher values of Reynolds shear stress than that for uniform OCF, however in the range of y/h > 0.5 uniform flow contains higher values of Reynolds shear stress. The Reynolds shear stress distributions in this study are consistent with previous works reported by Song and Chiew (2001), Afzalimehr and Anctil (1999), and Emamzadeh *et al.* (2010).

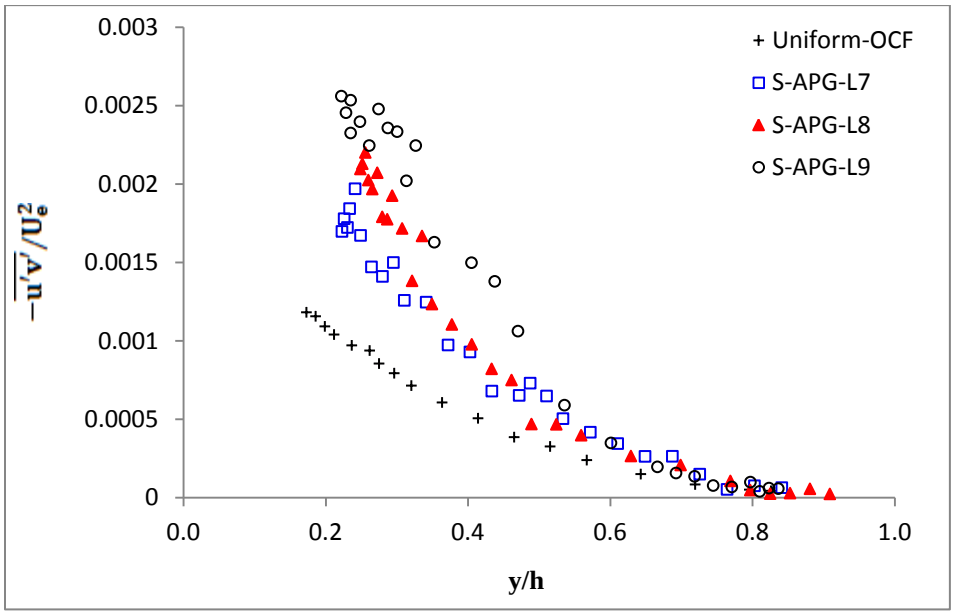

Figure 4.21 Reynolds shear stresses subject to APG flow over a smooth bed.

4.4 Effect of Pressure Gradient on Rough Bed Open Channel Flows

In order to investigate the combined effects of the roughness and pressure gradient on the open channel flow, the profiles of selected turbulence statistics in a non-uniform rough bed open channel flows are compared with a profile of the smooth bed

data as well as a rough NZPG data. The data sets presented here provide information about the development of the flow and the influence of the pressure gradient, as well as the surface roughness, on the turbulent characteristics of an open channel flow. Details of the experimental conditions and various parameters of the non-uniform experiments on the rough bed are summarized in Tables 3.1, 3.2, 4.1 and 4.2.

4.4.1 Favourable Pressure Gradient Over Rough Open Channel Flows

In this section, the experimental results of the effect of the favourable pressure gradient on the rough bed are presented. In what follows, the mean velocity, u_{RMS}, v_{RMS}, and the Reynolds shear stress profiles, measured at two streamwise stations will be discussed

4.4.1.1 Mean Velocity Profile

Figure 4.22 shows the mean velocity profiles for the FPG open channel flow over a rough bed. Two features can be seen in Figure 4.22. The roughness effect causes the FPG velocity profiles to shift to the right side of the smooth FPG profile, especially in the range $y/h < 0.6$. This could be due to the higher resistance generated by the roughness. Figure 4.22 also indicates that the roughness effect is no longer important far from the bed ($y/h > 0.6$), where all smooth and rough bed profiles tends to overlap with each other. The k_s^+ values for test stations L2 and L3 are 65.8 and 64.4 respectively, which are in a fully rough regime and fairly close to each other. To highlight the FPG effect, the rough FPG data are compared with the smooth FPG case. It is clearly visible from Figure 4.22 that in comparison with the NZPG data, the combination effects of FPG and surface roughness would increases the velocity magnitudes and pushes the mean profiles to the left side. The maximum deviation of the rough FPG data from the rough NZPG data

occurs in the region of $0.1 < y/h < 0.3$. It can be seen from Table 3.2 and Figure4.22 that there is no Reynolds number dependency since Re_θ for rough FPG for stations L2 and L3 are very close and $Re_\theta \sim 4762$ and 4461. The mean velocity defect of the rough FPG profiles is plotted and presented as an inset in Figure 4.21. The velocity defect profile of the test station L2 overlaps with the smooth FPG case at the station L3. However, rough FPG data at station L3 collapse below the smooth FPG data with the lower values of velocity. This could be due to the non-equilibrium nature of the flow at these stations, where there is influence from the upstream conditions. It can be seen from the inset profile that due to the acceleration of the flow in the FPG cases, the velocity deficit magnitudes are decreased. Surprisingly, the combined effect of roughness and FPG is remarkable for the test station L3, which is located at 13h from the start of the accelerating ramp or 3.3h from the intersection of the accelerating ramp and the flat bed. For this station both effects of the surface roughness and FPG appeared throughout the entire flow depth. Overall it can be conclude that the favourable pressure gradient increase the mean velocity and decrease the deficit velocity as indicated in Figure 4.22.

Figure 4.23 illustrates the log-law format of the mean velocity profiles for rough FPG open channel flow. The rough FPG profiles were compared with smooth FPG and rough NZPG profiles. Figure 4.23 shows the expected shift from the smooth FPG data for both rough FPG test cases ($\Delta U^+ = 7.0$), confirming that the effect of the surface roughness on the mean flow for both cases are the same. The rough wall data agree well with the classical logarithmic law at the range of $400 < y^+ < 300$. In comparison with rough NZPG, FPG effect causes a reduction in the region which can be represented with the classical log-law. Thus, a visible deviation from the log-law occurs at $y^+ > 300$ due to the

acceleration of the flow. This configuration has also been reported by Cardoso *et al.* (1991). In addition in the outer layer, the profiles including wake region collapse below the classical log-law. Figure 4.23 reveals that the combined effects of roughness and FPG causes the complete loss of the wake region, however, it keeps the logarithmic region, which agree well with the results of Bourassa and Thomas (2009).

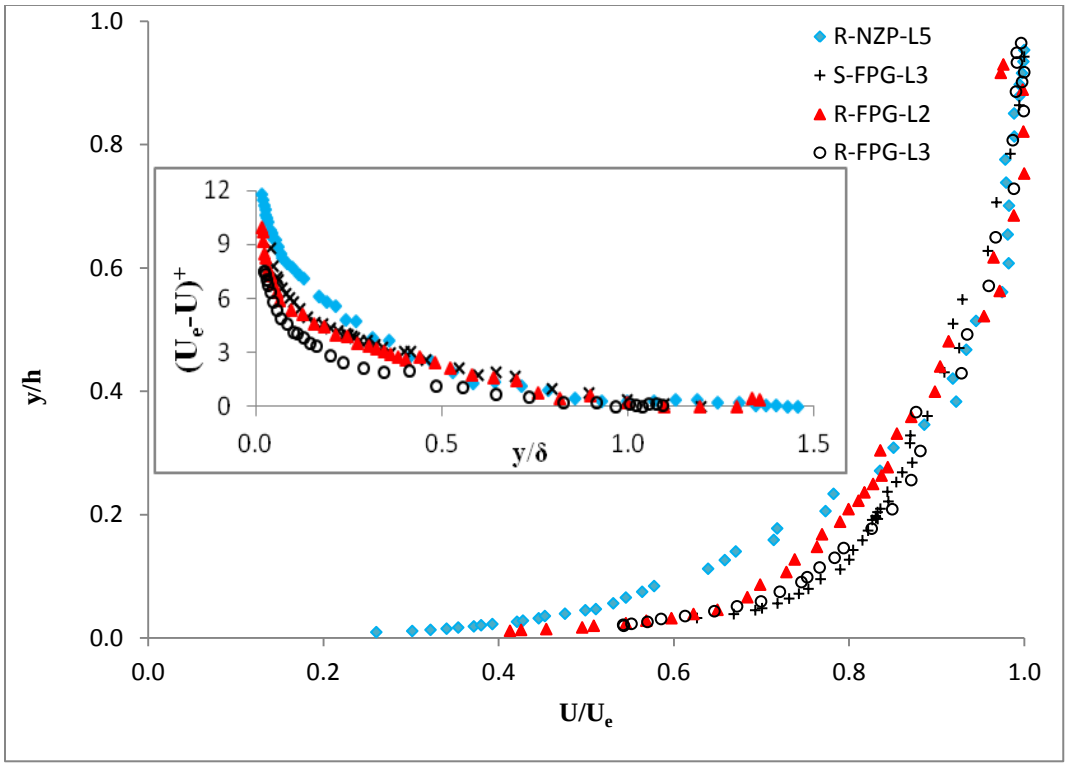

Figure 4.22 Streamwise mean velocity profile and the velocity defect profile for the rough FPG open channel flow.

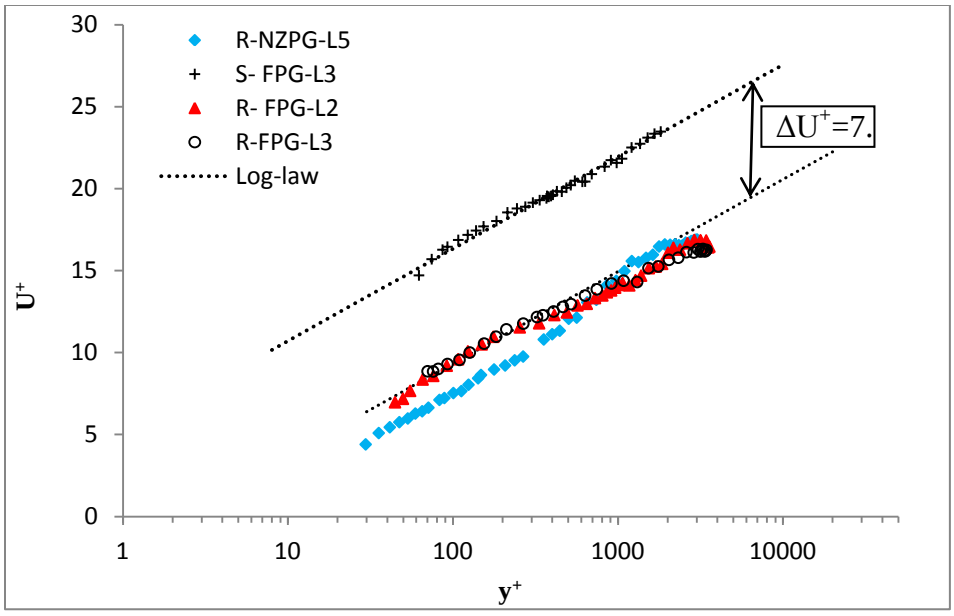

Figure 4.23 Inner scaling profiles of the mean velocity at three streamwise locations for rough and smooth FPG open channel flows.

4.4.1.2 Turbulence Intensity

4.4.1.2.1 Streamwise Turbulence Intensity

Typical streamwise turbulence intensity profiles for rough FPG open channel flow were presented in the Figure 4.24. The outer and the inner scaling are used in order to normalize the length and velocity fluctuations in Figures 4.24(a) and b. For all test conditions, one can note that the maximum streamwise turbulence intensity occurs near the wall with the exception of the rough NZPG case, for which the maximum value occurs at y/h = 0.3. By using of the inner scaling variables in Figure 4.24(a) show that there is no difference between turbulence intensities of the rough and the smooth FPG flow cases near the bed. Using outer variable scaling in Figure 4.24(b) indicates that roughness causes a notable increase in the streamwise turbulence intensities. Near the wall (y/h <0.2), the streamwise turbulence intensity is not affected by the favourable pressure gradient. Moreover, both Figures 4.24(a) and (b) confirmed that the combined

effects of the surface roughness and favourable pressure gradient tends to increase the turbulence intensity in a region close to the bed at $0.2 < y/h < 0.4$. Then, in the rest of the outer layer ($y/h > 0.4$) NZPG data indicate to be less turbulent that FPG ones. This could be because of the tendency of the flow to be re-laminarized due to the favorable pressure gradient effect. The maximum deviation of the FPG from NZPG occurs near the free surface around $y/h = 0.9$. Figure 4.24(b) also represents that from the channel bed up to about $y/h < 0.2$, turbulence intensity decreases gently and then increased slightly up to about $y/h < 0.4$, then keep decreasing up to the free surface. In addition, from both Figures 4.24(b) it can be noted, that the roughness effect is more effective than FPG effect in case of increasing in u_{RMS}. It can be conclude from these two Figures that the streamwise turbulence intensity of the rough FPG flow is faced with a systematic deviation from the smooth FPG flow for the entire depth.

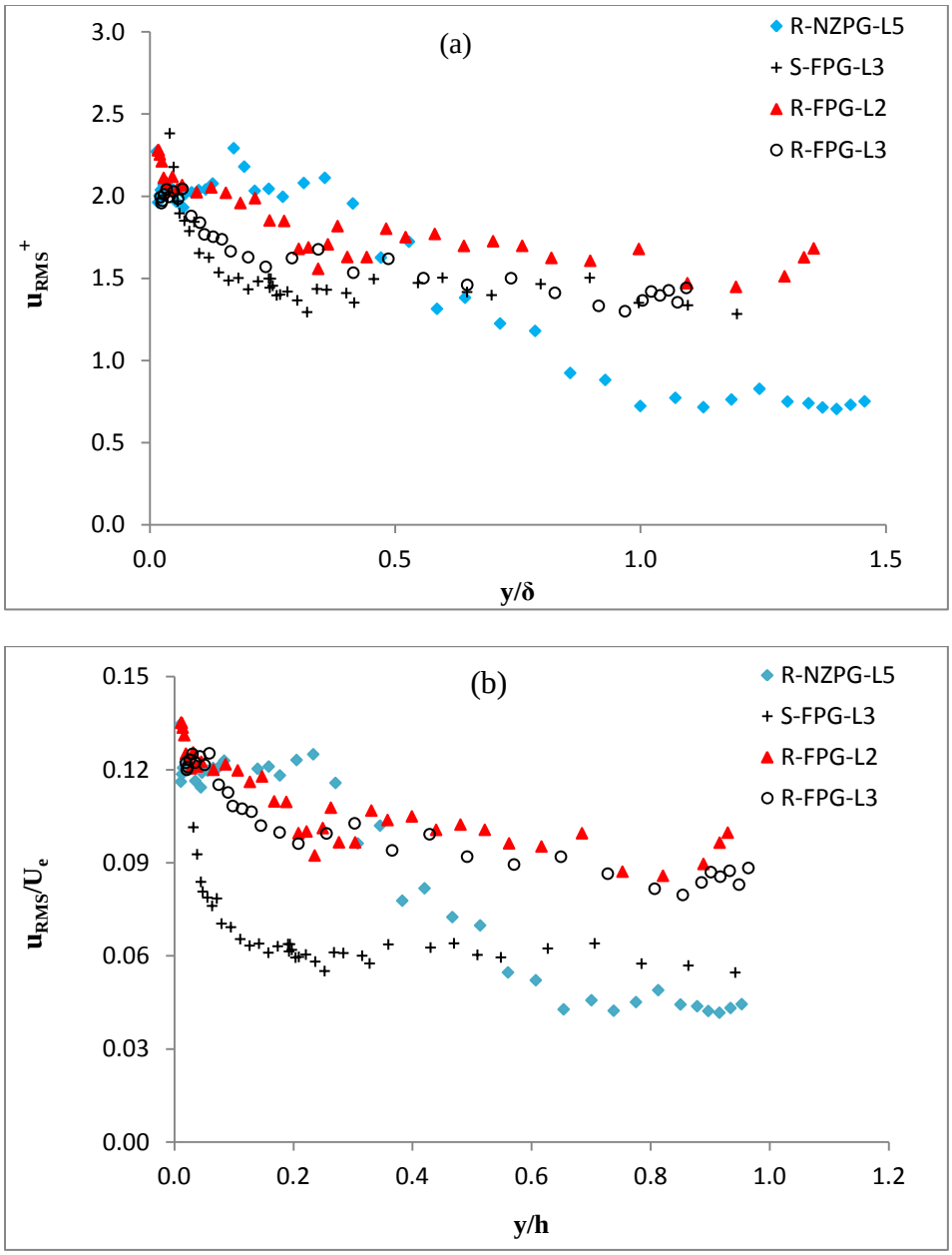

Figure 4.24 Streamwise turbulence intensity in (a) inner scaling and (b) outer scaling for the FPG flow over rough and smooth beds.

4.4.1.2.2 Vertical Turbulence Intensity

Figure 4.25 shows the distribution of the vertical turbulence intensity for the rough FPG open channel flow. In general, for all test stations presented in Figure 4.25, vertical turbulence intensity start to increase from the bed to about y/h ≈ 0.6, then

decreases slightly towards the free surface. The most important aspect of this figure is that the vertical turbulence intensity is significantly affected by favourable pressure gradient. This could be related to the existence of non-zero wall-normal velocity, which produced a downward velocity (Song and Chiew, 2001). One can note that the surface roughness increases the vertical turbulence intensity and causes a right side shift in the profiles. The maximum deviation of the vertical turbulence intensity due to the roughness is about 30%, while the deviation due to the pressure gradient changes from zero to 60%. Therefore, it can be noted that combined effects of the surface roughness and FPG will enhance turbulence productions. From Figure 4.25 and Table 4.2 it can be seen that for rough FPG cases even any small increase in k_s^+ (3%) can amplify the vertical turbulence intensity. In addition, from y/h = 0.6 towards the depth, the free surface effects dominates over pressure gradient and roughness effects therefore, vertical turbulence intensity slightly decreases.

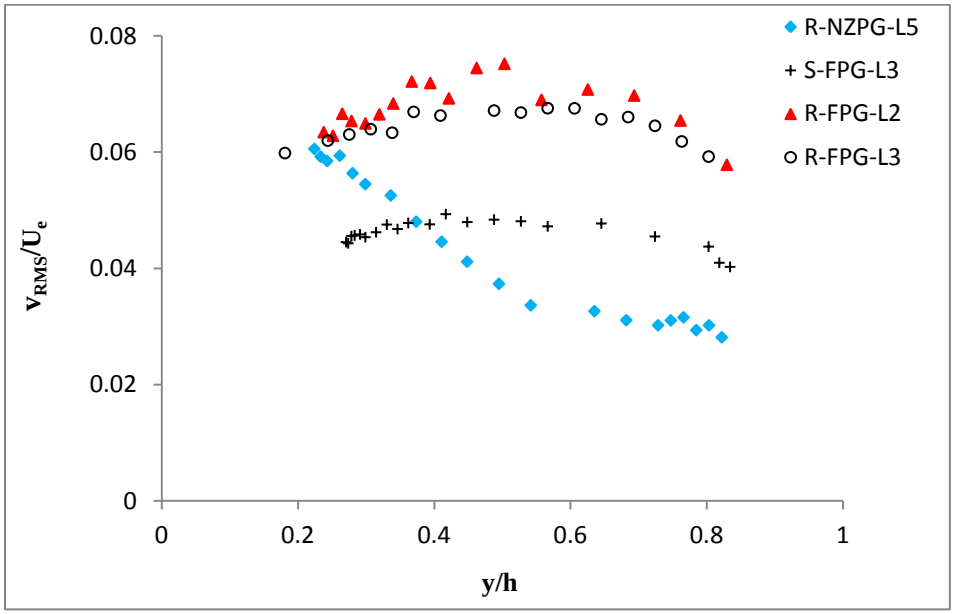

Figure 4.25 Vertical turbulence intensity in the outer scaling, for FPG over rough and smooth beds.

4.4.1.3 Reynolds Shear Stress

The Reynolds shear stress distributions in outer variables for the rough FPG open channel flow are shown in Figure 4.26. This figure includes NZPG velocity profile at section L5 over rough bed as well as a FPG velocity profile over a smooth bed. In Figure 4.26, the magnitude of the Reynolds shear stress has a small value close to the bed. At y/h > 0.3, $-\overline{u'v'}$ increases until it reaches a maximum at around y/h ≈ 0.4 and decrease non-linearly towards the free surface. This trend agrees well with the gradually accelerated data by Song and Chiew (2001). In order to discuss the surface roughness effect, the smooth bed FPG profiles will be compared with the rough bed profiles. It can be seen from Figure 4.26 that the rough profiles are shifted to the right side with higher magnitude of the Reynolds shear stresses due to the roughness effect. For the test station L2, the value of k_s^+= 65.8 which is slightly higher than the value obtained in test station L3 (k_s^+ = 64.8). The higher k_s^+ values of station L2 lead to higher values of the Reynolds shear stress in station L2 compared to station L3. A small increase of in the k_s^+, therefore result into 20 % - 32% increases in the Reynolds shear stress. In addition, a comparison between the rough NZPG profile and the rough FPG profile shows that the Reynolds shear stress for the rough NZPG decreases towards the free surface. However, the combined effects of the surface roughness and FPG will increase the Reynolds shear stress in the region 0.25 < y/h < 0.45. The reason is that the local wall shear stress decreases as flow accelerate. The occurrence of the maximum shear stress above the bed in FPG flow appears to be in contrast with the conclusion one may infer from Eq. (2.14). According to this equation, regardless of the types of the bed (smooth or rough), the bed shear stress τ_w should be higher than the Reynolds shear stress due to the negative

pressure gradient ($\partial P/\partial x < 0$); therefore the maximum shear stress should form near the bed.

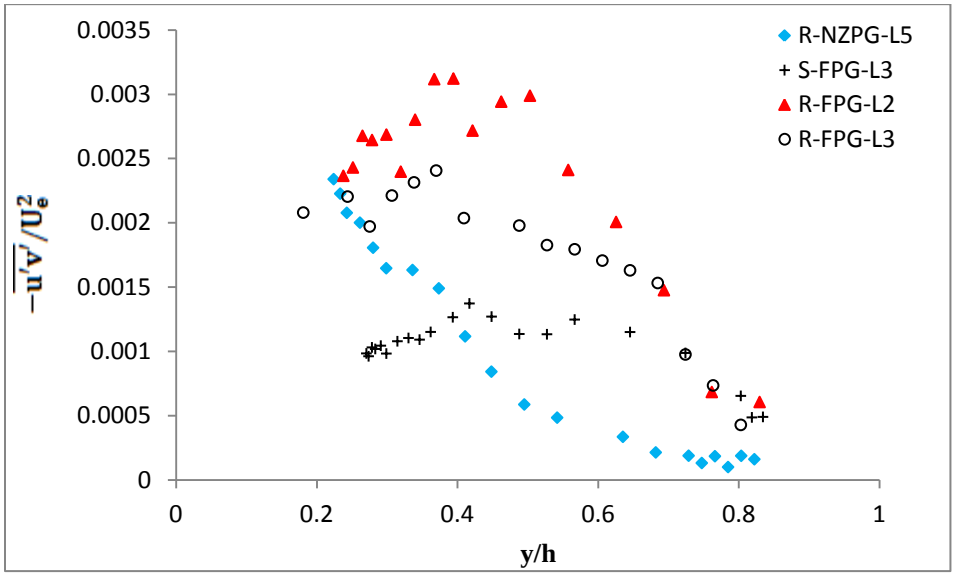

Figure 4.26 Reynolds shear stresses profiles subject to smooth and rough FPG.

4.4.2 Adverse Pressure Gradient Over Rough Open Channel Flows

The combined effects of the roughness and adverse pressure gradient on the open channel flow are discussed in this section. The profiles of selected turbulence statistics in the rough surface APG flow are compared with a profile of a smooth wall APG data.

4.4.2.1 Mean Velocity Profile

Figure 4.27 shows the streamwise mean velocity profiles in outer coordinates. As it can be seen from the rough wall APG data, the profiles do not overlap each other. The reason could be related to several factors such as APG parameter (β) and equivalent sand roughness (k_s^+). For example, the test station L8 is located at 4.3h from the beginning of decelerating ramp with $\beta = 0.944$ and $k_s^+ = 89.5$. The test station L9 is also located at 5.6h from the intersection of the zero sloped bed and decelerating ramp or 8.1h from the end of the decelerating ramp consists $\beta = 0.77$ and $k_s^+ = 100$. Figure 4.27 shows that all

profiles of the mean velocities of rough APG flows are located on the left hand side of the rough NZPG and smooth APG profile. The combined effects of APG and roughness are to further reduce velocity (U) consistent with the flow deceleration. Similar results was reported by Yang and Chow (2008) and Tsikata and Tachie (2013). Velocity defect profiles are plotted and presented as an inset in Figure 4.27. The APG and rough NZPG defect profiles deviate from the smooth APG profile for the ($0.1 < y/\delta < 0.8$). All of the rough profiles are shifted downward, which indicates that the roughness effects dominate over the pressure gradient effect. In addition, surface roughness shows its effects very clearly on the range $y/\delta < 0.7$, especially in the near wall region. The APG profiles fall in between the smooth APG and Rough NZPG deducing that the roughness decreases the magnitude of the velocity deficit while the APG increases it. Close to the free surface ($y/\delta > 0.9$) all effects are absorbed by the selected length and velocity scaling.

The distributions of the streamwise mean velocity in the inner coordinates for the rough APG open channel flows are displayed in Figure 4.28. All rough APG profiles agree with the classical log-law in the range of $300 < y^+ < 800$. However, for the test station L8, which has the lowest value of Π (~ 0.464), the log-law region seems to be extended $200 < y^+ < 1500$) and the wake region is slightly smaller than that for other rough APG profiles. Two important aspects can be discussed separately in Figure 4.27. First, all rough APG profiles deviate to a downward shift from the presented smooth APG profile. This phenomenon is expected due to the significant value the roughness function ($\Delta U^+ = 15$), which represented in Equation (2.10). In comparison, with the smooth wall APG data, the rough wall APG profiles show smaller wake region. The reason might be due to the smaller values of Π for rough APG (1.25, 1.92, and 1.47 for

L7, L8, and L9 respectively) in comparison with those for rough APG (0.604, 0.464, and 0.643 for L7, L8, and L9 respectively). The second aspect is that the NZPG profile is located above the APG profiles, which indicates a consist increase of the friction velocity with adverse pressure gradient (see Table 4.2). The NZPG mean flow velocity profiles seems to follow the standard logarithmic trend in the region $30 < y^+ < 400$, and APG effects shift this region to approximately $300 < y^+ < 1000$. Figure 4.28 and Table 4.2 represent changes in the profiles due to the combine effects of the APG and roughness effects. These changes can be seen for different parameters such as u^*, Π, k_s^+. For example, from the smooth NZPG flow to smooth APG, the friction velocity increases about 5%, while it increases about 24% from the rough NZPG flow to the rough APG flow. It also can be seen that, the combined effects of roughness and APG, cause the log region to be extended and makes the wake region smaller.

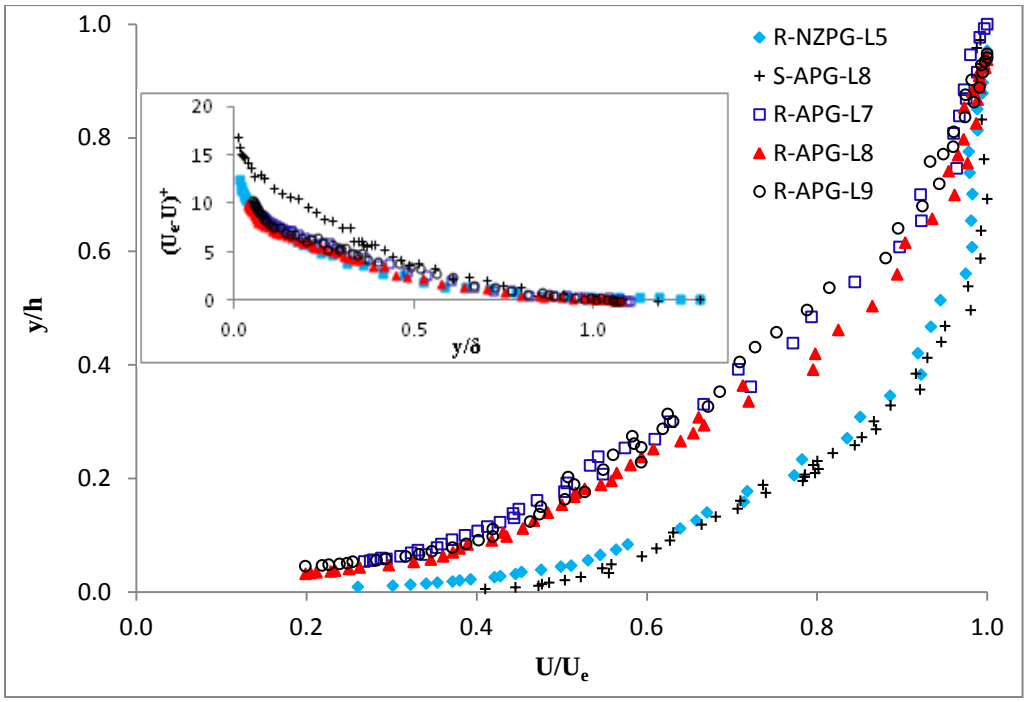

Figure 4.27 Streamwise mean velocity and the velocity defect profiles for the APG flow over a rough bed.

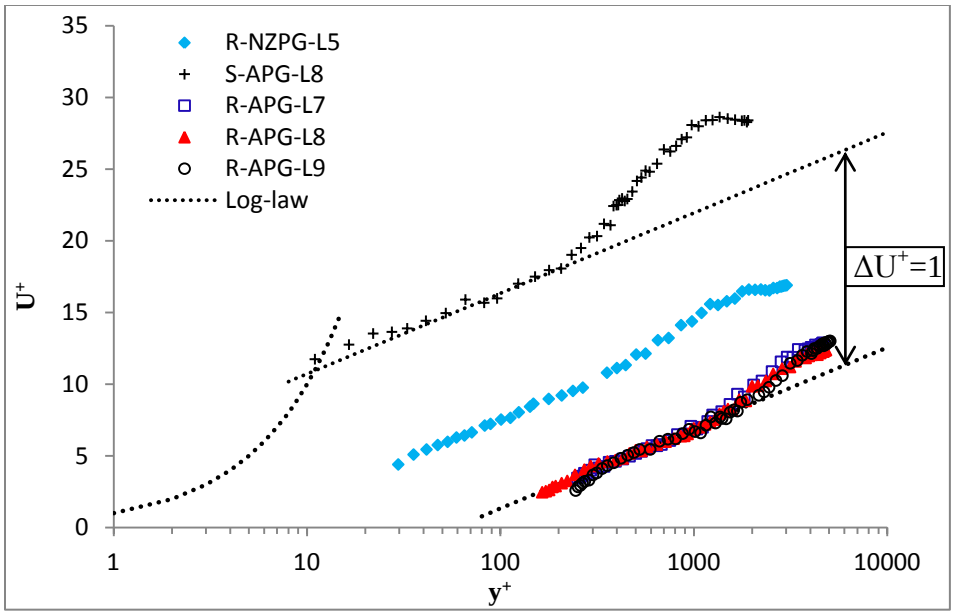

Figure 4.28 APG velocity profiles over smooth and rough bed.

4.4.2.2 Turbulence Intensity

4.4.2.2.1 Streamwise Turbulence Intensity

The effects of roughness and APG on the streamwise turbulence intensities are shown in Figure 4.29(a) and (b). Figure 4.29(a) shows the combined effects of the roughness and APG cause the streamwise turbulent intensity to deviate from the smooth APG data. In the near bed region($y/\delta < 0.1$), the streamwise turbulent intensity profiles increases and reach a maximum values at $y/\delta \approx 0.3$. In the outer region ($y/\delta > 0.3$) a decrease of the streamwise turbulent intensity towards the free surface is noted. Streamwise turbulent intensity profiles in the outer scaling are shown in Figure 4.29(b). Figure 4.29(b) illustrates that in the rough APG flow, streamwise turbulent intensity increases in the range of $0.05 < y/h < 0.3$. However, in the smooth APG flow streamwise turbulent intensity increases in a smaller range of $0.05 < y/h < 0.2$. The test station L9, which is located at 5.6d from the decelerating bed slope ($Re_\theta = 9461$), seems to be more turbulent in the region $0.4 > y/h > 1.0$. This is due to the higher depth of the flow in this

station in comparison with other stations and also the highest value of k_s^+ (~ 100) which obtained for this station. It can be conclude from Figure 4.29(a and b) that streamwise turbulence intensity is higher thought the flow for rough APG case in comparison with the smooth APG and rough NZPG, and the maximum deviation takes place in the outer region where the peak values of turbulence intensities occur. The results obtained for the pressure gradient parameter (β) in the case of rough APG show that the flow conditions is non-equilibrium as β varies from 0.94 to 0.77 along the decelerating ramp. This condition may results a non-linear distribution of turbulence intensity for rough APG flow as it can be seen in Figures 4.29(a) and (b).

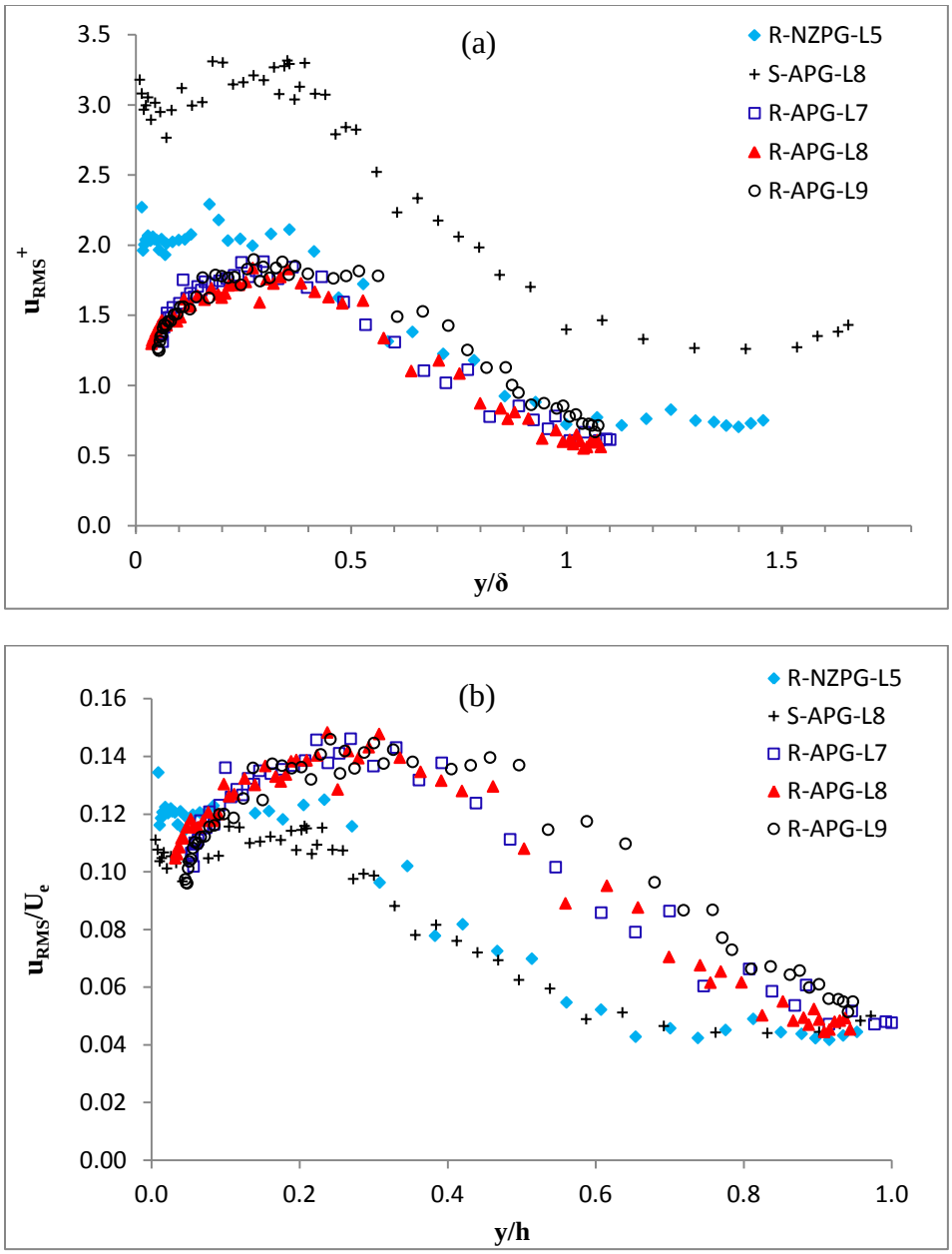

Figure 4.29 Streamwise turbulence intensity profiles in (a) inner and (b) outer scaling, over smooth APG flow.

4.4.2.2.2 Vertical Turbulence Intensity

Figure 4.30 shows the distribution of the vertical turbulence intensity in outer scaling for the rough APG open channel flow compared with that for smooth APG and rough NZPG flows. Except in a very small region close to the bed (y/h ~ 0.2), all test

station profiles of Figure 4.30 show that, the vertical turbulence intensity decreases almost linearly trough the depth towards free surface. The near bed region is very important zone of open channel boundary layer flow in terms of turbulence production. In Figure 4.30 the vertical turbulence intensity is higher throughout the flow for all rough APG cases. The test cases L7 (at 3.2h) and L8 (at 4.2h), have almost the same values of k_s^+; 89.8 and 89.5 respectively, thus their profiles overlap each other. However, the test case L9 (at 5.6h), which has the largest value of k_s^+ (= 100), deviates further from the smooth APG profile, and seems to be more turbulent. This value of k_s^+ accompanying with the APG generate more turbulence in station L9. Moreover, Figure 4.30 shows that the maximum deviation of vertical turbulent intensity of the rough APG flow from the smooth ones is in the region ($y/h < 0.5$). However, close to the free surface, the vertical turbulence intensities for all APG flow cases tend to attain similar constant value. Overall, Figure 4.30 reveals that for open channel flow, although values of vertical turbulence intensity for rough NZPG and smooth APG flows are approximately similar, but the combine effects of the roughness and APG significantly increase the turbulence level in the entire depth.

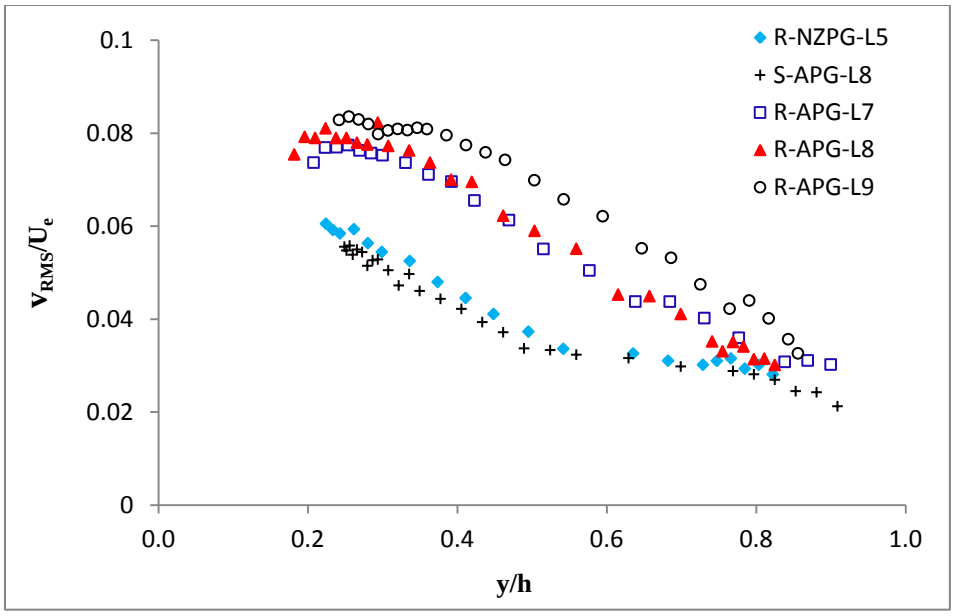

Figure 4.30 Vertical turbulence intensity in outer scaling, for APG over a rough surface.

4.4.2.3 Reynolds Shear Stress

The Reynolds shear stress profiles are examined to study the behavior of the turbulence in the presence of roughness and APG. The distribution of $-\overline{u'v'}$ normalized using U_e^2 and the vertical axis scaled with total depth (h) are shown in Figure 4.31. Recently, Tsikata and Tachie (2013) reported that the Reynolds shear stresses are substantially larger over rough walls compared to these on the smooth walls in turbulent boundary layer. For decelerating flows over rough surfaces, the Reynolds shear stress profiles have a convex shape in the region 0.2 > y/h > 0.4 as shown in Figure 4.31. The maximum value of the Reynolds shear stress is observed at y/h ~ 0.3. A gradual decrease of the Reynolds shear stress is observed close to the free surface. It can be noted from Figure 4.31 and Table 3.2 that, as Re_θ increases from 7935 for station L7 to 9461 for the station L9, respectively. The Reynolds shear stress profiles of the smooth APG and rough

NZPG shows similar distribution through the depth, however, the combination of the roughness effect and APG effect, generated higher values of the Reynolds shear stress.

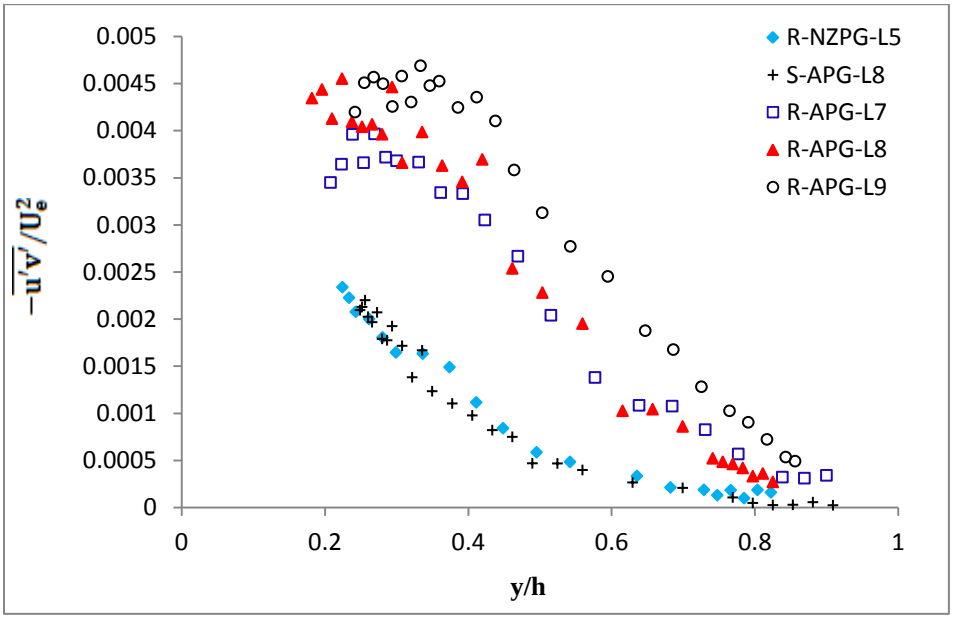

Figure 4.31 Reynolds shear stresses subject to FPG for smooth surface.

4.5 Power-law Analysis

As stated in Chapter II, the log-law is applicable for the overlap region, while the power-law could be fitted to the velocity measurements for the overlap region and entire outer flow. The application of power-laws to smooth and rough wall results and various approaches that have recently used by researchers are presented in section 2.4. In this section, the application of the power-law to the results of the current study will be discussed.

4.5.1 Power-law Analysis for Open Channel Flow Over Smooth Bed

The flow conditions for the case of smooth surface include friction velocity and power-law constants are given in Table 4.3 for the NZPG, FPG and APG open channel flows. In order to determine of the friction velocity the power-law method proposed by

Buschmann and Meinert (1999) is used. The reason for choosing this approach is that this method is independent of Reynolds number and would be appropriate for use in determining the friction velocity in smooth open channel flows, especially when there is no data obtained in the viscous sub layer (Balachandar *et al.* 2002). In this method, a plot of Ln(u) versus Ln(y) was provided and the best fit line was found.

$$\ln U = \alpha_L \ln y + \beta \tag{4.2}$$

The constants α_L and β can be found from the selected fit line. Then below equations were used to find the friction velocity and power-law constants.

$$C_L = \frac{\sqrt{3}+5\alpha_L}{2\alpha_L} \tag{4.3}$$

$$u^* = exp\left(\frac{\beta+\alpha_L \ln \nu - \ln C_L}{\alpha_L+1}\right) \tag{4.4}$$

Using the determined friction velocity, U^+ versus y^+ was plotted and then the best power trend was found for the plot. The computed constants C and α for the power-law Eq. (2.25) for all smooth test cases are listed in Table 4.3. The data of this Table for the case of NZPG can be compared with the results of Tachie (2001) which determined for two cases of smooth flat plate experiments. In the case of the formulation proposed by George and Castillo (1997) which he applied, the constants C and α found to be 8.8 and 0.133 respectively. These values are very close to the average values of C and α which have been found for the data of this study. With the formulation proposed by Buschmann and Meinert (1999) which is used in this study, the average values of C and α (for three test stations L4, L5 and L6) found to be 9.17 and 0.129 correspondingly.

Figures 4.32(a, b and c) show the velocity distributions in terms of inner coordinates for three NZPG experiments over a smooth surface OCF. The corresponding fits to the power-law and logarithmic law (κ = 0.41 and B = 5.1) are also shown in these

figures for comparison. For all three test stations considered on the smooth surface (L4, L5, and L6), the power-law formulation shows wider range of velocity profile in the overlap region ($50 < y^+ < 300$) than log-law. With the coefficients obtained for the NZPG flow over the smooth surface (see Table 4.3), equation (2.25) for the test stations L4, L5, and L6 found to be $U^+=7.97y^{+0.1514}$, $U^+=8.83y^{+0.1338}$, and $U^+=10.32y^{+0.1042}$, respectively. As it can be seen from the Table 4.2, as Re_θ decreases, the values of the constant C increases, however the constant α decreases. By the averaging of the constant values (C and α) it can be found a general power-law velocity profile for all three NZPG test stations as:

$$U^+ = 9.17y^{+0.129} \tag{4.5}$$

Figures 4.33(a, b, and c) present the mean velocity profiles for three test stations (L1, L2, and L3) over a smooth FPG using inner coordinates, as well as the matching power-law fit and the classical log-law. It should be noted that for all three Figures 4.33(a, b, and c) due to the existence of the small wake region, both power-law and log-law show an extended overlap region. In addition for the test station L3, it is difficult to distinguish power-law from the log-law in the overlap the most part of the outer region. With the coefficients obtained for the FPG flow over the smooth surface (see Table 4.3), equation (2.27) for the test stations L1, L2, and L3 found to be $U^+=8.82y^{+0.1357}$, $U^+=9.15y^{+0.1291}$, and $U^+=9.55y^{+0.1222}$, respectively. The general power-law velocity profile for all three stations with the average values of C and α for the FPG data of this study found to be:

$$U^+ = 9.04y^{+0.1298} \tag{4.6}$$

The region of the velocity profile fitted by the log-law is compared to that of the power-law in the inner coordinates for the APG open channel flow, is demonstrated in

Figure 4.34(a, b, and c). Both power-law and log-law represent a smaller wake region for APG flow in comparison with the FPG and the NZPG flows. In the region $30 < y^+ < 150$ the power-law and the log-law are closely matched. The maximum deviation of friction velocity obtained by power-law from that for log-law for the test stations L7, L8, and L9 is 1.9%, 0.5%, and 1.2% respectively. This observation supports the conclusion reported by Buschmann and Gad-el-Hak (2003) and Akinlade and Bergstrom (2007). With the coefficients obtained for the APG flow over the smooth surface (see Table 4.3), equation (2.27) for the test stations L7, L8, and L9 found to be $U^+=6.75y^{+0.2042}$, $U^+=7.07y^{+0.1908}$, and $U^+=6.63y^{+0.2006}$, respectively. A slight Reynolds number dependency is observed from the obtained constants. The general power-law velocity profile for all three APG flow cases of this study with the average values of C and α is:

$$U^+ = 6.81y^{+0.1985} \tag{4.7}$$

4.5.2 Power-law Analysis for Open Channel Flow Over Rough Bed

The flow conditions for all of the rough surface test cases include friction velocity and power-law constants are given in Table 4.4 for the NZPG, FPG and APG open channel flows. Balachandar *et al.* (2002) reported that the method proposed by Buschmann and Meinert (1999) cannot predict the friction velocity with an acceptable accuracy, therefore another approach will be used for rough surface flow experiments. Kotey *et al.* (2003) reported that the power-law formulation proposed by George and Castillo (1997) is appropriate to apply on the rough surface experiments and can predict a good estimate of the friction velocity. In the current study, the power-law formulation proposed by George and Castillo (1997) will be used to determine the friction velocity over rough surface OCF experiments (NZPG, FPG, and APG). The determination of the skin friction coefficient using the power-law profiles proposed by George and Castillo

(1997) required the determination of four coefficients C_i, E, γ and ξ, as given in the equation (2.36). The comparison of the log-law and power-law for NZPG, FPG, and APG flows over rough surface open channel flow will be presented in this section. Table 4.4 presents the required values as well as the obtained friction velocities using by George and Castillo power-law approach. In comparison with the data of Table 4.3, the power-law constants listed in Table 4.4 reveals that the power-law constants are dependent of pressure gradient and roughness. The FPG flows contain the maximum values of the constant C_R and the minimum values of the constant γ_R. Whereas the APG flows have the minimum values of C_R and the maximum values γ_R. The optimized power-law fits in the inner coordinate will be discussed in this section.

Figure 4.35 shows the experimental data in terms of inner coordinates for NZPG open channel flow experiments over a rough surface. The power-law determined from Eq. (2.38) and logarithmic law (κ = 0.41 and B = 5.1) are included in Figures 4.35(a, b, and c) for comparison. As it can be seen from Figure 4.35(a, b, and c) the power-law formulation shows the velocity profile in the overlap region over wider range than log-law. In the test station L4, the power-law and the log-law deviate from the experimental data in a wide region. In addition, the maximum error in determining the friction velocity occurs for this test station with $\Delta u^* = 3.7$. This station has highest value of k_s^+ (~ 80) among all of the NZPG test cases. However, the data of the test station L5 and L6 given in Figure 4.35 (b and c), which have the same values of k_s^+ (= 75), show a well matched power-law velocity profile with that for log-law in a wider overlap region ($50 < y^+ < 400$). With the coefficients obtained for the NZPG flow over the rough surface given in Table (4.3), equation (2.38) for the test stations L4, L5, and L6 found to be

$U^+=2.054y^{+0.2878}$, $U^+=1.896y^{+0.2985}$, and $U^+=1.99y^{+0.2853}$, respectively. By the averaging of the constant values it can be found a general power-law velocity profile for all three NZPG test stations as:

$$U^+ = 1.978y^{+0.2905} \tag{4.8}$$

Figure 4.36 presents the mean velocity profiles on a rough surface FPG for three test stations (L1, L2, and L3) using inner coordinates. Both power-law and classical log-law are included in Figures 4.36 (a), (b), and (c) for comparison. It can be seen from the Figure 4.36(a) that power-law and log-law are well matched in the range of $y^+ < 200$, and they show a very small overlap region in this station. This region for the experimental data of Figure 4.36 (b) is $50 < y^+ < 400$, and for the data of Figure 4.36(c) is $70 < y^+ < 1000$. Therefore, it can be conclude that as k_s^+ and wake parameter changes, the deviation of the power-law from the log-law can be different. This represents that a common region which described by both the log-law and power-law relations is various for different flow conditions. It should be noted here that the good agreement between measurements and fitted profile is remarkable in Figure 4.36(c). With the coefficients obtained for the FPG flow over the rough surface given in Table 4.4, Eq. (2.25) for the test stations L1, L2, and L3 found to be $U^+=5.37y^{+0.1435}$, $U^+=4.07y^{+0.1627}$, and $U^+=5.61y^{+0.137}$, respectively. The general power-law velocity profile for all three stations with the average constant values for the rough surface FPG open channel flow (data of this study) found to be:

$$U^+ = 5.01y^{+0.1477} \tag{4.9}$$

The region of the velocity profile fitted by the log-law is compared to that of the power-law in the inner coordinates for the rough surface APG open channel flow, is demonstrated in Figure 4.37. It should be noted here that data points in the range of $y^+ < 200$ were not considered due to the difficulties in finding the virtual origin. Therefore, it

was difficult to fit power-law on rough wall data in that range. It is observed that C_R diminishes with the combined effects of the APG and surface roughness, whereas γ_R increases with APG and roughness. This is agree well with the results reported by Tsikata and Tachie (2013). They concluded that the lower C_R is related to the reduction in the mean velocity produced by roughness, and higher γ_R is due to the larger wake component subjected to the APG. For the whole velocity profile from the inner layer to the outer region include wake zone, the log-law and the power-law are well matched in all of the test stations. From Figures 4.37(a), (b), and (c) and also Table 4.4, it can be seen that the friction velocity obtained from the log-law and the power-law for the APG open channel flow over a rough surface have very small deviation in comparison with most of the experimental data of this study ($\Delta u^* \leq 1.7$). With the coefficients obtained for the APG flow over the rough surface open channel flow given in Table 4.3, equation (2.38) for the test stations L7, L8, and L9 found to be $U^+=0.2771y^{+0.4614}$, $U^+=0.4421y^{+0.3941}$, and $U^+=0.4772y^{+0.3873}$, respectively. It can be noted that the experimental data of rough surface APG open channel flow of this study have the smallest values of (C_i/E) and the largest values of ($\gamma+\xi$). The general power-law velocity profile for all three APG flow cases of this study with the average constant values is:

$$U^+ = 0.3988y^{+0.4142} \tag{4.10}$$

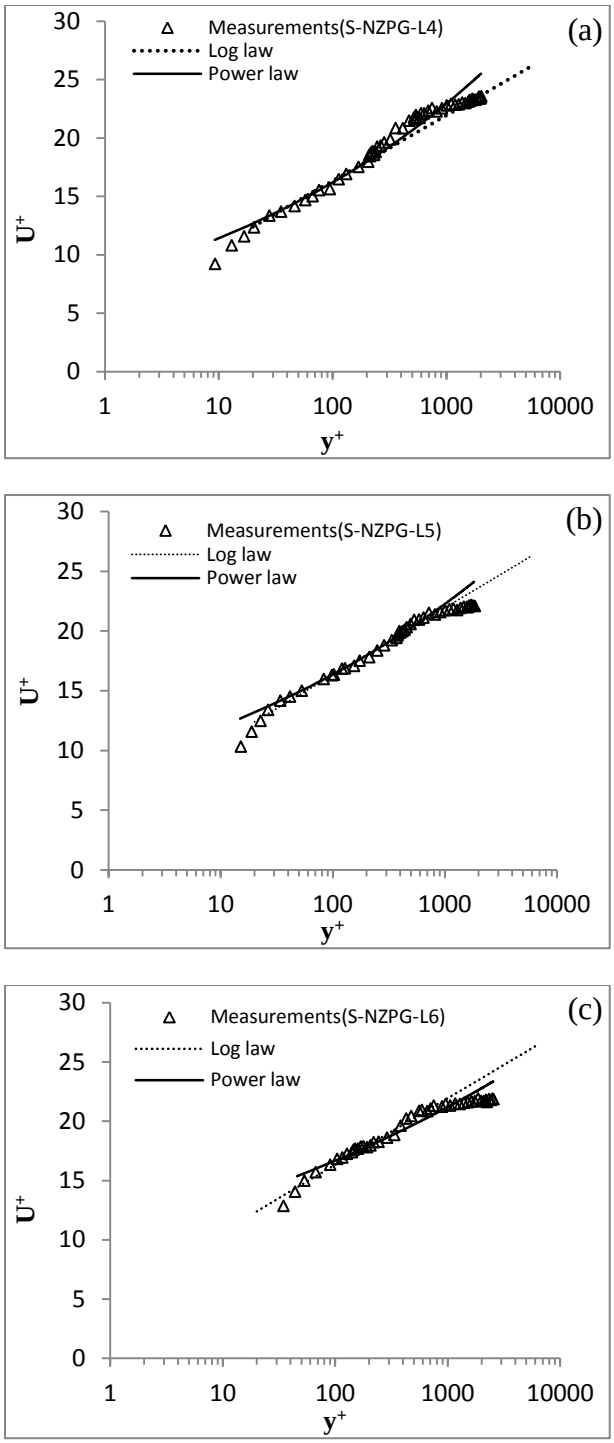

Figure 4.32 Mean velocity profile in inner variables and their corresponding fits using log-law and power-law for smooth NZPG open channel flow.

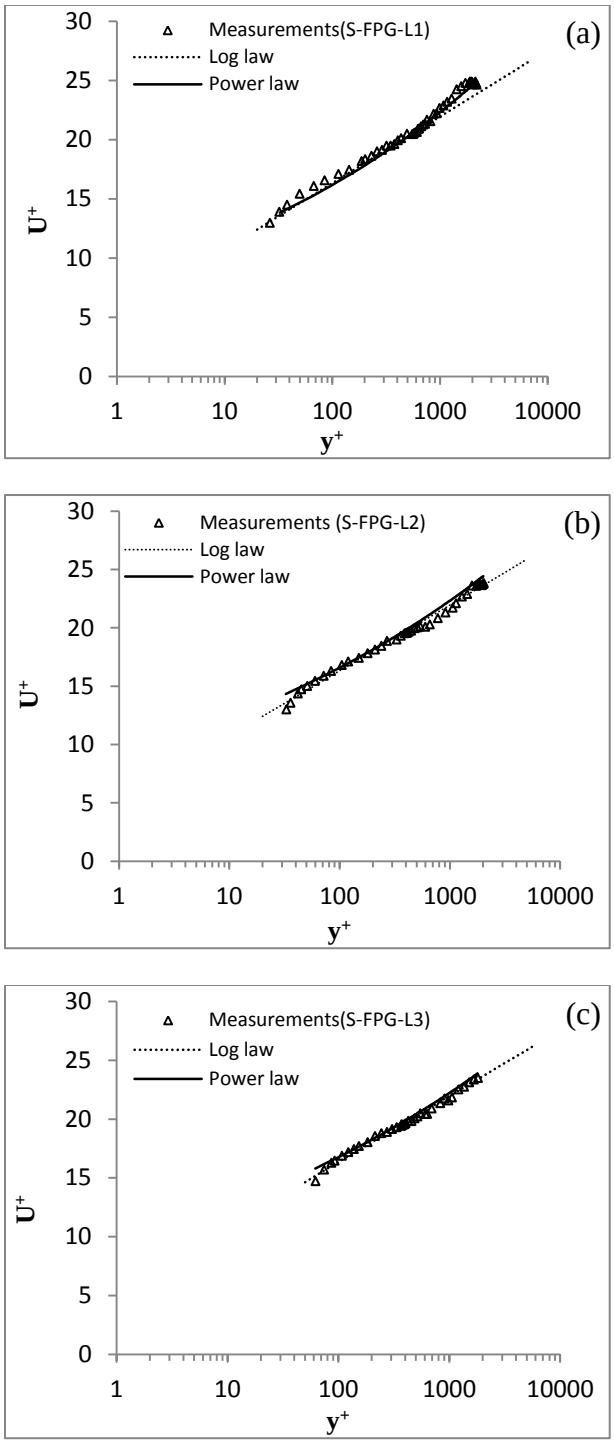

Figure4.33 Mean velocity profile in inner variables and their corresponding fits using log-law and power-law for smooth FPG open channel flow.

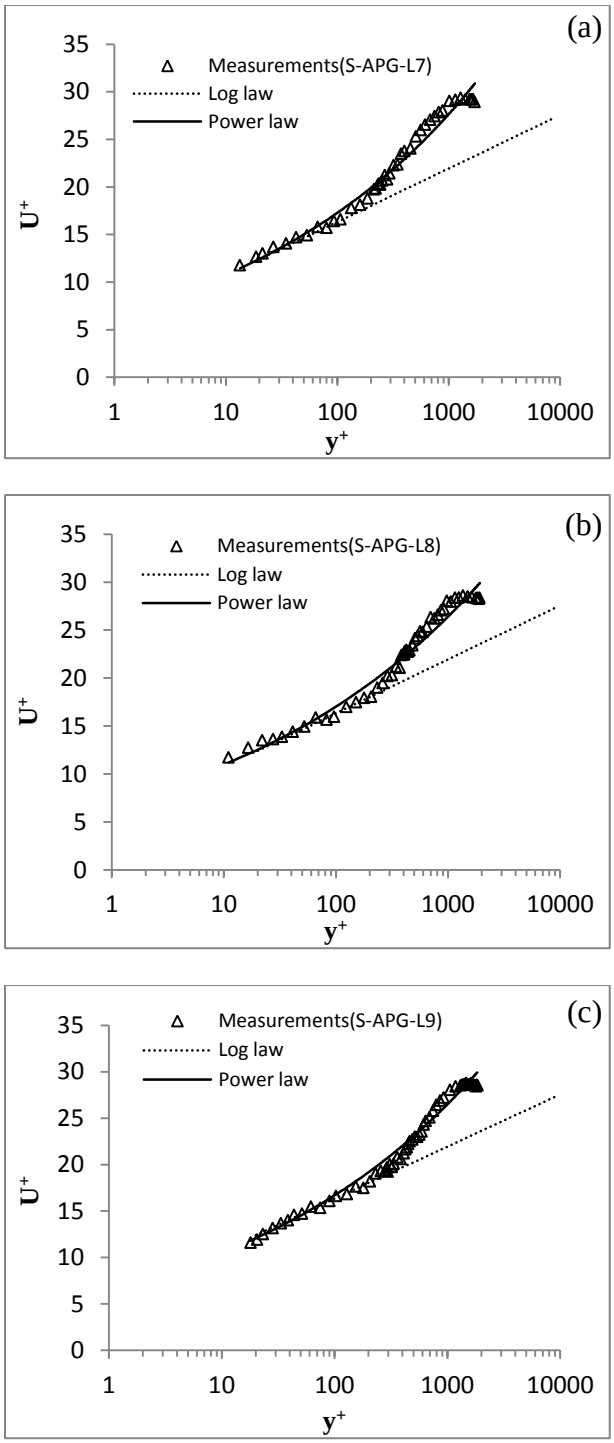

Figure 4.34 Mean velocity profile in inner variables and their corresponding fits using log-law and power-law for smooth APG open channel flow.

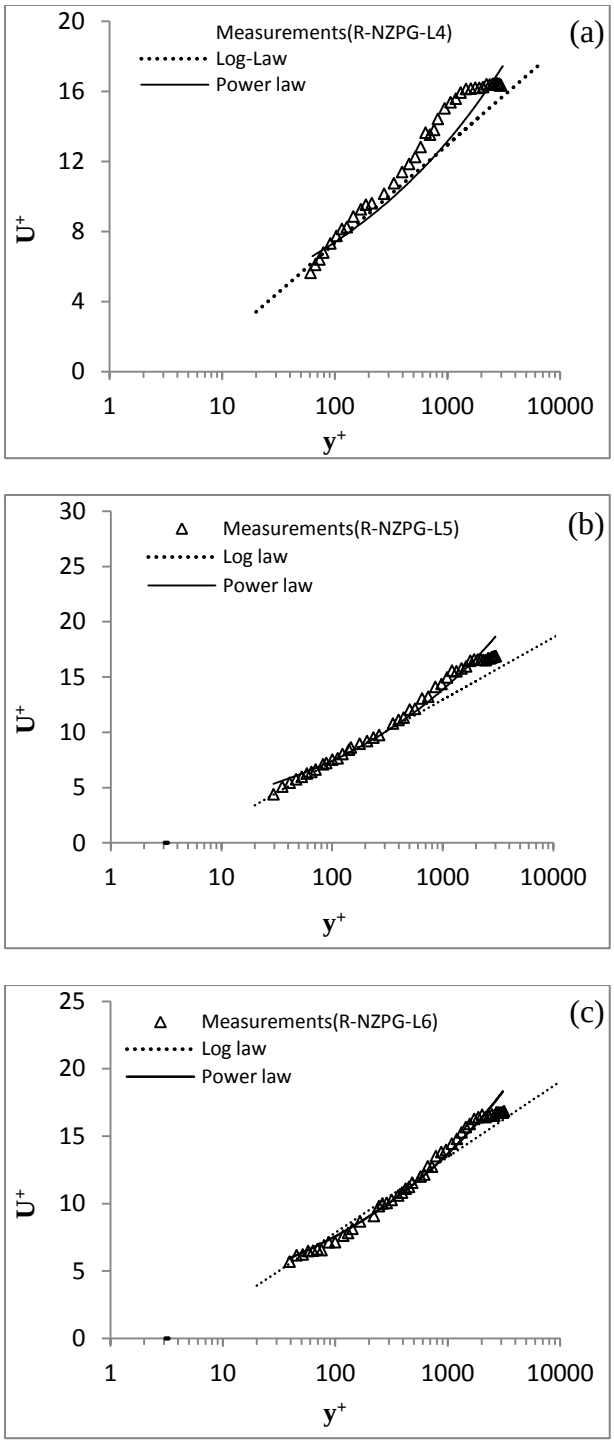

Figure 4.35 Mean velocity profile in inner variables and their corresponding fits using log-law and power-law for rough NZPG open channel flow.

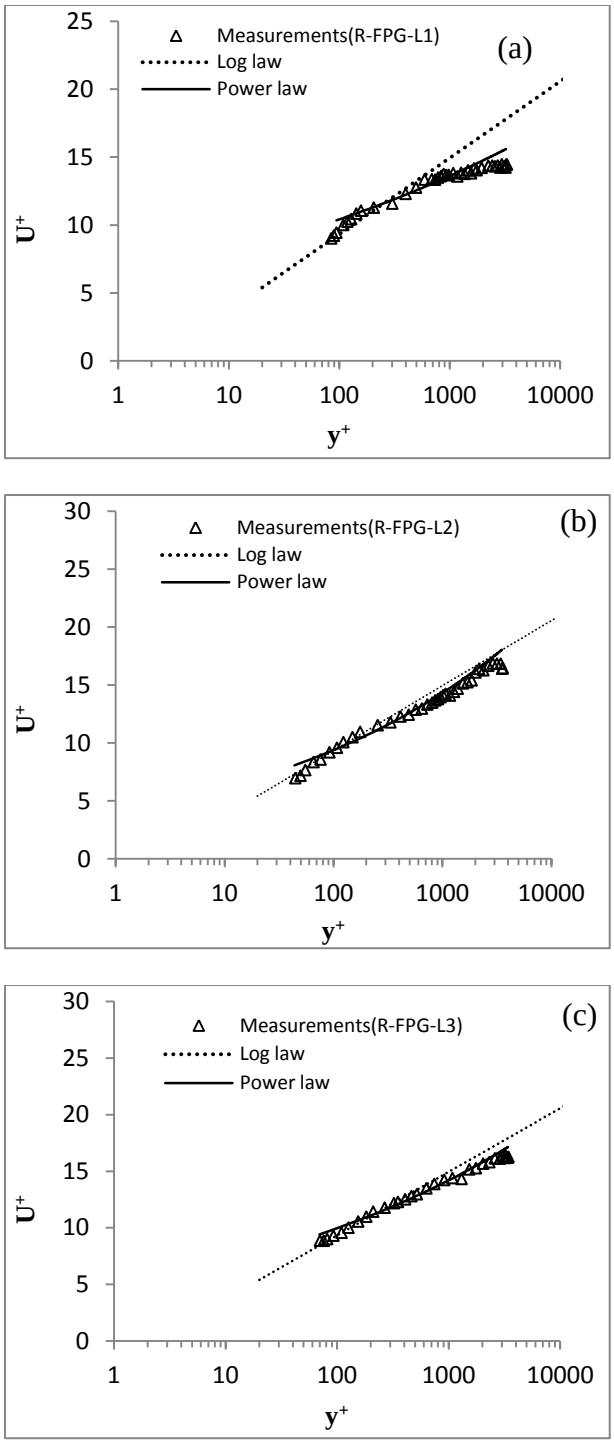

Figure 4.36 Mean velocity profile in inner variables and their corresponding fits using log-law and power-law for rough FPG open channel flow.

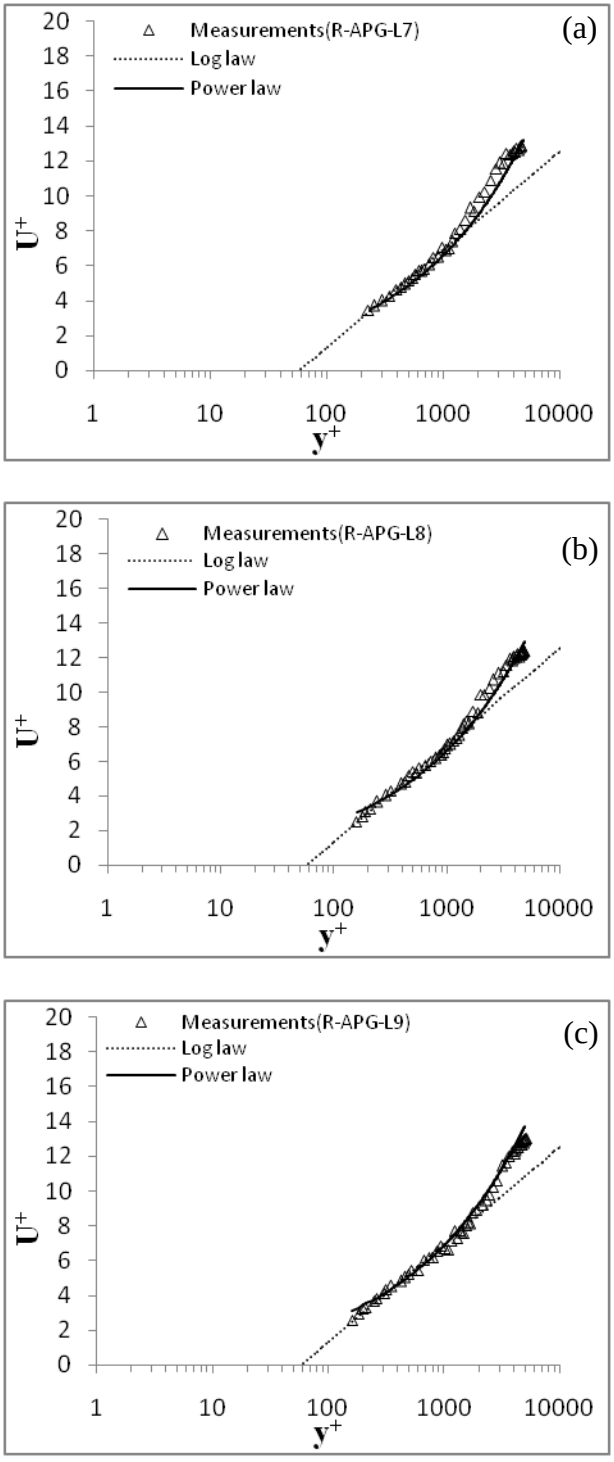

Figure 4.37 Mean velocity profile in inner variables and their corresponding fits using log-law and power-law for rough APG open channel flow

Table 4.1 Summary of Flow Parameters

Test condition	Test station	u^* (m/s)	Π	ε (mm)	k_s^+	ΔU^+
SMOOTH	L1	0.013	0.475	-	-	-
	L2	0.014	0.302	-	-	-
	L3	0.014	0.199	-	-	-
	L4	0.018	-0.268	-	-	-
	L5	0.018	-0.366	-	-	-
	L6	0.019	-0.391	-	-	-
	L7	0.019	1.251	-	-	-
	L8	0.020	1.192	-	-	-
	L9	0.021	1.476	-	-	-
ROUGH	L1	0.023	-0.502	0.55	70.5	7.0
	L2	0.021	0.203	0.43	65.8	7.0
	L3	0.021	-0.165	0.45	64.4	7.0
	L4	0.027	0.115	0.8	79.2	9.0
	L5	0.025	0.386	0.9	75	9.0
	L6	0.025	0.439	0.8	75	9.0
	L7	0.031	0.604	0.12	89.8	15.0
	L8	0.031	0.464	0.13	89.5	15.0
	L9	0.032	0.643	0.14	100	150

Table 4.2 Summary of the FPG and APG Flow Experiments

Test condition	Test Station	u^* (m/s)	Π	ε (mm)	k_s^+	ΔU^+	$K \times 10^{-6}$	β
SMOOTH	L1	0.013	0.475	-	-	-		-
	L2	0.014	0.302	-	-	-	5.25	-
	L3	0.014	0.199	-	-	-	4.55	-
	L7	0.019	1.251	-	-	-	-	
	L8	0.020	1.192	-	-	-	-	1.93
	L9	0.021	1.476	-	-	-	-	1.73
ROUGH	L1	0.023	-0.502	0.55	70.5	7.0		-
	L2	0.021	0.203	0.43	65.8	7.0	7.79	-
	L3	0.021	-0.165	0.45	64.4	7.0	6.08	-
	L7	0.031	0.604	0.12	89.8	15.0	-	
	L8	0.031	0.464	0.13	89.5	15.0	-	0.94
	L9	0.032	0.643	0.14	100	150	-	0.77

Table 4.3 Summary of .Friction Velocity and Power-law Constants for Smooth Surface Data

Test Condition	Test station	Re_θ	u^* (m/s)		Δu^* (%)	C	α
			Log-law	Power-law			
FPG	L1	3221	0.013	0.0128	1.5	8.824	0.1357
	L2	2240	0.014	0.0135	3.5	9.15	0.1291
	L3	2106	0.014	0.0142	1.4	9.55	0.1222
NZPG	L4	4769	0.0175	0.017	3.4	7.973	0.1514
	L5	4257	0.018	0.0182	1.6	8.8364	0.1338
	L6	3422	0.019	0.0192	1.4	10.324	0.1042
APG	L7	4060	0.019	0.0186	1.9	6.7465	0.2042
	L8	4267	0.02	0.019	0.5	7.0702	0.1908
	L9	4320	0.021	0.0207	1.2	6.6258	0.2006

Table 4.4 Summary of Friction Velocity and Power-law Constants for Rough Surface Bata

Test Condition	Test station	Re_θ	u^* (m/s)		Δu^* (%)	C_R	γ_R	E	ζ
			Log-law	Power-law					
FPG	L1	2206	0.0198	0.0192	3.0	5.371	0.1435	1.64	0.0078
	L2	4461	0.021	0.205	2.3	4.701	0.1627	1.95	0.0336
	L3	4262	0.023	0.0225	2.1	5.607	0.137	1.70	0.0148
NZPG	L4	3088	0.027	0.026	3.7	2.054	0.2878	3.88	0.1364
	L5	4601	0.025	0.0245	2.0	1.896	0.2985	4.66	0.1647
	L6	4637	0.025	0.0246	1.6	1.998	0.2853	5.17	0.1811
APG	L7	7935	0.031	0.0315	1.6	0.277	0.4614	24.35	0.2572
	L8	7826	0.0305	0.031	1.6	0.442	0.3941	15.99	0.2033
	L9	9461	0.028	0.0275	1.7	0.477	0.3873	13.88	0.1867

CHAPTER V

CONCLUSIONS AND RECOMMENDATIONS

5.1 Conclusion

This study was undertaken to provide better understanding for the turbulence structure of the non-uniform open channel flow. Particularly, the combined effects of the non-uniformity due to pressure gradient as well as surface roughness in open channel flow are investigated. The experiments were carried out in an laboratory flume and two component laser Doppler velocimetry technique is used to measure the velocity and turbulence parameters at various locations. Three types of the flow were used to maintain non-uniform flow conditions accelerating, decelerating, and near zero pressure gradient (flat plate). The flow in the present study is affected by the upstream conditions and can be described as a connected flow system. Conclusions related to the non-uniformity effects on the smooth and rough bed are presented in this chapter.

5.1.1 Effect of Non-uniformity on Smooth Bed Open Channel Flow

Inspection of the velocity profile shows slight increase in the streamwise mean velocity from FPG flow to NZPG flow. On the APG ramp the flow decelerate and the velocity are reduced. The velocity distributions in all measurement locations obey to the classical logarithmic law of the wall. The overlap region exist $50 < y^+ < 300$ for FPG and NZPG cases. On the decelerating ramp, under the APG flow, the velocity distributions are found to have a larger wake and to deviate from the log law at $y^+ > 300$. A reduction of the streamwise turbulent intensity distributions were found for FPG flow case at $y/d < 0.3$ in comparison with the uniform OCF (Roussinova *et al*., 2008). However, the opposite trend was found for the APG case where an increase in the turbulence intensity

is observed. Different values of the pressure gradient parameters (β) for both favourable and adverse pressure gradient flow cases confirms that the flow is in non-equilibrium condition. This suggest that the length of the accelerating ramp was short to establish gradually accelerating flow. In this case the velocity profiles do not conform to the standard boundary layer trends. The upstream effect was significant for the flow over flat plate which was mildly accelerated. The effect of the non-uniformity on turbulence intensities and Reynolds shear stresses was further investigated. Both turbulence intensity and Reynolds shear stress are found to have higher values in comparison with NZPG and FPG.

5.1.2 Effects of the Non-uniformity on Rough Bed Open Channel Flow

Significant changes in mean velocity profiles and turbulence intensities were observed for the combined effects of the surface roughness and pressure gradient. The effect of roughness on the turbulence structures is found to be predominant through most of the flow depth. A difference in the values of the roughness equivalent height (k_s^+) are found for all test cases due to the various flow conditions such as bed slope and friction velocity (all the cases are in the fully rough region). In addition, for all FPG, NZPG, and APG flows the boundary layer parameters such as δ, δ^*, and θ were increased in Rough bed experiments. The rough FPG results show the complete loss of the wake region in comparison with the smooth ones. The pressure gradient decreases the turbulence in mid-depth. However, in the inner layer, roughness enhances the turbulence level and improve the flow development. Therefore, to attain equilibrium condition, rough surface beds need shorter length of the ramp in comparison with the smooth beds. Moreover, for all test cases the combined effects of the surface roughness and non-uniformity causes an

increasing in both streamwise and wall normal turbulence intensities and as well as increasing in the Reynolds shear stress for all test cases.

5.1.3 Power-law Analysis

The results of the power-law analysis show that the power-law is applicable for the velocity profile obtained in both smooth and rough bed non-uniform open channel flow . Both approaches which used in the current study could predict the friction velocity with an acceptable accuracy ($\Delta u^* < 3.0$). The power-law constants are found to be dependent of both pressure gradient and surface roughness. For the smooth results, the power-law constants are also found to be similar for NZPG and FPG ($\Delta C = 1.4\%$ and $\Delta\gamma = 0.6\%$), but the roughness effect make larger differences for those constants ($\Delta C = 60\%$ and $\Delta\gamma = 49\%$). However, for the APG power-law constants are significantly different than other test cases.

5.2 Recommendations for Future Works

On the basis of above conclusions and understanding of the non-uniform open channel flow, the following recommendations are relevant to future work:

1. Investigate a numerical analysis with the same flow fields to enable comparison with the results of this study.
2. Study of the effect of non-uniformity on the longer accelerating and decelerating ramps to achieve equilibrium flow conditions.
3. Examine the other types of the surface roughness on the inclined and declined bed.
4. Perform a similar experimental study with higher bed slopes.

5. Perform PIV measurements on the discontinuity areas where two succession beds are connected.
6. Further study of the effect of the various Reynolds number on the non-uniform open channel flow.

APPENDIX A

UNCERTAINTY ESTIMATES

The uncertainty estimates in the LDV measurements is presented in this section. The uncertainty in the determination of the frequency of each burst signal is one of the main sources of error in the LDV measurements. In addition, the uncertainty in the beam spacing calculation can be another important source of error in the LDV measurements. The uncertainty in statistical quantities will also depend on the sample size (N). In this experimental study, at each measurement station, 10000 validated samples were acquired.

A methodology for estimating uncertainty in LDV measurements was developed by Yanta and Smith (1973) and Schwarz *et al.* (1999). Tachie (2001) and Faruque (2009) outlined this methodology. In order to estimate the uncertainty of the various parameters, following relationships were used:

The uncertainty in the streamwise component of the mean velocity:

$$\frac{\sigma_U}{U} = \left[(\sigma_0)^2 + \frac{1}{N}\left(\frac{u}{U}\right)^2\right]^{1/2} \tag{A.1}$$

The uncertainty in the vertical component of the mean velocity:

$$\frac{\sigma_V}{U} = \left[(\sigma_0)^2 + \frac{1}{N}\left(\frac{v}{U}\right)^2\right]^{1/2} \tag{A.2}$$

The corresponding expression for the streamwise and vertical components of turbulence fluctuation and the Reynolds shear stress are, respectively:

$$\frac{\sigma_u}{u} = \left[(\sigma_0)^2 \left(\frac{\langle uv\rangle}{u^2}\right)^2 + \frac{1}{2N}\right]^{1/2} \tag{A.3}$$

$$\frac{\sigma_v}{v} = \left[(\sigma_0)^2 \left(\frac{\langle uv\rangle}{v^2}\right)^2 + \frac{1}{2N}\right]^{1/2} \tag{A.4}$$

$$\frac{\sigma_{\langle uv\rangle}}{\langle uv\rangle} = \left[(\sigma_0)^2\left(1+\frac{u^2}{\langle uv\rangle}\right)^2 + \frac{1}{2N}\left(\frac{2}{R}\right)^2\right]^{1/2} \quad \text{(A.5)}$$

Here, σ_o is the error due to uncertainty in the determination of the beam-crossing angle, N is the number of samples and R is the shear stress correlation coefficient. Following Tachie (2001) a value of σ_o = 0.4 is adopted in the current study. Results of the determination of uncertainty estimates for different flow conditions are given in Tables A.1 and A.2.

Typical estimates for uncertainties for the turbulence intensities like mean velocity and its fluctuations are shown in Tables A.1 and A.2. As it can be seen from these tables, the values are very similar to those obtained by Tachie (2000) and Faruque (2009), in their open channel flow LDV measurements.

Table A.1 Typical uncertainty estimates for smooth bed experiments

Test Condition	Test station	U (%)	V (%)	u_{RMS} (%)	v_{RMS} (%)	$-\overline{u'v'}$ (%)
FPG	L1	0.40	0.40	0.093	0.19	2.02
	L2	0.40	0.40	0.093	0.18	2.23
	L3	0.40	0.40	0.102	0.19	2.73
NZPG	L4	0.40	0.40	0.056	0.153	3.37
	L5	0.40	0.40	0.058	0.16	3.23
	L6	0.40	0.47	0.053	0.14	4.38
APG	L7	0.40	0.43	0.053	0.19	5.81
	L8	0.40	0.40	0.055	0.18	7.22
	L9	0.40	0.40	0.058	0.18	5.55

Table A.2 Typical uncertainty estimates for rough bed experiments

Test Condition	Test station	U (%)	V (%)	u_{RMS} (%)	v_{RMS} (%)	$-\overline{u'v'}$ (%)
FPG	L1	0.40	0.40	0.036	0.07	2.58
	L2	0.40	0.40	0.092	0.21	2.23
	L3	0.40	0.40	0.084	0.17	4.76
NZPG	L4	0.40	0.40	0.065	0.18	3.00
	L5	0.40	0.40	0.053	0.16	3.74
	L6	0.40	0.40	0.057	0.18	3.51
APG	L7	0.40	0.40	0.068	0.23	2.86
	L8	0.40	0.40	0.066	0.22	3.00
	L9	0.40	0.40	0.078	0.25	2.52

REFERENCES

[1] Afzal, B., Faruque, M.A.A., Balachandar, R., 2009, "Effect of Reynolds number, near-wall perturbation and turbulence on smooth open channel flows". *J. of Hydr. Res.*, 47(1), pp. 66-81

[2] Afzal, N., 2001, ''Power law and log law velocity profiles in fully developed turbulent boundary layer flow: Equivalent relations at large Reynolds numbers''. *Acta Mech.*, 151, pp.195

[3] Afzalimehr, H., Anctil, F., 1999, "Velocity distribution and shear velocity behavior of decelerating flows over a gravel bed". *Canadian J. of Civil Eng.*, 26, pp. 468–475

[4] Afzalimehr, H., Anctil, F., 2000, "Accelerating shear velocity in gravel-bed channels",. *Hydrol. Sci J.*, 45, pp. 113-124

[5] Afzalimehr, H., Dey, S., Rasoulianfar, P., 2007, "Influence of decelerating flow on incipient motion of a gravel-bed stream". Sadhana *Proc Indian Acad Sci*; 32(5), pp. 545–559

[6] Afzalimehr, H., Rennie C.D., 2009, "Determination of bed shear stress in gravel-bed rivers using boundary layer parameters". *Hydrol. Sci. J.*; 54(1), pp. 147–159

[7] Amir, M., Castro, I.P., 2011, "Turbulence in rough-wall boundary layers: universality issues". *Exp. Fluids* 51, pp. 313–326

[8] Akinlade, O.G., Bergstrom, D.J., 2007, "Effect of surface roughness on the coefficients of a power law for the mean velocity in a turbulent boundary layer". *J. of Turbulence*, 8(18), pp. 1-27

[9] Antonia, R.A., Bisset, D., Brownel, W.B., 1990 "Effect of Reynolds number on the topology of the organised motion in a turbulent boundary layer". *J. Fluid Mech.*, 213, pp. 267-286

[10] Aubertine, C.D., Eaton, J.K., 2005, "Turbulence development in a non-equilibrium turbulent boundary layer with mild adverse pressure gradient". *J. Fluid Mech*. 532, pp. 345–364

[11] Bakken, O.M., Krogstad, P.A., Ashrafian, A., Andersson, H. I., 2005, "Reynolds number effects in the outer layer of the turbulent flow in a channel with rough walls". *Phys. Fluids* 17, 065101

[12] Balachandar, R., Bhuiyan, F., 2007, "Higher-order moments of velocity fluctuations in an open channel flow with large bottom roughness". *J. of Hydr. Eng.*, 133(1), pp. 77-87

[13] Balachandar, R., Blakely, D., Tachie, M., Putz, G., 2000, "Turbulent boundary layers in open channel flows". Proceedings of the National Conference of the American Society of Mechanical Engineers, Fluids Engineering Division, Boston, Mass

[14] Balachandar, R., Hagel, K., Blakely, D., 2002, "Velocity distribution in decelerating flow over rough surfaces". *Can. J. Civil. Eng.*, 29, pp. 211-221.

[15] Balachandar, R. Patel, V.C. 2005, "Velocity measurements in a developed open channel flow in the presence of an upstream perturbation". *J. Hyd. Res.*, ASCE 43(3), pp. 258-266.

[16] Balachandar, R., Patel V.C., 2002, "Rough wall boundary layer on plates in open channels". *J. of Hydr. Eng.*, 128(10), pp. 947-951

[17] Balachandar, R., Ramachandran, S., 1999, "Turbulent boundary layers in low Reynolds number shallow open channel flows". *J. of Fluids Eng.*, 121, pp.684–689

[18] Balachandar, R., Tachie, M.F., 2001, "A study of boundary layer-wake interaction in shallow open channel flows". *Exp. Fluids* 30(5), pp. 511–525

[19] Barenblatt, I., 1993, ''Scaling laws for fully developed turbulent shear flows. Part 1. Basic hypothesis and analysis''. *J. Fluid Mech*., 248, pp. 513-520

[20] Barenblatt, I., Prostokishin V.M., 1993, ''Scaling laws for fully developed turbulent shear flows. Part 2. Processing of experimental data''. *J. Fluid Mech*., 248, pp. 521-529

[21] Barenblatt, I., Chorin, J., Prostokishin V.M., 1997, ''Scaling laws for fully developed turbulent flow in pipes: Discussing of experimental data''. *Proc. Natl. Acad. Sci. USA*, 94, 773

[22] Bigillon, F., Niňo, Y., Garcia, M.H. 2006, "Measurements of turbulence characteristics in an open-channel flow over a transitionally-rough bed using particle image velocimetry". *Exp. in Fluids,* 41(6), pp. 857-867

[23] Bourassa, C., Thomas, F.O., 2009, "An experimental investigation of a highly accelerated turbulence boundary layer". *J. Fluid Mech*., 634, pp. 359-404

[24] Blinco, P.H., partheniades, E., 1971, "Turbulence characteristics in free surface flows over smooth and rough boundaries". *J. Hydr. Res.*, IAHR 9, pp. 43– 69

[25] Buschmann M.H., Gad-el-Hak, M., 2003, "Generalized logarithmic law and its consequences". *AIAA journal*, 41, pp. 40-48

[26] Buschmann M.H., Gad-el-Hak, M., 2006, "Turbulent boundary layer: reality and myth". *On Boundary and Interior Layers, BAIL*, © University of Göttingen, Germany

[27] Buschmann M.H., Meinert, J., 199, "Power law or log law for turbulent boundary layers with low Reynolds number?". *Colloquium Fluid Dynamics*, 99, Prague

[28] Cal, R.B., Brzek, B., Johansson, T.G., Castillo, L., 2009, "The rough favourable pressure gradient boundary layer". *J. Fluid Mech.*, 641, pp. 129-155

[29] Cal, R.B., Brzek, B., Johansson, G.T., Castillo, L., 2006, "Upstream condition effects on rough favourable pressure gradient turbulent boundary layers". *Proceedings of the 44th AIAA Aerospace Sciences Meeting*, Reno, Nevada, pp. 3945–3961

[30] Cardoso, A.H., Gust, G., Graf, W.H., "Steady gradually accelerating flow in a smooth open channel". *J. Hydr. Res*. 29(4), 1991, pp. 525-543

[31] Castillo, L., George, W.K., 2001, "similarity analysis for turbulent boundary layer with pressure gradient: Outer flow". *AIAA Journal*, 39, pp. 41-47

[32] Cebeci, T., Smith, M., 1974, "Analysis of turbulent boundary layer". *J. Hydr. Eng.*, 112, pp. 335-355

[33] Clauser, F.H., 1954, "Turbulent boundary layer in adverse pressure gradient". J. *Aero. Sci*., 21, pp. 91– 108

[34] Coleman, H.W., Moffatt, R.J., Kays, W.M., 1977, "The accelerated fully rough turbulent boundary layer". *J. Fluid Mech*. 82, 507

[35] Coleman, H.W., Steele, W.G., 1995, "Eng. application of experimental uncertainty analysis". *AIAA Journal*, 33(10), pp. 1888– 1896

[36] Coles, D.E., 1956, "The law of the wake in the turbulent boundary layer". *J. Fluid. Mech.*, 1, pp. 191–226.

[37] Connelly, J.S., Schultz, M.P., Flack, K.A., 2006, ''Velocity-defect scaling for turbulent boundary layers with a range of relative roughness''. *Exp. Fluids* 40, pp. 188–195

[38] Das, D.K., 1987, "A numerical study of turbulent separated flows". *Amer. Soc. Mech. Engineers*, Forum on Turbulent Flows, FED, 1(1), pp. 83-99

[39] Dienidi L., Dubief, Y., Antonia, R.A., 1997, ''Advantages of using power law in the low Re_θ boundary layers''. *Exp. in Fluids*, 22, pp.348-350

[40] Durbin, P.A., Belcher, S.E., 1992, "Scaling of adverse-pressure-gradient turbulent boundary layer". *J. Fluid Mech.*, 238, pp. 699-722

[41] Emamzadeh, A., Yee, M.C., Afzalimehr H. 2010, "Effect of accelerating and decelerating flows on incipient motion in sand bed streams". *Advance in Water Resources*, 33, pp. 1094-1104

[42] Faruque, M.F., 2009, Smooth and Rough Wall Open Channel Flow Including Effects of Seepage and Ice Cover, PhD thesis, University of Windsor, Windsor, Canada

[43] Flack, K.A., Schultz, M.P., Shapiro, T.A., 2005, "Experimental support for Townsend's Reynolds number similarity hypothesis on rough walls". *Phys. Fluids* 17, 035102

[44] George W.K., Castillo, L., 1997, ''Zero-pressure gradient turbulent boundary layer''. *Applied. Mechanics. Review*. 50(11), pp. 689-72

[45] Graf, W.H., Altinakar, M.S.,1998, "Fluvial hydraulics-flow and transport. processes in channels of simple geometry". Wiley

[46] Granville, P.S., 1976 "A modified law of the wake for turbulent shear layers". Trans. ASME I, *J. Fluids Eng*., 98, pp. 578–580

[47] Grass, A.J., 1971 "Structural features of turbulent flow over smooth and rough boundaries". *J. of Fluid Mech.*, 50(2), pp. 233-255

[48] Hinze, J.O., 1959, "Turbulence: an introduction to its mechanism and theory". McGraw- Hill, New York.

[49] Ippen, A.T., Raichlen, F., 1957, "Turbulence in civil engineering: Measurements in free surface streams". *J. Hydr. Div., Am. Soc. Civ. Eng.*, 83(5), pp. 1–27

[50] Jimenez, J., 2004, "Turbulent flows over rough walls". *Annu. Rev. Fluid Mech.* 36, pp. 173–196

[51] Kaftori, D., Hetsroni, G., Banerjee, S., 1995, "Particle behavior in the turbulent boundary layer. I. Motion, deposition, and entrainment". *Physics of Fluids,* 7(5), pp. 1095-1106

[52] Karman T.V., 1930, "Mechanische ahnlichkeit und turbulenz". Nachr Ges. Wiss. Gottingen, Math. Phys. Klasse 58-76

[53] Kirkgoz, M.S., Ardichoglu, M., 1997, "velocity profiles of developing and developed open channel flow". *J. Hydr. Eng.*, 123(1), pp. 1000-1105

[54] Kironoto, B.A., Graf, W.H., 1995, "Turbulence characteristics in rough non-uniform open channel flow". *Proc Instin Civ Eng Wat, Marit Energy*; 112, pp. 336–348

[55] Knight, D.W., Patel, H.S., 1985, "Boundary shear in smooth rectangular ducts". *J. Hydr. Eng.,* ASCE, 111, pp. 29-47

[56] Kotey, N.A., Bergstrom, D.J., Tachie, M.F, 2003, "Power laws for rough wall turbulent boundary layers". *Physics of Fluids,* 15 No. 6, pp. 1396-1404

[57] Krogstad, P.A., Antonia, R.A., 1999, "Surface roughness effects in turbulent boundary layers". *Exp. in Fluid,* 27, pp. 450-460

[58] Krogstad, P., Antonia, R., Browne, L.W.B., 1992, “Comparison between rough and smooth-wall turbulent boundary layers”. *J. of Fluid Mech.,* 245, pp. 599-617

[59] Krogstad, P.A., Skare, P.E., 1995, “Influence of a strong adverse pressure gradient on the turbulent structure in a boundary layer”. *Physics Fluid*, 7(8), pp. 2014-2024

[60] Launder, B.E., 1964, “Laminarization of the turbulent boundary layer in a severe acceleration”. *Tech. Rep. 77*. MIT Gas Turbine Lab. Cambridge, MA, USA

[61] Lee J.H., Sung, H.J., 2007, “Direct numerical simulation of the turbulent boundary layer over a rod-roughened wall”. *J. Fluid Mech*. 584, pp. 125–146

[62] Lee, J.H., Sung, H.J., 2008, “Effects of an adverse pressure gradient on a turbulent boundary layer”. *Int. J. Heat Fluid Flow*, 29, pp. 568–578

[63] Lee, J.H., Sung, H.J., 2009, “Structures in turbulent boundary layers subjected to adverse pressure gradients”. *J. Fluid Mech*., 639, pp. 101–131

[64] Lee, J., Lee, J.H., Sung, H.J., 2010, “Coherent structures in turbulent boundary layers with adverse pressure gradients”. *J. Turbul.*, 11(28), pp. 1–20

[65] Long, L., Chen, T.C., 1981, ‘‘Experimental evidence for the existence of the ‘Mesolayer in turbulent system’’. *J. of Fluid Mech.*, 150, pp. 19-52

[66] Marusic, I., McKeon, B.J., Monkewitz, P.A., Nagib, H.M., Smits, A.J., Sreenivasan, K.R., 2010, “Wall-bounded turbulent flows at high Reynolds numbers: recent advances and key issues”. *Phys. Fluids*, 22(065103), pp. 1–24

[67] Marusic, I. Perry, A.E., 1995, “A wall-wake model for the turbulence structure of boundary layers”. Part 2. Further experimental support. *J. Fluid Mech*., 298 pp. 389–407

[68] Monty, J.P., Harun, Z., Marusic, I., 2011 “A parametric study of the adverse pressure gradient turbulent boundary layers”. *Int. J. of Heat and Fluid flow*, 32, pp. 575-585

[69] Nagib, H.M., Chauhan, K.A., 2008. “Variations of von Karman coefficient in canonical flows”. *Phys. Fluids*, 20(101518), pp. 1–10

[70] Nagano, Y., Houra, T., 2002, “Higher-order moments and spectra of velocity fluctuations in adverse-pressure-gradient turbulent boundary layer”. *Exp. Fluids*, 33, pp. 22–30

[71] Nagano, Y., Tagawa, M. Tsuji, T., 1991, “Effects of adverse pressure gradients on mean flows and turbulence statistics in a boundary layer”. *Proc. 8th Symp. on Turb. Shear Flows*, pp. 7-20

[72] Nagano, Y., Tsuji, T., Houra, T., 1998, “Structure of turbulent boundary layer subjected to adverse pressure gradient”. *Int. J. Heat and Fluid Flow*, 19, pp. 563–572

[73] Nakagawa, H.I., Nezu, A., Ueda, H., 1975, “Turbulence of open channel flow over smooth and rough beds”. *Proc. of Japan Soc. Civil Eng*., 241, pp. 155-168

[74] Nezu, I, 2005, “Open channel flow turbulence and its research prospect in the 21st century”. *J. Hydraul. Eng.*, 131(4), pp. 229–246

[75] Nezu, I., Kadota, A., Nakagawa, H., 1994, “Turbulence structure in accelerating and decelerating open-channel flows with laser Doppler anemometers”. *In Proceedings of the ninth congress*, APD-IAHR; pp. 413–420

[76] Nezu, I., Nakagawa, H., 1991, “Response of velocity and shear stress to abrupt irregularity of bed roughness in streams”. Proc. 24th IAHR Congress., A, Delf, Netherland, pp. 233-242

[77] Nezu, I., Nakagawa, H., 1993a, “Turbulence in open channel flow”. *J. Hydr. Eng.*, 112, pp. 335-355

[78] Nezu, I., Nakagawa, H., 1993b, “*Turbulence in Open Channel Flows*”. International Association for Hydraulic Research, A.A. Balkema Publishers, Rotterdam

[79] Nezu, I., Nakagawa, H., 1993c, “Three dimensional structure of coherent vortices generated behind dunes in turbulence free surface flows”. Proc. 5th Int. Symo. on Refined Flow Modeling and Turbulence Measurements., pp. 603-612

[80] Nezu, I., Rodi, W., 1986, “Open channel flow measurements with a laser Doppler anemometer”. *J. Hydr. Eng.*, 112(5), pp. 335-355

[81] Nikora, V.I., Goring, D.G., McEwan, I., Griffiths, G., 2001, “Spatially averaged open channel flow over rough bed”. *J. Hydr. Eng.*, 127, pp. 123– 133

[82] Österlund, J.M., Johansson, A.V., Nagib, H.M., Hites, M.H., 2000, ‘‘A note on the overlap region in turbulent boundary layers’’. *Phys. Fluids*, 12, pp.1 -4

[83] Pearce, N.F., Denissenko, P., Lockerby, D.A., 2013, “An experimental study into the effects of streamwise and spanwise acceleration in a turbulent boundary layer”. *Exp. Fluids*, 54(1414), pp. 1-17

[84] Perry, A., Schofield, W., Joubert, P., 1969, “Rough wall turbulent boundary layers”. *J. of Fluid Mech.*, 37 pp. 383-413

[85] Prandtl, L., 1925, “Über die ausgebildete Turbulence”. *ZAMM*, 5: 136

[86] Rashidi, M., Hetsroni, G., Banerjee, S., 1990, “Particle-turbulence interaction in a boundary layer”. *International J. of Multiphase Flow*, 16(6), pp. 935-949

[87] Raupach, M.R., 1981, "Conditional Statistics of Reynolds Stress in Rough-wall and Smooth-wall Turbulent Boundary Layers". *J. Fluid Mech.,* 108, pp. 363-382

[88] Raupacham, R. Antonia, Rajaqopalans, R.A., 1991, "Rough-wall turbulent boundary layers". Appl. Mech., Rev., 44, pp. 1-25

[89] Roussinova, V., Balachandar, R., Biswas, N., 2009, "Reynolds stress Anisotropy in open-channel flow". *Hydraul. Eng.*, 135, Issue 10, pp. 812-825

[90] Roussinova,V., Biswas, N., Balachandar, R., 2006, "Revisiting turbulence in smooth uniform open channel flow". *J. of Hydr. Res.,* 46(Extra Issue 1), pp. 36-48

[91] Schlichting, H. 1979, "*Boundary-layer theory*". 7th ed., McGraw-Hill, New York

[92] Schultz, M.P., Flack, K.A., 2005, ''Outer layer similarity in fully rough turbulent boundary layers''. *Exp. in Fluids,* 38, pp. 328-340

[93] Schultz, M.P., Flack, K.A., 2007, ''The rough-wall turbulent boundary layer from the hydraulically smooth to the fully rough regime''. *J. of Fluid Mechanic,* 580, pp. 381-405

[94] Schultz, M.P., Wain, G.W., 1999, "The effect of biofilms on turbulent boundary layers". *J. of Fluids Eng.*, 21(1), pp. 44–51

[95] Schwarz, A., Plesniak, M.W., Murthy S.N.B., 1999, "Turbulent boundary layer subjected to multiple strains". *Trans. SME, J. Fluids Eng.*, 121, pp. 526-632

[96] Shah, M.K., Tachie, M.F., 2008, "PIV study of turbulent flow in asymmetric converging and diverging channels". *ASME J. of Fluid Engrg*., 130, pp.1-15

[97] Skare, P.E., Krogstad, P.A., 1994, "A turbulent equilibrium boundary layer near separation". *J. Fluid Mech.*, 272, pp. 319–348

[98] Skote, M., Henningson, D.S., 2002, “Direct numerical simulation of a seperated turbulent boundary layer”. *J. Fluid Mech.,* 471, pp. 107–136

[99] Song, T., 1994, “Velocity and turbulence distribution in non-uniform and unsteady open channel flow”. *Ecole Polytech. Federale De Lausanne*

[100] Song T, Chiew Y.M., 2001 “Turbulence measurement in non-uniform open channel flow using Acoustic Doppler Velocimeter (ADV)”. *J. of Eng Mech,* 127(3), pp.219–232

[101] Song, T., Graf, W.H., 1994, “Non-uniform open-channel flow over a rough bed”. *J of Hydroscience and Hydr. Eng.*, 12(1), pp. 1–25

[102] Song Z.Y., yan, Y.X., Lv, G.N., 2009, “Vertical distribution of tidal flow Reynolds stress in shallow water”.Chaina ocean Eng., 23(2), 10933-10949

[103] Spalart, P.R., Watmuff, J.H., 1993, “Experimental and numerical study of a turbulent boundary layers with pressure gradients”. *J. Fluid Mech.*, 249, pp. 337-371

[104] Spalding D.B., 1961, “A single formula for the " law of the wall"”. *J. of applied Mech.*, 28, pp. 455-458

[105] Sreenivasan, K.R., Narasimha, R., 1982, “Equilibrium parameters for two dimensional turbulent wake”. *J. Fluid eng.,* 104, pp. 167-170

[106] Steffler, P.M., Rajaratnam, N., Peterson, A.W., 1985, “LDA measurements in open channel”. *J. Hydr. Eng*., 111(1), pp. 119–130

[107] Tachie, M.F., 2001, “Open-channel turbulent boundary layers and wall jets on rough surfaces”. PhD thesis, University of Saskatchewan, Saskatchewan, Canada

[108] Tachie, M.F., 2007, “Particle image velocimetry study of turbulent flow over transverse square ribs in an asymmetric diffuser”. *Phys. Fluids,* 19(065106)

[109] Tachie, M.F., Bergstrom, D.J., Balachandar, R., 2000, "Rough wall turbulent boundary layers in shallow open channel flow". *J. of Fluids Eng.,* 122, pp. 533-541

[110] Tachie, M.F., Bergstrom, D. J., Balachandar, R., 2003, "Roughness effects in low- Re_θ open-channel turbulent boundary layers". *Exp. in Fluids*, 35, pp. 338-346

[111] Tachie, M.F., Shah, M., 2008, "Favorable pressure gradient turbulent flow over straight and inclined ribs on both channel walls". *Physics of Fluids,* 20(095103), pp. 20-21

[112] Tani, I., Munakatha, H., Matsumotoa, A., Abe, K., 1988, "Turbulence management by groove roughness". *In Turbulence Management and Relamimrisation,* Springer, (ed. H. W. Liepmann & R. Narasimha), pp. 161-172

[113] Tay, G.F.K., Kuhn, D.C.S., Tachie, M.F., 2009. ''Influence of adverse pressure gradient on rough-wall turbulent flows''. *Int. J. Heat Fluid Flow,* 30(2), pp. 249–265

[114] Tennekes, H., Lumley, J,L., 1972, ''*First Course in Turbulence*''. MIT, Cambridge, MA

[115] Townsend, A.A., 1976, "*Turbulent Structure of Turbulent Shear Flow*". Cambridge University Press

[116] Tsikata, J.M., Tachie, M.F., 2013, "Adverse pressure gradient turbulent flows over rough walls". *Int. J. of Heat and Fluid* Flow, 39, pp. 127-145

[117] Tsujimoto, A., Cardoso, A.H., Saito, A., , 1990, "Open channel flow with spatially varied bed shear stress". *J of Hydroscience and Hydr. Eng*, 8,(2), pp.1–52

[118] Volino, R.J., Schultz, M.P., Flack, K.A., 2009 "Turbulent structure in a boundary layer with two-dimensional roughness". *J. Fluid Mech.,* 635, pp. 75–101

[119] White, F.M., 1974, "*Viscous Fluid Flow*". McGraw-Hill, New York

[120] Wosnik, M., Castillo, L., George, W.K., 2000, "A theory for turbulent pipe and channel flows". *J. Fluid Mech.,* 421, pp.115–145

[121] Yang, S., 2009, "Velocity distribution and wake-law in gradually deceleration flows". *J. of Hydr. Res.,* 47(2), pp. 177-184

[122] Yang, S., Lee, J.V., 2007, "Reynolds shear stress distribution in gradually varied flow". *J. of Hydr. Res.,*, 45(4), pp. 426-471

[123] Yang, S.Q., Chow, A.T., 2008, "Turbulence structures in non-uniform flows". *Advances in Water Resources*, 31, pp. 1341-1351

[124] Yang, S., Tan, S., Lim, S., 2004, "Velocity and sediment concentration profiles in sediment-laden flows". China Ocean Eng., 18(2), pp. 229–44

[125] Yang, S. Tan, S. Lim., 2004, "Velocity distribution and dip phenomena in smooth and straight open channel flow". *J. Hydr. Eng*., ASCE 130(12), pp. 1179–86

[126] Yang, S.Q., Xu, W.L., Yu, G.L., 2006, "Velocity distribution in a gradually accelerating free surface flow". *Adv Water Res*, 29(12), pp. 1969–1980

[127] Yanta, W.J., Smith, R.J., 1973, "Measurements of turbulence transport properties with a laser Doppler velocimetry". *AIAA Paper.*, 73, pp. 73-169

[128] Zagarola, M.V., Perry, A.E., Smits, A.J., 1997, ''Log laws or power laws: The scaling in the overlap region''. *Phys. Fluids,* 9, 2094

[129] http://water.me.vccs.edu

VITA AUCTORIS

NAME:	Mohammad H. Asgari Kaji
PLACE OF BIRTH:	Ardal, Iran
YEAR OF BIRTH:	1977
EDUCATION	SUT-MUT, Tehran, Iran
	1997-2001, B.Sc. Aerospace Engineering
	SUT, Tehran, Iran
	2008-2010, M.Sc. Aerospace Engineering
	University of Windsor, Windsor, Ontario
	2001-2013, M.A.Sc., Civil and Environmental Engineering